AROMATICITY AND FLEXIBILITY OF TRANSMEMBRANE HELIX 12 CONTRIBUTE TO SUBSTRATE RECOGNITION AND TRANSPORT IN HUMAN P-GLYCOPROTEIN

by

Jason Anthony Goebel

A Dissertation

Submitted to the Faculty of Purdue University

In Partial Fulfillment of the Requirements for the degree of

Doctor of Philosophy

Department of Chemistry

West Lafayette, Indiana

December 2020

THE PURDUE UNIVERSITY GRADUATE SCHOOL

STATEMENT OF COMMITTEE APPROVAL

Dr. Christine A. Hrycyna

Department of Chemistry

Dr. Jean A. Chmielewski

Department of Chemistry

Dr. Angeline M. Lyon

Department of Chemistry

Dr. Shalini T. Low-Nam

Department of Chemistry

Approved by:

Dr. Christine A. Hrycyna

Dedicated to my family and friends

ACKNOWLEDGMENTS

I want to first thank my parents Tony Goebel and Donna Simoneaux Svenson for all their support, I would not be here without them. Dad, you inspired and supported my love of science from the very beginning and help me realize the potential I had within. Mom, your love and support were a constant reminder that I could achieve whatever I set my mind to. I cannot begin to express how thankful I am to the both of you here, but I am so thankful to both of you for helping me become the individual I am today and giving me the opportunity to realize my dreams. I want to thank my bothers Gerard and Jeff Ramos for being my role models growing up. Gerard, you showed me that with drive and determination anything is possible. Jeff, you showed me how much can be achieved with good leadership and teamwork. I want to thank my grandparents, Donald and Gloria Simoneaux, and the rest of my family, who are too numerous to name here, for all their support and words of encouragement while I chased this crazy desire to stay in school.

Second, I want to thank those who helped me through my educational career. Len Hamner and Mark Nabors were ironically my teachers in my two least favorite high school subjects, history and English, but were so important in the early development of my education. Ms. Hamner saw the potential I had in the classroom and pushed me to take a more active role in my education showing me what I could accomplish when I applied myself. Coach Nabors sparked the expansion of my perspective of the world with on simple statement; baseball and football are the only two sports. It is a definitional argument that made me consider a different perspective than my own and opened my mind to an expanded way of thinking. Next the University Fellows program at Samford University took what Coach Nabors taught me to the wider Western Intellectual Tradition. WIT was a giant, challenging sidestep from biochemistry that would ultimately help shape my understanding and perspective of myself and the world. The University Fellows expanded my perspective in so many aspects that have been indispensable in my understanding of and approach to biochemistry. Finally, I want to thank my research advisors Dr. Andy Lampkins and Dr. Steve Donaldson and the Chemistry and Biochemistry department at Samford University. Dr. Lampkins was my first experience in a research lab and that lab is where I confirmed my passion for chemistry and experienced how rewarding research can be.

I want to thank all of my friends for their support. I want to thank Zach and Megan Brown, David Meadows, Taylor Alan Burgess (TAB), Sean Altendorf, Scott Simpson, and Evan Elmore.

You all have been a constant support and source of encouragement over the years. Dnd, Magic, Bee game and so on were always a great outlet and random, impromptu conversations were always welcomed. Also, I want to thank Alana Perković whom I would always joke about curing cancer with some day back in high school. Those memories and your compassion for others have motivated me to continue to strive to help others through research.

Finally, I want to thank my lab and all of my lab mates. Allison Lange, you were my mentor and helped me to get started in the lab as well as being a good friend. Elias Beretta, I may not have mentored you on all of the organic side of the project, but we have worked through many of the difficulties of our project together. I want to thank Anna Ratliff who was a friend before joining the lab and was my contemporary in grad school. I also want to thank all current and previous lab members: Ari, Chelsea, Shanica, Akansha, Erh-Ting, and all the other members. Liz Garland-Kuntz, where would the lab be without you; you have helped us all so much. Dr. Christine Hrycyna, emphasis on the sin, thank you for being my advisor, for pushing me, and helping me find confidence in the lab.

TABLE OF CONTENTS

LIST OF TABLES

LIST OF FIGURES

LIST OF ABBREVIATIONS

ABC	ATP Binding Cassette
ADME	Adsorption, Distribution, Metabolism, and Excretion
APS	Ammonium Persulfate
ATP	Adenosine Triphosphate
ATPase	Adenosine Triphosphate Hydrolase
BD	Bodipy
BME	Basal Medium Eagle
BSA	Bovine Serum Albumin
CFTR	Cystic Fibrosis Conductance Regulator
CL	Cysteine-less
Cryo-EM	Cryo-electron Microscopy
DiOC2	3,3’-Diethyloxacarbocyanine Iodide
DMEM	Dulbecco's Modified Eagle Medium
DMSO	Dimethyl Sulfoxide
ECD	Extra Cellular Domain
FBS	Fetal Bovine Serum
FSC	Forward Scatter
HDL	High Density Lipoprotein
His_6	6-Histidine Tag
ICD	Intracellular Domain
IF	Inward Facing
IH	Intracellular Helix
IRES	Internal Ribosomal Entry Site
MDR	Multidrug Resistance
MFI	Mean Fluorescence Intensity
MHC	Major Histocompatibility Complex
MOI	Multiplicity of Infection
*m*P-gp	Mouse P-glycoprotein

MRP	Multidrug Resistant Protein
NBD	Nucleotide Binding Domain
NBS	Nucleotide Binding Site
NCS	Newborn Calf Serum
NTP	Nucleotide Triphosphate
OABP	Organic Anion-Binding Protein
OF	Outward Facing
PAGE	Polyacrylamide Gel Electrophoresis
PBS	Phosphate Buffer Saline
PBST	Phosphate Buffer Saline plus Tween
PCR	Polymerase Chain Reaction
PFIC	Progressive Familial Intrahepatic Cholestasis
P-gp	Human P-Glycoprotein
PK	Protein Kinase
P-loop NTPase	P-loop Containing Nucleoside Triphosphate Hydrolase
SDS	Sodium Dodecyl Sulfate
Sf9	*Spodoptera frugiperda*
SSC	Sideways Scatter
STDG	Stargardt Disease
TAP1/2	Transporter Associated with Antigen processing 1/2
TEMED	N,N,N’,N’-Tetramethylethylenediamine
TM	Transmembrane
TMD	Transmembrane Domain
TMH	Transmembrane Helix
VLCFA	Very Long Chain Fatty Acids
WT	Wild Type

ABSTRACT

Human p-glycoprotein (P-gp) is an ATP-binding cassette transporter that actively transports a diverse set of substrates at the plasma membrane. Specifically, P-gp is expressed most highly at important blood tissue barriers on the lumenal side of endothelial cells and secretory tissues asymmetrically where it provides generalized protection against xenobiotics due to its promiscuous substrate binding pocket. Substrates typically interact with P-gp within the inner leaflet of the plasma membrane before being effluxed through large conformation changes driven by ATP binding and hydrolysis. Since many small molecule drugs are substrates of P-gp and P-gp has the ability to transport chemically and structurally diverse molecules, delivery of bioavailable small molecule therapies and treatment of diseases beyond blood-tissue barriers may be difficult. In cancer, expression of P-gp may confer a multidrug resistance phenotype due to upregulation of the MDR1 gene, which encodes P-gp, in response to treatment with chemotherapies. Treatments of diseases beyond blood-tissue barriers and some cancers may be more complex given the protective role of P-gp coupled with it promiscuous substrate binding site.

Many studies of P-gp have been centered around understanding the structure function relationship of how P-gp effluxes small molecules across the plasma membrane. Here we have used a transient Vaccinia virus expression system to rapidly express many mutants of P-gp in human cells for analysis. Transient expression using the Vaccinia system was optimized to produce a large amount of protein while avoiding significant cell death. Optimization of the Vaccinia expression system has also helped to show that changes in P-gp surface expression are not correlated to changes in substrate accumulation within cells expressing P-gp, a topic that has yet to be addressed within the field of P-gp study. Reduced surface expression of P-gp to 68% maintained the same level of reduced cellular accumulation of two substrates, calcein-AM and rhodamine 123, relative to a WT P-gp control. Further study of P-gp mutations revealed a Y998A mutation had a 90% reduction of surface expression but the same reduction of cellular accumulation of rhodamine 123 further supporting that changes in surface expression do not correlate to changes in substrate transport.

We then sought to demonstrate how flexibility in transmembrane helix (TMH) 12 of P-gp affected overall stability and transport ability *in vitro*. TMH 12 in inward facing conformations shows a region of decreased hydrogen bonding in the backbone of the helix leading to a “kink”

present in many crystal structures of *C. elegans* and mouse P-gp as well as in an occluded structure of human P-gp. Outward facing crystal structures of *C. elegans*, mouse, and human P-gp show TMH 12 where the backbone of the helix is fully hydrogen bonded and ordered. The change in hydrogen bonding pattern and the presence of the kink in TMH 12 suggest the importance of flexibility in the function of TMH 12. Clustal Omega was used to align the primary structure of P-gp between 8 species and a conserved sequence of 996-PDYAKA-1001 was identified aligning with the kink observed in crystallographic data. The kinked nature of this region led to our development of a rigid poly-alanine mutation and a flexible poly-glycine mutation based on the propensity of these amnio acids to form helices. The more flexible poly-glycine mutation obtained no significant transport while the poly-alanine mutation maintained some ability to transport fluorescent substrate relative to a WT control. Crosslinking of the nucleotide binding domains (NBDs) revealed a decrease of NBD dimerization likely correlating to decreased transport. Thus, some degree of flexibility within the kink region is critical for substrate transport as rigid and flexible mutations of this region abrogate transport of fluorescent substrates.

While the substrate binding pocket it located towards the interior of P-gp within the lipid bilayer, it has been theorized that substrates may interact with P-gp at the lipid-protein interface of the inner leaflet near portals for substrate entry formed by pairs of helices either side of the protein. To test this hypothesis, aromatic residues on TMH 12 and adjacent elbow helix 2 near the interface region of the inner leaflet, that have also been observed to interact with a cyclic peptide in a crystal structure of P-gp, were mutated to alanine. Y998, on TMH 12, was shown to interact with the cyclic peptide and is ideally located at the protein-lipid interface near a surface formed by elbow helix 2 and TMH 9 and was observed to have the largest effect on substrate accumulation. Accumulation of fluorescent substrates, relative to WT P-gp, was increased though not all substrates were affected similarly. No increase of accumulation was observed with rhodamine 123 while accumulation of BD-prazosin increased 65% relative to WT P-gp. It is to be expected that the large diversity of substrates recognized by P-gp would interact preferentially with carrying residues at the protein-lipid interface similar to observations of substrate binding at the substrate binding pocket. Variability in accumulation signifies that substrates do interact with P-gp at the lipid-protein interface and substrates interact differently at this interface similarly to substrate interaction at the substrate biding pocket.

CHAPTER 1. INTRODUCTION TO THE STRUCTURE AND FUNCTION OF ABC TRANSPORTERS AND HUMAN P-GLYCOPROTEIN

1.1 ABC Transporters

ATP Binding Cassette (ABC) transporters are integral membrane proteins found in all domains of life.[1,2] These transporters utilize energy from ATP hydrolysis to transport a wide variety of substrates across membranes including ions, amino acids, polypeptides, sugars, lipids, metabolites, ligands, xenobiotics, and synthetic small molecules such as those related to drugs, pesticides, and so on.[3–7] Eukaryotic ABC transports typically consist of two conserved domains in pairs: a nucleotide binding domain (NBD) and a transmembrane domain (TMD) though there are some exceptions. These four domains do not have to be encoded by the same polypeptide. ABC transporter NBDs contain commonly conserved ATP binding motifs, many of which are observed in other common ATP binding proteins. TMDs consists of several transmembrane helices that form binding sites and channels for substrate transport in ABC transporters. ABC transporters undergo large conformational changes from inward to outward or outward to inward facing conformations to transport substrate. While many prokaryotic transporters are importers, most eukaryotic ABC transporters are exporters.[8,9]

1.1.1 Eukaryotic ABC Transporters

Eukaryotic ABC transporters have been classified into seven ABC transporter families from ABCA to ABCG based on domain organizations (Figure 1.1) and primary sequence homology.[10–15] Members of these families are widely distributed in eukaryotes and can vary drastically. ABCE and ABCF, despite being classified as ABC transporters, do not function as transporters but are instead involved in other cellular functions, including translational control and ribonuclease inhibition.[16,17] This is primarily due to the fact that these two families no longer contain TMD domains and adopt a NBD-NBD conformation. Organization of ABC domains in a NBD-TMD-NBD-TMD or TMD-NBD-TMD-NBD are designated full transporters while organization of domains in a NBD-TMD or TMD-NBD designate half transporters.[18] Half transporters can form homodimers or heterodimers to adopt a full transporter structure.[19] A small

number of transporters consist of single TMD and NBD domains that come together to form the full transporter.[9] Unlike bacterial ABC transporters, the majority of eukaryotic transporters are exporters.[8,9] Eukaryotic transporters are present in virtually all cell types and transport a plethora of substrates across cellular and organelle membranes with the likely exception of the nuclear membrane.

1.1.2 Human ABC Transporters

The human ABC superfamily consists of 49 ABC genes designated into seven subfamilies labeled A to G. These genes encode mostly transporters, as exporters, that move a large variety of substrates from one side of a membrane to the other. Substrates range from ions, peptides, amino acids, fats, and sugars to metabolites and a large number of hydrophobic compounds. The ABC gene family is part of the P-loop containing nucleoside triphosphate hydrolase superfamily (P-loop NTPase) which contains a large number of genes associated with nucleotide binding and hydrolysis.[20,21]

12 genes are associated with subfamily A which make up some of the largest ABC transporters with ABCA13 containing 5058 residues.[22] ABCA transporters are typically involved in lipid trafficking throughout most tissues.[23] ABCB contains 11 genes that are unique to mammals. Many ABCB transporters confer the multidrug resistance (MDR) phenotype and is thus commonly referred to as the MDR family of ABC transporters though they are not the only family to confer this phenotype. ABCB1, human P-glycoprotein (P-gp), is the trademark of this family and has been heavily implicated in MDR leading it to be one of the most studied ABC transporters and is the focus of this thesis. Subfamily C includes 13 genes and is involved in ion transport as well as transport of fungal and bacterial toxins. Like the ABCB family, ABCC transporters also display the MDR phenotype with the MRP genes ABCC1-5.[24] ABCC7 is unique among the ABC superfamily in that it is an cAMP-regulated chlorine ion channel and not an active transporter.[25] Deficiencies in ABCC7, also known as CFTR, are directly linked to cystic fibrosis.

Peroxisomal or ALD transporters make up the ABCD family of ABC transporters.[26] This family contains 4 genes that encode half transporters that can either homo or heterodimerize to make functional full transporters. ABCD transporters primarily transporter fatty acids in peroxisomes or lysosomes and are involved in the transport of very long chain fatty acids (VLCFA).[27]

ABCE1 is the only member of its ABC transporter family and lacks a transmembrane (TM) domain encoding just the NBD domain. ABCE1 binds organic anions and is known more commonly as the organic anion-binding protein, OABP. Instead of transporting molecules across membranes, ABCE1 instead is part of ribosomal regulation and recycling.[28] The 3 genes of the ABCF family, like the ABCE family, do not contain TM domains instead only encoding for the NBD domains. ABCF genes are upregulated by necrosis factor-α thus it is believed that ABCF proteins are involved in inflammatory responses.[29]

Finally, the ABCG family encodes 5 genes that are half transporters and primarily transport sterols while some family members transporter a larger variety of substrates. ABCG2, or the breast cancer resistance protein (BCRP), is the most well known of the ABCG family as it has been implicated in acquired MDR phenotypes of some breast cancers.

Human ABC transporters are critically important in a large variety of physiological functions and studying this superfamily is critical for the diseases and MDR phenotypes associated with the ABC transporter superfamily.

1.2 Diseases Associated with Human ABC Transporters

Human ABC transporters so far have been shown to be involved in many substrate transport activities, transporting a large variety of substrates, and are almost ubiquitously found throughout tissues in the human body. With 49 genes in the human ABC family there are several diseases associated with loss of function either through mutation or loss of expression. Defects in 14 ABC transporter genes have been associated with human disease. Tangier disease is an autosomal genetic disease associated with high-density lipoprotein (HDL) deficiencies, sterol deposition in macrophages, and atherosclerosis. Autosomal recessive mutations in ABCA1 have been directly linked to Tangier disease and other familial HDL deficiencies.[30] ABCA4, a retinoid transporter, has been linked to another autosomal recessive disease in Stargardt disease (STGD).[31] Deficiencies in ABCA4 in STGD lead to age-related macular degeneration.[32] ABCB2 and ABCB3, also known as TAP1/TAP2, are half transporters that heterodimerize to form a full transporter of major histocompatibility complex (MHC) molecules.[33] Decreased expression of either ABCB2 or ABCB3 leads to age related immune deficiencies.[34] ABCB4 and ABCB11, transporters of bile-acids, have been linked to progressive familial intrahepatic cholestasis (PFIC) 3 and 2 respectively.[35,36] Transport of Fe-S clusters at mitochondria has been linked to ABCB7 and as such

defects in ABCB7 function or expression lead to iron deficiency related disease.[37] Suppression of the ABCB7 gene x-linked sideroblasts and anemia.[38,39] Dubin-Johnson syndrome, which causes black liver due to a buildup of conjugated bilirubin, is caused by mutation in ABCC2, a bile acid transporter.[40] ABCC6 deficiencies have been linked to cardiovascular disease and pseudoxanthoma elasticum.[41,42] No known substrate of ABCC6 has been identified which has made the underlying cause of the associated disease difficult to determine.[43] ABCC7, CFTR, an ion channel and not a typically ABC transporter is linked most cases of cystic fibrosis or the buildup of fluid in the lungs of patients.[44] Decreased transport of VLCFAs into peroxisomes by low expressing ABCD1 phenotypes is linked to x-linked adrenoleukodystrophy in both children and adults.[45] Cholesterol and other sterols are typically excreted in kidneys by ABCG5 and ABCG8. Disruption of these genes leads to sitosterolemia where buildup of dietary sterols is observed.[46]

1.2.1 Multidrug Resistance Associated with ABC Transporters

Many ABC transporters have the ability to transport a large number of chemically and structurally diverse molecules due to highly heterogeneous TMDs allowing for the binding pocket of these proteins to be promiscuous. The most common function of the most promiscuous of the ABC transporters is typically linked to a protective roll by effluxing xenobiotics at important blood-tissue barriers and excretory organs. A consequence of the protective nature of these proteins is that these transporters can affect the pharmacokinetic profile of absorption, distribution, metabolism, and excretion (ADME) of many drugs.[47] Conversely inhibition or decreased genetic expression of these transporters can lead to pharmacokinetic changes and even toxicity due to alterations in ADME and drug-drug interactions.[48] Many studies done with cell culture models and animal models show efflux activity of ABC transporters mediates multidrug resistance.[49–51]

P-gp (ABCB1), BCRP (ABCG2), and MRP1 (ABCC1) are the most studied transporters of the 49 ABC transporter genes.[51] These ABC transporters transport a considerable number of pharmacologically important substrates including but not limited to anti-cancer drugs, tyrosine kinase inhibitors, steroids, anti-epileptics, analgesics, antibiotics, cholesterol-lowering agents, anthelmintics, Ca^{2+} channel blockers, calmodulin antagonists, cardiac glycosides, HIV protease inhibitors, immunosuppressive agents, ionophores and so on.[52–54] While P-gp, ABCG2, and MRP1 are typically most often associated with MDR other ABC transporters, mostly in the ABCA – C

families, have also been shown to be able to transport a variety of substrates and have been associated with the MDR phenotype.[55–58] Occurrence of MDR phenotypes and the difficulty to treat disease with therapeutics effluxed by these proteins makes the study of ABC transport mediated MDR of great importance.

1.3 Characterization of P-Glycoprotein

1.3.1 General Characterization of P-Glycoprotein

P-glycoprotein is a member of the ABC superfamily of proteins and was the first discovered ABC transporter as well as being one of the most studied ABC transporters. It was discovered through its contribution to MDR in cultured cancer cells subjected to increasing levels of toxic compounds. Specifically, Chinese hamster ovary cells were exposed to increasing levels of colchicine until the cells became resistant to a number of chemically and structurally unrelated chemotherapeutics thus acquiring MDR.[59] Over time, this observed phenotype in MDR CHO cells was correlated to expression of a 170 kDa glycoprotein through purification of protein from colchicine resistant CHO cells and later became known as P-gp.[60] Since P-gp's discovery an entire superfamily of genes have been described.

Human P-gp is encoded by the ABCB1 gene and contains 1280 amino acids in its most common isoform. Its domain structure follows the NBD-TMD-NBD-TMD form where the two halves of the P-gp protein are homologous (Figure 1.2). Homogeneity between the halves of the protein follows a likely gene duplication event which resulted in the creation of the ABCB1 gene.[61] The NBDs are cytosolic facing while the TMDs, each containing 6 TM helices, span the plasma membrane. Substrates of P-gp are effluxed into extra-cellular space through large dynamic conformational changes driven by the NBDs and hydrolysis of ATP. Localization of P-gp is observed at several organs and barriers in the body including kidney, liver, gastrointestinal tract, and epithelial cells including blood-tissue barriers such as the blood brain barrier (BBB).[62] P-gp is asymmetrically trafficked in these tissues and primarily resides on the lumenal side of these tissues to help in secretion or protection from xenobiotics.[63]

P-gp has many post translational modifications involved in cell surface tracking, protease protection, and degradation. After translation, P-gp is approximately 145 kDa before being post-translationally modified and trafficked to the membrane. Protein kinase (PK) A, PKC, and the

proto-oncogene PIM-1 phosphorylate P-gp at S661, S667, S671, and S683 allowing for proper cellular trafficking. Mutations at these residues lead to decreased surface expression and an increase of degradation products in surface expression assays and immunoblots.[64–67] N-glycosylation occurs on the first extracellular loop at Asn 91, 94, and 99 and protect from proteolysis in the ER during maturation.[68] Several lysine residues also become ubiquitinated as part of protein degradation.[69]

Quality of P-gp crystal structures have improved significantly over the past few years with improved techniques using both X-ray crystallography and more recently cryo-electron microscopy (Cryo-EM). Initially many human crystal structures were based on and fitted to *M. musculus* as mouse P-gp (*m*P-gp) has a sequence identity of 87% to human P-gp (P-gp). The most reliable crystal structures now are human P-gp in the closed, outward facing conformation and a mouse-human chimera in the open, inward conformation both in nanodisks with cryo-EM.[70–72] These improved structures along with biochemical data collected in the past 4 decades have significantly strengthened our understanding of the structure function relationship of P-gp.

1.3.2 Expression and Localization of P-Glycoprotein in Human Tissues

P-gp is expressed typically on the apical membrane side of endothelial, epithelial, and secretory tissues and normally acts to stop the absorption of xenobiotics.[11,62] This protects tissues and organs from potential harm, but also can make it difficult to administer small molecule therapies. Expression of P-gp is observed in the liver, lung, kidney, intestines, and at important blood-tissue barriers such as the BBB. Other blood tissue barriers include the blood-testis barrier and blood-placenta barrier. Tight junctions in endothelial cells do not allow molecules to pass directly from the blood to tissue thus expression of P-gp and other ABC transporters along with these tight junctions form a selective barrier that molecules must pass through to reach protected tissue.[73] Expression of P-gp directly affects the pharmacokinetics of many therapies as expression in the intestines affects oral bioavailability, expression in the lungs affects pulmonary/ nasal bioavailability, expression in the kidneys affects the rate at which drugs are secreted, and expression at blood-tissue barriers affects absorption of drugs across those barriers.[74–76]

1.3.3 Secondary Structure Organization of P-Glycoprotein

As previously described, P-gp's domain organization is TMD-NBD-TMD-NBD organized to form two homologous halves of the protein. These domains are not discretely organized in the crystal structures of P-gp but instead are intricately combined for close interactions between domains and even mixing of secondary structures between tertiary domains. ATP binding drives interaction between the two NBDs as the Walker A motif of one of the nucleotides interacts with the ABC signature motif of the other in binding ATP.[77] NBDs directly interact with the TMDs through 4 intracellular helices (IH).[78] IH1 forms from an intracellular loop between TM segments 2 and 3 and IH3 forms from an intracellular loop between TM segments 7 and 8 and both IH1 and 3 contact NBD1. Conversely IH2 and 4 are formed from intracellular loops between Tm segments 4 & 5 and 10 & 11 respectively and contact NBD2. Mutations in 3 of these 4 helices can cause a decrease in ATPase activity and transport kinetics.[79] Unlike many integral TM helices, P-gp's TM helices extend beyond the plasma membrane and into the cytoplasm and partially into extracellular space.[52] The extension of these TM helices beyond the plasma membrane are commonly referred to as intracellular domains (ICD) 1 & 2 and extracellular domains (ECD) 1 & 2.

TMDs refer to the 12 TM helices that span the plasma membrane and bundle together to form the substrate binding pocket. 6 helices come from each of the two homologous halves of P-gp but intertwine to create the two TMDs. Helices 1, 2, 3, 10, 11, and 6 form TMD1 while helices 7, 8, 9, 4, 5, and 12 form TMD2.[80] Intertwined mixing of TM helices likely permits communication and signal transduction between the two homologous halves.[81] Based on inward, open crystal structures we observe two drug entry gates on either side of the protein between helices 4 and 6 on TMD1 and 10 and 12 on TMD2.[52] During drug transport the TMDs undergo significant conformational changes and completely reorder to form a surface facing extracellular space.[82] Reordering of the TMD helices is directly correlated to NBD dimerization between the un-dimerized inward facing (IF) conformation where NBDs are separated by a significant distance and a binding surface is exposed towards the inside of the cell and outward facing (OF) driven by NBD dimerization where the inward binding surface becomes outward facing and exposed to extracellular space.[81]

1.3.4 Nucleotide Binding Domain Motifs and Transmembrane Domain Structure

NBD structures between different ABC transporters tend to be highly conserved and typically have high degrees of percent similarity even outside specific conserved nucleotide binding structures.[2] The NBD structure of P-gp and other ABC transporters are part of the P-loop containing NTPase superfamily and have a RecA-type binding core which consists of six-stranded β-sheet core surrounded by four α-helices (Figure 1.3 A).[83] Eukaryotic ABC transporter NBDs add prosthetic groups to these RecA-type cores in their complete structures.[84] NBDs contain many similar motifs to other NTP binding cores including the Walker A and B motifs, the A, D, and Q-loops as well as the H-switch and including the ABC specific signature binding motif (Figure 1.3 B). The signature motif is highly conserved in ABC transporters and has the consensus sequence of LSGGQ.[85]

Nucleotide binding is primarily directed by interaction with the phosphate-coordinating Walker A, P-loop, and the A-loop (Figure 1.3 C).[83] Aromatic π-π interactions between the nucleotide base and A-loop is observed. Lysine from the P-loop and the Walker B motif coordinate a Mg^{2+} ion with a glutamine from the Q loop that also senses the γ-phosphate. Catalytic glutamate immediately follows the Walker B motif, and the histidine of the H-switch stabilizes the transition state of NTP hydrolysis. D-loop residues likely have help position water in the nucleophilic attack of the γ-phosphate. Finally, the signature motif of the opposite NBD contributes to ATP-induced-dimerization of the two NBDs (Figure 1.3 D). Since there are two NBDs in P-gp, as in most ABC transporters, there are two binding sties for ATP as each NBD contains all the previously described structural motifs used in ATP binding.

ABC transporters are least conserved in their TMDs as seen in the varying number of helices making up TMDs between ABC families as wells as the low sequence identity between the same gene of even closely related species. In comparison, NBDs are highly conserved due to the very specific function of ATP hydrolysis versus the much more ambiguous nature of substrate binding at the TMDs. P-gp contains 6 TM helices in each TMD for a total of 12 TM helices. TMD 1 and 2 comprise helices from both halves of the protein and adopt many conformations of which IF, occluded, and OF conformations are well described. [70,80,86] IF allows for substrate binding as the TMDs open towards the cytosolic side of the membrane.[87] The TMDs in the occluded state are more tightly packed and most notably TMHs 4 and 10 are bent significantly towards each other to occlude the binding pocket from substrate entry.[88] Finally, the OF conformation changes the

conformation of the TMDs so that the binding pocket becomes solvent exposed to extracellular space allowing for substrate to diffuse out of the cell.[70] TMD structure is constantly changing to sample a large range of conformations and is likely a factor in the promiscuity of P-gp to transport many different substrates. Large sampling of conformational states is supported by relatively high basal levels of ATPase activity observed even when no substrate is present.[89]

1.3.5 ATP Binding and Nucleotide Binding Domain Dimerization

ATP binding induces NBD dimerization and does so asymmetrically such that ATP is sandwiched between both NBDs but only one ATP at one of the two nucleotide binding sites (NBS) is in catalytic contact with both NBDs simultaneously. Dimerization has been confirmed biochemically through crosslinking of the two NBDs under various conditions. Crosslinking residues near the Walker A and signature motifs caused complete loss of ATPase activity while incubation with ATP beforehand inhibited crosslinking allowing for normal ATPase activity.[90]

ATP hydrolysis is also asymmetrical and has been shown biochemically through mutations of many residues in the nucleotide binding motifs.[77,91] Mutating residues at one NBS did not abolish ATPase activity at the other NBS. Biophysical techniques such as attenuated total reflection infrared spectroscopy have also been used to more directly observe the asymmetrical nature of the NBDs in P-gp.[92] Interestingly, symmetrical mutations between the NBDs did not lead to the same effects on ATPase activity and vanadate trapping which led to the discover of the NBDs being structurally similar but functionally different.[92] Double electron-electron resonance, through substitutions of residues on opposing NBDs, has shown a "two-stroke" hydrolysis of ATPs where one ATP is discretely hydrolyzed followed by the second ATP before release of ADP and Pi from the NBDs.[81] Through we know ATP hydrolysis is coupled to substrate efflux the exact mechanism of ATP hydrolysis and TMD conformational changes has not been fully elucidated.

1.3.6 P-glycoprotein Substrate Binding Sites

Many techniques have been utilized to determine how substrates bind and interact with P-gp. Early biochemical techniques used site-directed mutagenesis to determine residues important in substrate binding, ATPase activity, and enzyme kinetics.[93–95] These techniques revealed at least two distinct binding sites correlated to rhodamine 123 and Hoechst 33342 binding.[86,94] Further

analysis using mutagenesis revealed how prazosin bound in a third distinct site and how prazosin binding could modulate ATPase activity in combination with rhodamine and Hoechst 33342 binding.[96] Further investigation of the substrate binding pockets of P-gp revealed substrates could bind in many unique orientations not congruent with previously defined binding sites and that the substrate binding pocket of P-gp should be considered a large hydrophobic binding pocket with the ability to bind substrates in many different orientations and conformations.[86,97–99] Interestingly, it was also observed that substrates can bind multiply to the substrate binding pocket.[88,99] In the IF conformation, measurements of crystallographic data from *m*P-gp reveal a binding pocket that is roughly 6000 $Å^3$ in size.[86] The ability of P-gp to bind substrates in multiple orientations, locations, and multiply results in the large promiscuity seen in substrate recognition by P-gp. This promiscuity makes P-gp an important but difficult target for study in the delivery of small molecule drugs.

1.3.7 Substrates and Inhibitors of P-Glycoprotein

P-glycoprotein recognizes a large variety of substrates and inhibitors that are chemically and structurally different.[86,100] Commonly studied substrates of P-gp include anticancer agents such as anthracyclines, camptothecins, epipodophyllotoxins, taxanes, tyrosine kinase inhibitors, and vinca alkaloids.[100–103] Many other small molecules are also transported such as antiarrhythmic, antibacterial, anticonvulsant, antidepressant, antiemetic, antihypertensive, anti-inflammatory, antiparasitic, antiviral, immunosuppressant, opioids, steroids, and so on.[74] P-gp substrate recognition is not limited to small molecules as it can also bind with and transport organic cations, lipids, carbohydrates, amino acids, and to a limited extent small peptides.[3,74,104,105] Efforts to predict substrate recognition have determined some features that are common between small molecule substrates. Molecules containing two to three electron-donating groups separated by 2.5 or 4.6 Å, a log-P value > 2.9 (lipophilicity), and the presence of a tertiary amine are common candidates for recognition and transport by P-gp.[74,106]

Several known substrates were found to be inhibitors of P-gp ATPase activity and substrate transport and were the first substrates investigated as inhibitors of P-gp for a clinical setting for cancer: amiodarone, cyclosporine A, quinidine, and verapamil.[107] Promising results *in vitro* were not observed in a clinical setting as there were off-target effects and no observable reverse of drug resistance.[108] Second generation inhibitors had no better outcomes due to more off target

interactions. For example, vaslpodar is a potent inhibitor of P-gp but also is an inhibitor for cytochrome p450.[109] Third generation inhibitors were the first designed specifically to inhibit P-gp. These include biricodar, elacridar, dofequidar, tariquidar, and zosuquidar. However, coadministration of these inhibitors with other small molecule drugs did not lead to better clinical outcomes and also had many off-target effects likely due to inhibition of endogenous P-gp increasing toxicity in certain tissues.[107]

1.3.8 Mechanism of P-Glycoprotein Efflux and Substrate Transduction

How P-gp transports substrates across the plasma membrane has been heavily debated since its discovery. Much effort has been put into determining structure function relationships of P-gp using many different techniques from mutagenesis to double electron-electron resonance to crystallographic data.[82,88,110] However, exactly how ATP hydrolysis and substrate transport is coupled has remained elusive. As more experiments have been carried out an emerging consensus on the basic mechanism of ATP hydrolysis and substrate transport is generally accepted.[111] High concentrations of cytosolic ATP, ~1-3 mM, likely induces an ATP or ADP·Pi bound outward facing conformation. Release of ADP·Pi induces a conformational change that results in an open inward conformation at which point the drug binding pocket becomes available for substrate binding. Substrate and ATP can then bind and P-gp adopts an occluded conformation where the drug binding pocket becomes occluded.[88] Asymmetric hydrolysis of ATP or further rearrangement of the TMDs produces the outward facing structure of P-gp exposing the drug binding pocket to extracellular space where substrate can be effluxed.

Substrate transduction through P-gp in the transport cycle can be demonstrated through recent high resolution cryo-EM structures of human P-gp. Recent advancements in cryo-EM have greatly expanded our ability to understand the mechanism of substrate transport as new techniques have allowed the first high resolution cryo-EM structures of human P-gp to be solved specifically for the outward and occluded conformations of P-gp.[70,88,112] A cyclic peptide has been observed interacting with TMH 12 and EH 2 at the protein lipid interface on an exterior surface of P-gp that likely acts as a pre-binding site.[113] Though it has not been observed this interaction is possible on the opposing homologous half of P-gp with TMH 6 and EH 1. Substrates can then enter P-gp through portals made by TMHs 4 & 6 and 10 & 12 and bind to the substrate binding pocket at the apex of the TMDs.[114] TMHs 4 and 10 then undergo large conformational changes occluding the

drug binding pocket.[88] Conformational changes in TMHs 4 and 10 also reveal an access tunnel extending from the substrate binding pocket towards the inner leaflet formed by TMHs 5, 7, 8, 9, and 12. In the transition from the IF conformation to occluded state, the formation of the access tunnel by TMHs 4 and 10 may provide a pathway for substrate to enter the substrate binding pocket. There is an opening in the access tunnel in the inner leaflet adjacent to TMH 12 further suggesting a possible translocation pathway for substrates between IF and occluded conformations. Rearrangement of TMHs 4, 9, and 10 with TMH 12 rearranging to occupy the substrate binding pocket produces the outward facing conformation allowing for substrate efflux.[70,88]

Pre-binding of substrate at the lipid-protein interface is the only observation that has yet to be validated using biochemical or biophysical means and has only been observed in crystallographic data. Further understanding of how substrates first interact with P-gp at the lipid-protein interface would help in understanding how substrates are recognized by P-gp. Rational drug design could then be used to create drugs that have poor affinity for pre-binding interactions with P-gp potentially reducing efflux by P-gp which would be useful in treating MDR diseases or diseases that are beyond blood-tissue barriers.

1.4 Blood-Tissue Barriers and ABC Transporter Mediated Multidrug Resistance

1.4.1 P-Glycoprotein Expression at Blood-Tissue Barriers

P-glycoprotein is expressed at many blood-tissue barriers including the BBB. The BBB is a physical barrier formed by blood brain capillary endothelial cells that are conjoined through tight junctions forming a barrier that molecules must pass through to reach brain tissue. The role of the BBB is to maintain homeostasis of the brain and the function of the central nervous system by protecting them from potentially harmful and toxic xenobiotics.

A factor in maintaining the function of the BBB is the expression of several ABC transporters on the apical side of the capillary endothelial cells facing the lumen of the capillary.[115] Discovery of the importance of P-gp at the BBB was accidental when studying the two *mdr1* genes in knockout mice. P-gp deficient mice were more susceptible to many drugs and an increased accumulation of drugs in brain tissue was observed.[116] Further investigation led to the creation of *Abcb1ab*$^{-/-}$ mouse line used to study the role of P-gp at the BBB. *Abcb1ab*$^{-/-}$ mice were embryonically viable with no obvious defects and grew to maturity with no observed

developmental issues. Routine treatment of the mice cages with ivermectin, a common pesticide and neurotoxin, revealed the increased susceptibility to certain neurotoxic chemicals thus showing the importance of P-gp expression and its role at the BBB.[116,117]

Further study of P-gp and ABC transporter expression at the BBB revealed that many therapeutics developed for diseases that lie beyond the barrier were substrates of P-gp and had altered absorption into brain tissue due to the expression of P-gp.[118] Many therapeutics for CNS infections, HIV, epilepsy, schizophrenia, brain cancers, and so on have since been shown to be affected by expression of P-gp leading to research in strategies to increase drug delivery.[119,120] While many ABC transporters are expressed at the BBB, P-gp has been shown to have the largest effect of the expressed ABC transporters in efflux therapeutics at the BBB.[115] Thus research into the structure and function of P-gp in relation to the BBB remains important in treating diseases of the brain and central nervous system.

1.4.2 Acquired Multidrug Resistance in Cancer

A common and unfortunate outcome of long-term chemotherapy is accrued MDR to several chemically and structurally unrelated chemotherapeutics.[121] Despite major efforts to combat MDR, many patients with metastatic cancer will be overcome by their cancer due to the lack of response to chemotherapeutic treatment. Observations of MDR were first made in HeLa cells grown in selection media containing actinomycin D which later became resistant to a number of other unrelated drugs.[122] Initial observations were later confirmed in several cell lines from Chinese hamster cell cultures grown in increasing concentrations of actinomycin D. These new cell lines became resistant to several anticancer drugs including daunomycin, vincristine, and vinblastine.[123] It was later verified that expression of P-gp was responsible for the acquired MDR in cells grown in selection media as well as in some patients displaying MDR cancer.[124–126]

Overexpression of P-gp has been reported in leukemias, kidney, colon, breast, carcinoid tumors, adrenal, pancreas, lung cancers and more in relation to MDR.[127–131] P-gp expression confers MDR in cancer to a large number of unrelated anti-cancer drugs including anthracyclines, camptothecins, epipodophyllotoxins, taxanes, tyrosine kinase inhibitors, and vinca alkaloids.[100–103] As such, many poor outcomes in patients with expression of P-gp has been observed. For example, patients with expression of P-gp in non-small cell and small cell lung carcinomas have shown resistance to treatment with paclitaxel and cyclophosphamide, cis-platin, doxorubicin, and

vincristine, respectively.[132] Numerous more studies show that expression of P-gp through increased detection of mRNA confers MDR and poor outcomes to responses with chemotherapy.[127–129]

As such, much effort has been devoted to researching MDR in cancer and developing methodologies for circumventing P-gp. Thus, continued research into the structure and function of P-gp is important for developing new methodologies in defeating acquired MDR in cancer.

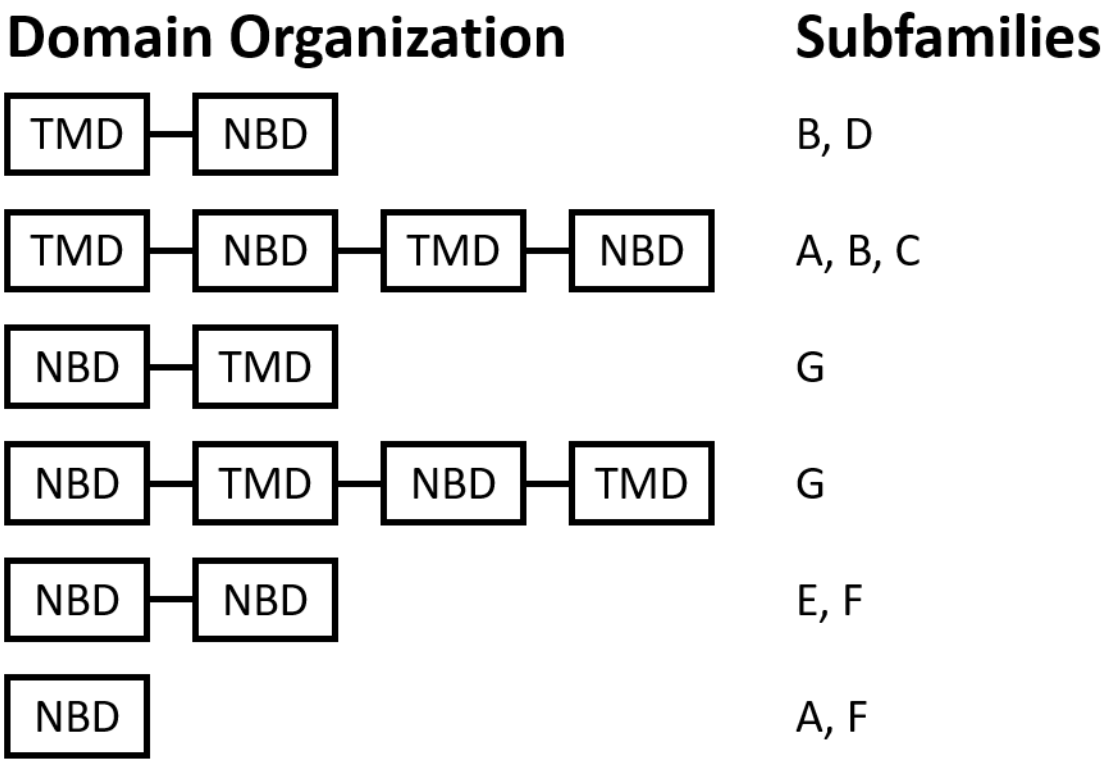

Figure 1.1: Domain Organization of the ABC Transporter Subfamilies

Subfamilies are partially characterized by the organization of their NBDs and/or TMDs. ABC transporter subfamilies A, B, C, and G can form full transporters with two NBDs and TMDs. Subfamilies B, D, and G can form half transporters with each contains one NBD and TMD. Finally, subfamilies A, E, and F contain members that are only comprised of one or two NBDs and are not traditional ABC transporters of substrates.

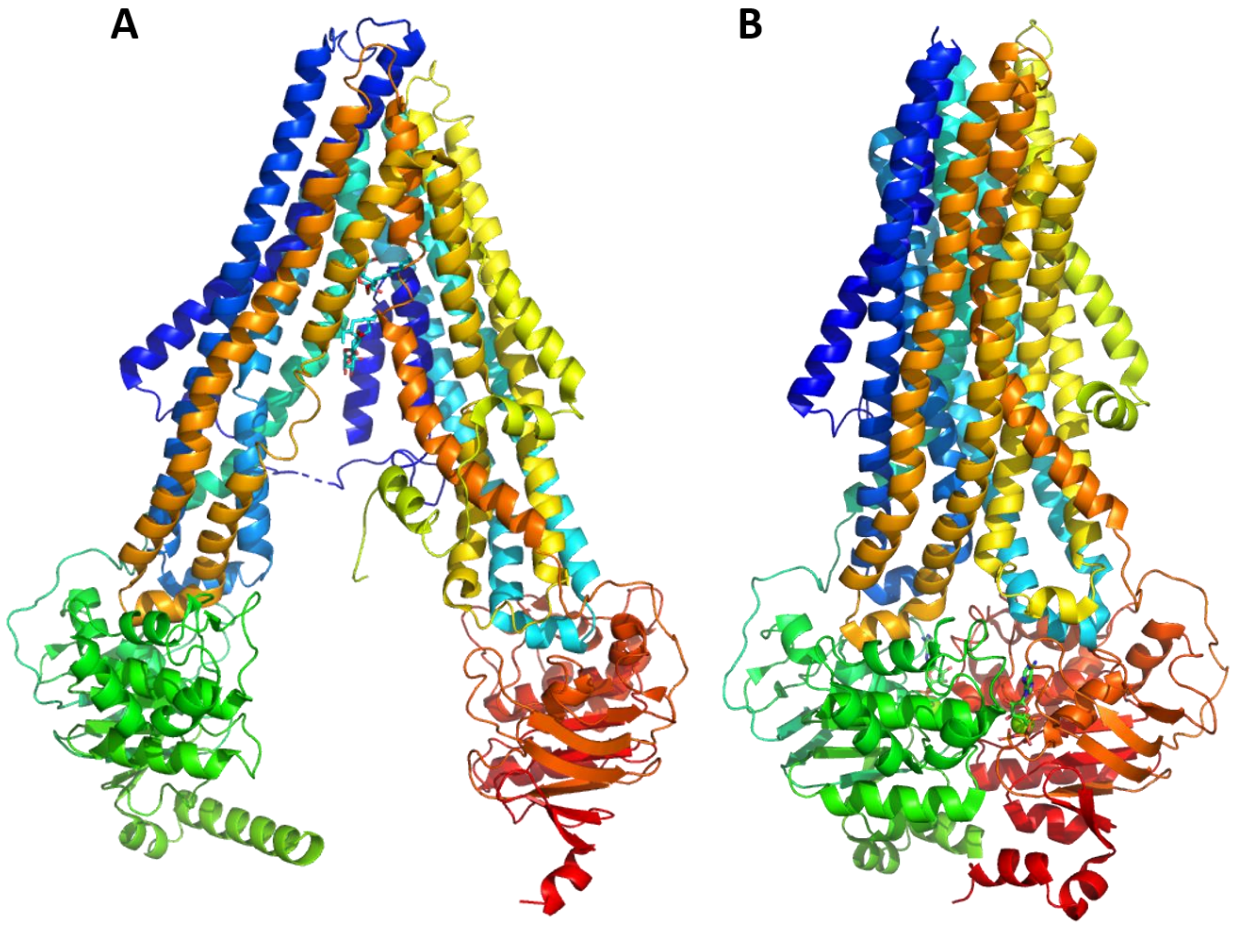

Figure 1.2: Crystal Structures of Open and Closed P-glycoprotein Show Nucleotide Domain Dimerization and TMD Reordering

P-glycoprotein adopts many conformations during NBD dimerization and reorganization of the TMDs during substrate efflux. (A) NBDs have been observed to be significantly distant when not ATP or ADP•Pi bound leading to an open, inward conformation giving access to substrate entry at the protein interface at the inner leaflet. (B) ATP or ADP•Pi bound conformations have the two NBDs in close proximity due to ATP induced dimerization. In this state a surface of the TMDs are facing extracellular space allowing substrate to diffuse out of the cell. It should be noted that these are only snapshots of the protein structure and that P-gp is highly dynamic in organization of its TMDs and NBDs depending on combinations of ATP, ADP•Pi, and substrate bound states. (PDB: 4F4C(A) and 6C0V(B))

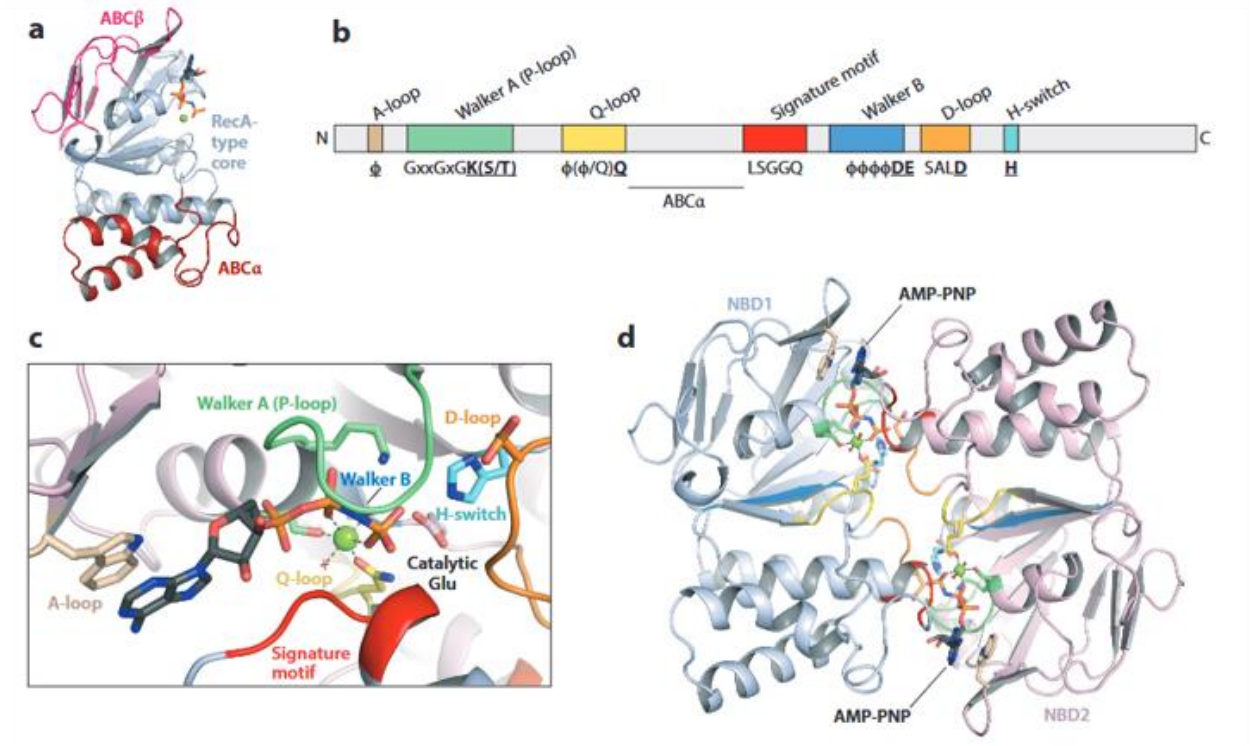

Figure 1.3: Nucleotide Binding Domain Structure of ABC Transporters

NBD of ABC transporters, nucleotide binding site formation, and NBD dimerization from PDB: 3RLF. (A) The NBD consists of a RecA-type ATP binding core with adjacent prosthetic groups. (B) Primary sequence arrangement of the ATP binding motifs observed in ABC transporters. (C) Organization of structural motifs involved with ATP and Mg^{2+} binding and catalysis of ATP hydrolyzation. (D) View from the membrane of NBD dimerization captured by a nonhydrolyzable ATP analog demonstrating how ATP is bound between two NBDs. Republished with permission of Annual Review of Biochemistry, from Structural and Mechanistic Principles of ABC Transporters, C. Thomas and R. Tampé, 89, 2020; permission conveyed through Copyright Clearance Center, Inc.

Table 1.1: P-glycoprotein Transports Common Therapeutic Drugs that are Structurally and Functionally Different

Class of Therapeutics	P-gp Therapeutic Substrate
Antiarrhythmic	Verapamil, Digoxin, Quinidine
Antibacterial	Tetracycline, Erythromycin, Ciprofloxacin
Anticancer	Taxol, Doxorubicin, Dasatinib, Vincristine
Anticonvulsant	Phenobarbital, Phenytoin
Antidepressant	Amitriptyline, Paroxetine, Citalopram
Antiemetic	Domperidon, Ondansetron
Antihypertensive	Celiprolol, Losartan, Diltiazem
Antiinflammatory	Methylprednisone, Dexamethasone
Antiparasitic	Emetine, Quinine, Ivermectin, Itraconazole
Antipsychotic	Quetiapine, Risperidone
Antiviral	Abacavir, Acyclovir, Saquinavir
Immunosuppressant	Cyclosporine, Tacrolimus, Sirolimus
Opioids	Morphine, Loperamide, Pentazocine
Steroid hormones	Aldosterone, Cortisol, Prednisolone

P-gp has been shown to be able to transport a large variety of structurally and functionally different molecules including common classes of therapeutics. The promiscuity of P-gp increases the difficulty of treating diseases that are beyond barriers where P-gp is expressed or cells that have developed P-gp mediated MDR.

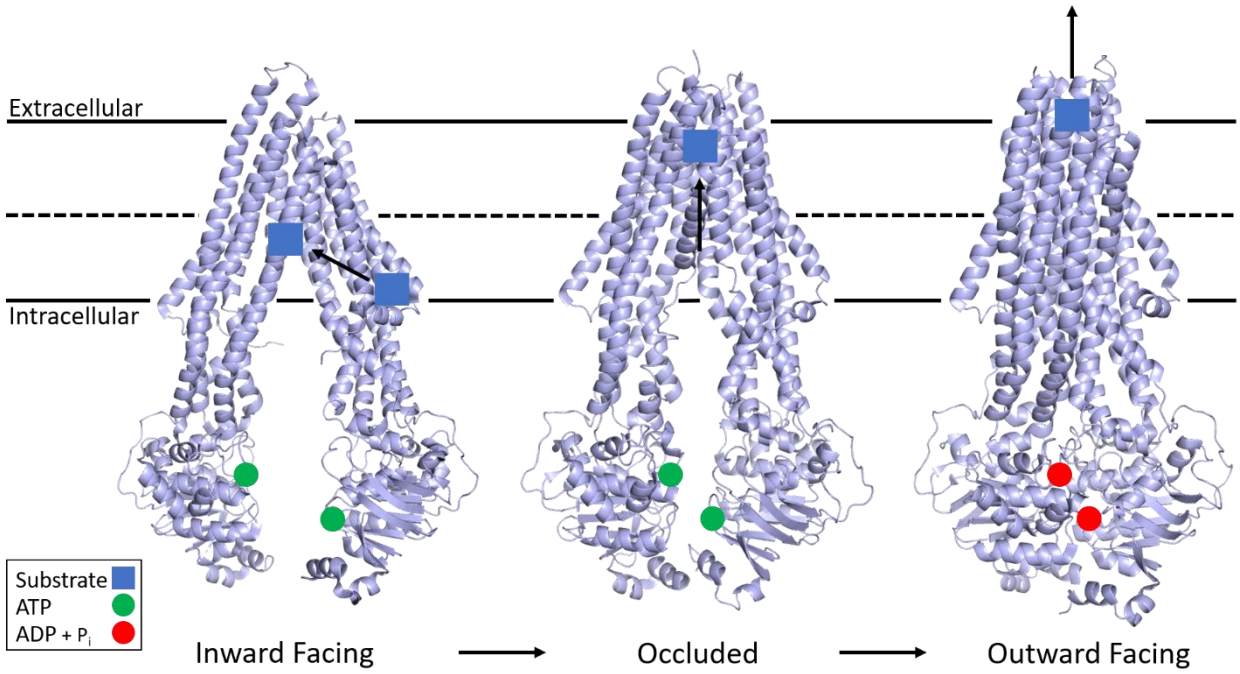

Figure 1.4: Substrate Transduction Pathway During the Catalytic ATP Hydrolysis Cycle of P-Glycoprotein

Substrate from the inner leaflet interacts with TMH 12 and EH 2 at the lipid-protein interface. Substrate can then occupy the substrate binding pocket at the apex of the IF structure. Large conformational changes by TMHs 4 and 10 then occlude the substrate binding pocket in an intermediate step. Finally, ATP hydrolysis drives large conformational changes in TMHs 4, 10, and 9 while TMH 12 reorders to occupy the substrate binding pocket to expose and efflux substrate into extracellular space. PDB: 5KPI (inward), 7A6C (occluded), and 6C0V (outward)

1.5 References

1. Higgins, C. F. ABC Transporters: From Microorganisms to Man. *Annu. Rev. Cell Biol.* **8**, 67–113 (1992).

2. Rees, D. C., Johnson, E. & Lewinson, O. ABC transporters: the power to change. *Nat. Rev. Mol. Cell Biol.* **10**, 218–227 (2009).

3. Linton, K. J. Structure and Function of ABC Transporters. *Physiology* **22**, 122–130 (2007).

4. Buss, D. S. & Callaghan, A. Interaction of pesticides with p-glycoprotein and other ABC proteins: A survey of the possible importance to insecticide, herbicide and fungicide resistance. *Pestic. Biochem. Physiol.* **90**, 141–153 (2008).

5. Tarling, E. J., Vallim, T. Q. de A. & Edwards, P. A. Role of ABC transporters in lipid transport and human disease. *Trends Endocrinol. Metab.* **24**, 342–350 (2013).

6. Hosie, A. H. F. & Poole, P. S. Bacterial ABC transporters of amino acids. *Res. Microbiol.* **152**, 259–270 (2001).

7. Yazaki, K. Transporters of secondary metabolites. *Curr. Opin. Plant Biol.* **8**, 301–307 (2005).

8. Holland, I. B. & Blight, M. A. ABC-ATPases, adaptable energy generators fuelling transmembrane movement of a variety of molecules in organisms from bacteria to humans. *J. Mol. Biol.* **293**, 381–399 (1999).

9. ter Beek, J., Guskov, A. & Slotboom, D. J. Structural diversity of ABC transporters. *J. Gen. Physiol.* **143**, 419–435 (2014).

10. Klein, I., Sarkadi, B. & Váradi, A. An inventory of the human ABC proteins. *Biochim. Biophys. Acta BBA - Biomembr.* **1461**, 237–262 (1999).

11. Dean, M., Hamon, Y. & Chimini, G. The human ATP-binding cassette (ABC) transporter superfamily. *J. Lipid Res.* **42**, 1007–1017 (2001).

12. Dean, M. & Allikmets, R. Complete Characterization of the Human ABC Gene Family. *J. Bioenerg. Biomembr.* **33**, 475–479 (2001).

13. Anjard, C., Consortium, the D. S. & Loomis, W. F. Evolutionary Analyses of ABC Transporters of Dictyostelium discoideum. *Eukaryot. Cell* **1**, 643–652 (2002).

14. Sheps, J. A., Ralph, S., Zhao, Z., Baillie, D. L. & Ling, V. The ABC transporter gene family of Caenorhabditis elegans has implications for the evolutionary dynamics of multidrug resistance in eukaryotes. *Genome Biol.* **5**, R15 (2004).

15. Klokouzas, A., Shahi, S., Hladky, S. B., Barrand, M. A. & van Veen, H. W. ABC transporters and drug resistance in parasitic protozoa. *Int. J. Antimicrob. Agents* **22**, 301–317 (2003).

16. Kerr, I. D. Sequence analysis of twin ATP binding cassette proteins involved in translational control, antibiotic resistance, and ribonuclease L inhibition. *Biochem. Biophys. Res. Commun.* **315**, 166–173 (2004).

17. Zhao, Z., Fang, L. L., Johnsen, R. & Baillie, D. L. ATP-binding cassette protein E is involved in gene transcription and translation in Caenorhabditis elegans. *Biochem. Biophys. Res. Commun.* **323**, 104–111 (2004).

18. Holland, B., Cole, S., Kuchlar, K. & Higgins, C. *ABC Proteins: From Bacteria to Man*. (Academic Press, 2003).

19. Locher, K. P. Mechanistic diversity in ATP-binding cassette (ABC) transporters. *Nat. Struct. Mol. Biol.* **23**, 487–493 (2016).

20. Leipe, D. D., Koonin, E. V. & Aravind, L. Evolution and classification of P-loop kinases and related proteins. *J. Mol. Biol.* **333**, 781–815 (2003).

21. Confalonieri, F. & Duguet, M. A 200-amino acid ATPase module in search of a basic function. *BioEssays News Rev. Mol. Cell. Dev. Biol.* **17**, 639–650 (1995).

22. Prades, C. *et al.* The human ATP binding cassette gene ABCA13, located on chromosome 7p12.3, encodes a 5058 amino acid protein with an extracellular domain encoded in part by a 4.8-kb conserved exon. *Cytogenet. Genome Res.* **98**, 160–168 (2002).

23. Peelman, F. *et al.* Characterization of the ABCA Transporter Subfamily: Identification of Prokaryotic and Eukaryotic Members, Phylogeny and Topology. *J. Mol. Biol.* **325**, 259–274 (2003).

24. Gradhand, U. & Kim, R. B. Pharmacogenomics of MRP Transporters (ABCC1-5) and BCRP (ABCG2). *Drug Metab. Rev.* **40**, 317–354 (2008).

25. Quinton, P. M. Physiological Basis of Cystic Fibrosis: A Historical Perspective. *Physiol. Rev.* **79**, S3–S22 (1999).

26. Trompier, D. & Savary, S. X-linked Adrenoleukodystrophy. *Colloq. Ser. Genet. Basis Hum. Dis.* **2**, 1–134 (2013).

27. Kawaguchi, K. & Morita, M. ABC Transporter Subfamily D: Distinct Differences in Behavior between ABCD1–3 and ABCD4 in Subcellular Localization, Function, and Human Disease. *BioMed Research International* vol. 2016 e6786245 https://www.hindawi.com/journals/bmri/2016/6786245/ (2016).

28. Pisarev, A. V. *et al.* The Role of ABCE1 in Eukaryotic Posttermination Ribosomal Recycling. *Mol. Cell* **37**, 196–210 (2010).

29. Liu, Y.-H., Chen, Y.-J., Wu, H.-H., Wang, T.-Y. & Tsai, F.-J. Single Nucleotide Polymorphisms at the PRR3, ABCF1, and GNL1 Genes in the HLA Class I Region Are Associated with Graves' Ophthalmopathy in a Gender-Dependent Manner. *Ophthalmology* **121**, 2033–2039 (2014).

30. Oram, J. F. Tangier disease and ABCA1. *Biochim. Biophys. Acta BBA - Mol. Cell Biol. Lipids* **1529**, 321–330 (2000).

31. Quazi, F. & Molday, R. S. ATP-binding cassette transporter ABCA4 and chemical isomerization protect photoreceptor cells from the toxic accumulation of excess 11-cis-retinal. *Proc. Natl. Acad. Sci.* **111**, 5024–5029 (2014).

32. Rivera, A. *et al.* A Comprehensive Survey of Sequence Variation in the ABCA4 (ABCR) Gene in Stargardt Disease and Age-Related Macular Degeneration. *Am. J. Hum. Genet.* **67**, 800–813 (2000).

33. Schumacher, T. N. *et al.* Peptide length and sequence specificity of the mouse TAP1/TAP2 translocator. *J. Exp. Med.* **179**, 533–540 (1994).

34. Witkowski, J. M., Gorgas, G. & Miller, R. A. Reciprocal Expression of P-Glycoprotein and TAP1 Accompanied by Higher Expression of MHC Class I Antigens in T Cells of Old Mice. *J. Gerontol. Ser. A* **51A**, B76–B82 (1996).

35. Sundaram, S. S. & Sokol, R. J. The multiple facets of ABCB4 (MDR3) deficiency. *Curr. Treat. Options Gastroenterol.* **10**, 495–503 (2007).

36. Park, J. S., Ko, J. S., Seo, J. K., Moon, J. S. & Park, S. S. Clinical and ABCB11 profiles in Korean infants with progressive familial intrahepatic cholestasis. *World J. Gastroenterol.* **22**, 4901–4907 (2016).

37. Qi, W., Li, J. & A. Cowan, J. A structural model for glutathione-complexed iron–sulfur cluster as a substrate for ABCB7-type transporters. *Chem. Commun.* **50**, 3795–3798 (2014).

38. Cavadini, P. *et al.* RNA silencing of the mitochondrial ABCB7 transporter in HeLa cells causes an iron-deficient phenotype with mitochondrial iron overload. *Blood* **109**, 3552–3559 (2007).

39. Nikpour, M. *et al.* The transporter ABCB7 is a mediator of the phenotype of acquired refractory anemia with ring sideroblasts. *Leukemia* **27**, 889–896 (2013).

40. Keitel, V. *et al.* A common Dubin-Johnson syndrome mutation impairs protein maturation and transport activity of MRP2 (ABCC2). *Am. J. Physiol.-Gastrointest. Liver Physiol.* **284**, G165–G174 (2003).

41. Westerterp, M. *et al.* ATP-binding cassette transporters, atherosclerosis, and inflammation. *Circ. Res.* **114**, 157–170 (2014).

42. Bergen, A. A. B., Plomp, A. S., Hu, X., de Jong, P. T. V. M. & Gorgels, T. G. M. F. ABCC6 and pseudoxanthoma elasticum. *Pflugers Arch.* **453**, 685–691 (2007).

43. Nitschke, Y. *et al.* Generalized arterial calcification of infancy and pseudoxanthoma elasticum can be caused by mutations in either ENPP1 or ABCC6. *Am. J. Hum. Genet.* **90**, 25–39 (2012).

44. Cheng, S. *et al.* Defective intracellular transport and processing of CFTR is the molecular basis of most cystic fibrosis. *Cell* **63**, 827–834 (1990).

45. Kemp, S. *et al.* ABCD1 mutations and the X-linked adrenoleukodystrophy mutation database: Role in diagnosis and clinical correlations. *Hum. Mutat.* **18**, 499–515 (2001).

46. Yu, L. *et al.* Disruption of Abcg5 and Abcg8 in mice reveals their crucial role in biliary cholesterol secretion. *Proc. Natl. Acad. Sci.* **99**, 16237–16242 (2002).

47. Hee Choi, Y. & Yu, A.-M. ABC Transporters in Multidrug Resistance and Pharmacokinetics, and Strategies for Drug Development. *Curr. Pharm. Des.* **20**, 793–807 (2014).

48. Montanari, F. & Ecker, G. Prediction of drug-ABC-transporter interaction - Recent advances and future challenges. *Adv. Drug Deliv. Rev.* **86**, 17–26 (2015).

49. Chang, G. Multidrug resistance ABC transporters. *FEBS Lett.* **555**, 102–105 (2003).

50. Ceballos, M. P. *et al.* ABC Transporters: Regulation and Association with Multidrug Resistance in Hepatocellular Carcinoma and Colorectal Carcinoma. *Curr. Med. Chem.* **26**, 1224–1250 (2019).

51. Fletcher, J., Williams, R., Henderson, M., Norris, M. & Haber, M. ABC transporters as mediators of drug resistance and contributors to cancer cell biology. *Drug Resist. Updat.* **26**, 1–9 (2016).

52. Sharom, F. J. The P-glycoprotein multidrug transporter. *Essays Biochem.* **50**, 161–178 (2011).

53. Litman, T. *et al.* The multidrug-resistant phenotype associated with overexpression of the new ABC half-transporter, MXR (ABCG2). *J. Cell Sci.* **113**, 2011–2021 (2000).

54. Allen, J. D., Brinkhuis, R. F., Deemter, L. van, Wijnholds, J. & Schinkel, A. H. Extensive Contribution of the Multidrug Transporters P-Glycoprotein and Mrp1 to Basal Drug Resistance. *Cancer Res.* **60**, 5761–5766 (2000).

55. Albrecht, C. & Viturro, E. The ABCA subfamily—gene and protein structures, functions and associated hereditary diseases. *Pflüg. Arch. - Eur. J. Physiol.* **453**, 581–589 (2007).

56. Childs, S., Yeh, R. L., Hui, D. & Ling, V. Taxol Resistance Mediated by Transfection of the Liver-specific Sister Gene of P-Glycoprotein. *Cancer Res.* **58**, 4160–4167 (1998).

57. Keppler, D. Multidrug Resistance Proteins (MRPs, ABCCs): Importance for Pathophysiology and Drug Therapy. in *Drug Transporters* (eds. Fromm, M. F. & Kim, R. B.) 299–323 (Springer, 2011).

58. Slot, A. J., Molinski, S. V. & Cole, S. P. C. Mammalian multidrug-resistance proteins (MRPs). *Essays Biochem.* **50**, 179–207 (2011).

59. Juliano, R. L. & Ling, V. A surface glycoprotein modulating drug permeability in Chinese hamster ovary cell mutants. *Biochim. Biophys. Acta* **455**, 152–162 (1976).

60. Riordan, J. R. & Ling, V. Purification of P-glycoprotein from plasma membrane vesicles of Chinese hamster ovary cell mutants with reduced colchicine permeability. *J. Biol. Chem.* **254**, 12701–12705 (1979).

61. Moitra, K. & Dean, M. Evolution of ABC transporters by gene duplication and their role in human disease. *Biol. Chem.* **392**, 29–37 (2011).

62. Thiebaut, F. *et al.* Cellular localization of the multidrug-resistance gene product P-glycoprotein in normal human tissues. *Proc. Natl. Acad. Sci.* **84**, 7735–7738 (1987).

63. Fromm, M. F. Importance of P-glycoprotein at blood–tissue barriers. *Trends Pharmacol. Sci.* **25**, 423–429 (2004).

64. Chambers, T. C., Pohl, J., Glass, D. B. & Kuo, J. F. Phosphorylation by protein kinase C and cyclic AMP-dependent protein kinase of synthetic peptides derived from the linker region of human P-glycoprotein. *Biochem. J.* **299**, 309–315 (1994).

65. Germann, U. A. *et al.* Characterization of Phosphorylation-defective Mutants of Human P-glycoprotein Expressed in Mammalian Cells. *J. Biol. Chem.* **271**, 1708–1716 (1996).

66. Goodfellow, H. R. *et al.* Protein Kinase C-mediated Phosphorylation Does Not Regulate Drug Transport by the Human Multidrug Resistance P-glycoprotein. *J. Biol. Chem.* **271**, 13668–13674 (1996).

67. Xie, Y., Burcu, M., Linn, D. E., Qiu, Y. & Baer, M. R. Pim-1 Kinase Protects P-Glycoprotein from Degradation and Enables Its Glycosylation and Cell Surface Expression. *Mol. Pharmacol.* **78**, 310–318 (2010).

68. Schinkel, A. H., Kemp, S., Dollé, M., Rudenko, G. & Wagenaar, E. N-glycosylation and deletion mutants of the human MDR1 P-glycoprotein. *J. Biol. Chem.* **268**, 7474–7481 (1993).

69. Akkaya, B. G. *et al.* The multidrug resistance pump ABCB1 is a substrate for the ubiquitin ligase NEDD4-1. *Mol. Membr. Biol.* **32**, 39–45 (2015).

70. Kim, Y. & Chen, J. Molecular structure of human P-glycoprotein in the ATP-bound, outward-facing conformation. *Science* 73–89 (2018).

71. Alam, A., Kowal, J., Broude, E., Roninson, I. & Locher, K. P. Structural insight into substrate and inhibitor discrimination by human P-glycoprotein. *Science* **363**, 753–756 (2019).

72. Alam, A. *et al.* Structure of a zosuquidar and UIC2-bound human-mouse chimeric ABCB1. *Proc. Natl. Acad. Sci. U. S. A.* **115**, E1973–E1982 (2018).

73. Begley, D. J. ABC transporters and the blood-brain barrier. *Curr. Pharm. Des.* **10**, 1295–1312 (2004).

74. Zhou, S.-F. Structure, function and regulation of P-glycoprotein and its clinical relevance in drug disposition. *Xenobiotica Fate Foreign Compd. Biol. Syst.* **38**, 802–832 (2008).

75. Cox, D. S., Scott, K. R., Gao, H., Raje, S. & Eddington, N. D. Influence of multidrug resistance (MDR) proteins at the blood-brain barrier on the transport and brain distribution of enaminone anticonvulsants. *J. Pharm. Sci.* **90**, 1540–1552 (2001).

76. Chen, L., Li, Y., Zhao, Q., Peng, H. & Hou, T. ADME Evaluation in Drug Discovery. 10. Predictions of P-Glycoprotein Inhibitors Using Recursive Partitioning and Naive Bayesian Classification Techniques. *Mol. Pharm.* **8**, 889–900 (2011).

77. Hrycyna, C. A. *et al.* Both ATP Sites of Human P-Glycoprotein Are Essential but Not Symmetric. *Biochemistry* **38**, 13887–13899 (1999).

78. Loo, T. W. & Clarke, D. M. Locking Intracellular Helices 2 and 3 Together Inactivates Human P-glycoprotein. *J. Biol. Chem.* **289**, 229–236 (2014).

79. Loo, T. W., Bartlett, M. C. & Clarke, D. M. Human P-glycoprotein Contains a Greasy Ball-and-Socket Joint at the Second Transmission Interface. *J. Biol. Chem.* **288**, 20326–20333 (2013).

80. Jin, M. S., Oldham, M. L., Zhang, Q. & Chen, J. Crystal structure of the multidrug transporter P-glycoprotein from Caenorhabditis elegans. *Nature* **490**, 566–569 (2012).

81. Verhalen, B. *et al.* Energy transduction and alternating access of the mammalian ABC transporter P-glycoprotein. *Nature* **543**, 738–741 (2017).

82. Dastvan, R., Mishra, S., Peskova, Y. B., Nakamoto, R. K. & Mchaourab, H. S. Mechanism of allosteric modulation of P-glycoprotein by transport substrates and inhibitors. *Science* **364**, 689–692 (2019).

83. Thomas, C. & Tampé, R. Structural and Mechanistic Principles of ABC Transporters. *Annu. Rev. Biochem.* **89**, 605–636 (2020).

84. Hung, L.-W. *et al.* Crystal structure of the ATP-binding subunit of an ABC transporter. *Nature* **396**, 703–707 (1998).

85. Ambudkar, S. V., Kim, I.-W., Xia, D. & Sauna, Z. E. The A-loop, a novel conserved aromatic acid subdomain upstream of the Walker A motif in ABC transporters, is critical for ATP binding. *FEBS Lett.* **580**, 1049–1055 (2006).

86. Aller, S. G. *et al.* Structure of P-glycoprotein reveals a molecular basis for poly-specific drug binding. *Science* **323**, 1718–1722 (2009).

87. Esser, L. *et al.* Structures of the Multidrug Transporter P-glycoprotein Reveal Asymmetric ATP Binding and the Mechanism of Polyspecificity. *J. Biol. Chem.* **292**, 446–461 (2017).

88. Nosol, K. *et al.* Cryo-EM structures reveal distinct mechanisms of inhibition of the human multidrug transporter ABCB1. *Proc. Natl. Acad. Sci.* **117**, 26245–26253 (2020).

89. Sharom, F. J. Complex Interplay between the P-Glycoprotein Multidrug Efflux Pump and the Membrane: Its Role in Modulating Protein Function. *Front. Oncol.* **4**, 1–19 (2014).

90. Loo, T. W. & Clarke, D. M. Drug-stimulated ATPase Activity of Human P-glycoprotein Is Blocked by Disulfide Cross-linking between the Nucleotide-binding Sites. *J. Biol. Chem.* **275**, 19435–19438 (2000).

91. Carrier, I., Julien, M. & Gros, P. Analysis of Catalytic Carboxylate Mutants E552Q and E1197Q Suggests Asymmetric ATP Hydrolysis by the Two Nucleotide-Binding Domains of P-Glycoprotein. *Biochemistry* **42**, 12875–12885 (2003).

92. Vigano, C., Julien, M., Carrier, I., Gros, P. & Ruysschaert, J.-M. Structural and Functional Asymmetry of the Nucleotide-binding Domains of P-glycoprotein Investigated by Attenuated Total Reflection Fourier Transform Infrared Spectroscopy. *J. Biol. Chem.* **277**, 5008–5016 (2002).

93. Loo, T. W. & Clarke, D. M. Cross-linking of Human Multidrug Resistance P-glycoprotein by the Substrate, Tris-(2-maleimidoethyl)amine, Is Altered by ATP Hydrolysis EVIDENCE FOR ROTATION OF A TRANSMEMBRANE HELIX. *J. Biol. Chem.* **276**, 31800–31805 (2001).

94. Loo, T. W. & Clarke, D. M. Determining the Dimensions of the Drug-binding Domain of Human P-glycoprotein Using Thiol Cross-linking Compounds as Molecular Rulers. *J. Biol. Chem.* **276**, 36877–36880 (2001).

95. Loo, T. W. & Clarke, D. M. Covalent Modification of Human P-glycoprotein Mutants Containing a Single Cysteine in Either Nucleotide-binding Fold Abolishes Drug-stimulated ATPase Activity. *J. Biol. Chem.* **270**, 22957–22961 (1995).

96. Shapiro, A. B., Fox, K., Lam, P. & Ling, V. Stimulation of P-glycoprotein-mediated drug transport by prazosin and progesterone. *Eur. J. Biochem.* **259**, 841–850 (1999).

97. Loo, T. W., Bartlett, M. C. & Clarke, D. M. Drug Binding in Human P-glycoprotein Causes Conformational Changes in Both Nucleotide-binding Domains. *J. Biol. Chem.* **278**, 1575–1578 (2003).

98. Mittra, R. *et al.* Location of contact residues in pharmacologically distinct drug binding sites on P-glycoprotein. *Biochem. Pharmacol.* **123**, 19–28 (2017).

99. Chufan, E. E. *et al.* Multiple Transport-Active Binding Sites Are Available for a Single Substrate on Human P-Glycoprotein (ABCB1). *PLOS ONE* **8**, e82463 (2013).

100. Gottesman, M. M. & Ambudkar, S. V. Overview: ABC Transporters and Human Disease. *J. Bioenerg. Biomembr.* **33**, 453–458 (2001).

101. K. Tiwari, A., Sodani, K., Dai, C.-L., R. Ashby, C. & Chen, Z.-S. Revisiting the ABCs of Multidrug Resistance in Cancer Chemotherapy. *Curr. Pharm. Biotechnol.* **12**, 570–594 (2011).

102. Schinkel, A. H. & Jonker, J. W. Mammalian drug efflux transporters of the ATP binding cassette (ABC) family: an overview. *Adv. Drug Deliv. Rev.* **64**, 138–153 (2012).

103. Assaraf, Y. G. *et al.* The multi-factorial nature of clinical multidrug resistance in cancer. *Drug Resist. Updat.* **46**, 100645 (2019).

104. Dolghih, E., Bryant, C., Renslo, A. R. & Jacobson, M. P. Predicting Binding to P-Glycoprotein by Flexible Receptor Docking. *PLoS Comput. Biol.* **7**, (2011).

105. Cirrito, J. R. *et al.* P-glycoprotein deficiency at the blood-brain barrier increases amyloid-β deposition in an Alzheimer disease mouse model. *J. Clin. Invest.* **115**, 3285–3290 (2005).

106. Seelig, A. A general pattern for substrate recognition by P-glycoprotein. *Eur. J. Biochem.* **251**, 252–261 (1998).

107. Binkhathlan, Z. & Lavasanifar, A. P-glycoprotein Inhibition as a Therapeutic Approach for Overcoming Multidrug Resistance in Cancer: Current Status and Future Perspectives. *Curr. Cancer Drug Targets* **13**, 326–346 (2013).

108. Gottesman, M. M., Fojo, T. & Bates, S. E. Multidrug resistance in cancer: role of ATP–dependent transporters. *Nat. Rev. Cancer* **2**, 48–58 (2002).

109. Leonard, G., Polgar, O. & Bates, S. E. ABC transporters and inhibitors: new targets, new agents. *Curr. Opin. Investig. Drugs* 1652–1659 (2002).

110. Al-Shawi, M. K. & Omote, H. The Remarkable Transport Mechanism of P-glycoprotein; a Multidrug Transporter. *J. Bioenerg. Biomembr.* **37**, 489–496 (2005).

111. Xia, D., Zhou, F. & Esser, L. Emerging consensus on the mechanism of polyspecific substrate recognition by the multidrug transporter P-glycoprotein. *Cancer Drug Resist.* **2**, 471–489 (2019).

112. Bai, X., McMullan, G. & Scheres, S. H. W. How cryo-EM is revolutionizing structural biology. *Trends Biochem. Sci.* **40**, 49–57 (2015).

113. Szewczyk, P. *et al.* Snapshots of ligand entry, malleable binding and induced helical movement in P-glycoprotein. *Acta Crystallogr. D Biol. Crystallogr.* **71**, 732–741 (2015).

114. Loo, T. W. & Clarke, D. M. Do drug substrates enter the common drug-binding pocket of P-glycoprotein through "gates"? *Biochem. Biophys. Res. Commun.* **329**, 419–422 (2005).

115. Shen, S. & Zhang, W. ABC transporters and drug efflux at the blood-brain barrier. *Rev. Neurosci.* **21**, 29–53 (2010).

116. Schinkel, A. H. *et al.* Disruption of the mouse mdr1a P-glycoprotein gene leads to a deficiency in the blood-brain barrier and to increased sensitivity to drugs. *Cell* **77**, 491–502 (1994).

117. Atkinson, D. E., Greenwood, S. L., Sibley, C. P., Glazier, J. D. & Fairbairn, L. J. Role of MDR1 and MRP1 in trophoblast cells, elucidated using retroviral gene transfer. *Am. J. Physiol. Cell Physiol.* **285**, C584-591 (2003).

118. Mahringer, A. & Fricker, G. ABC transporters at the blood-brain barrier. *Expert Opin. Drug Metab. Toxicol.* **12**, 499–508 (2016).

119. Siegal, T. & Zylber-Katz, E. Strategies for increasing drug delivery to the brain: focus on brain lymphoma. *Clin. Pharmacokinet.* **41**, 171–186 (2002).

120. Dong, X. Current Strategies for Brain Drug Delivery. *Theranostics* **8**, 1481–1493 (2018).

121. Patel, N. H. & Rothenberg, M. L. Multidrug resistance in cancer chemotherapy. *Invest. New Drugs* **12**, 1–13 (1994).

122. Goldstein, M. N., Slotnick, I. J. & Journey, L. J. In Vitro Studies with Hela Cell Lines Sensitive and Resistant to Actinomycin D. *Ann. N. Y. Acad. Sci.* **89**, 474–483 (1960).

123. Biedler, J. L. & Riehm, H. Cellular Resistance to Actinomycin D in Chinese Hamster Cells in Vitro: Cross-Resistance, Radioautographic, and Cytogenetic Studies. *Cancer Res.* **30**, 1174–1184 (1970).

124. Gros, P., Croop, J., Roninson, I., Varshavsky, A. & Housman, D. E. Isolation and characterization of DNA sequences amplified in multidrug-resistant hamster cells. *Proc. Natl. Acad. Sci.* **83**, 337–341 (1986).

125. Roninson, I. B. *et al.* Isolation of human mdr DNA sequences amplified in multidrug-resistant KB carcinoma cells. *Proc. Natl. Acad. Sci.* **83**, 4538–4542 (1986).

126. Ueda, K. *et al.* The mdrl gene, responsible for multidrug-resistance, codes for P-glycoprotein. *Biochem. Biophys. Res. Commun.* **141**, 956–962 (1986).

127. Goldstein, L. J. *et al.* Expression of Multidrug Resistance Gene in Human Cancers. *JNCI J. Natl. Cancer Inst.* **81**, 116–124 (1989).

128. Amiri-Kordestani, L., Basseville, A., Kurdziel, K., Fojo, A. T. & Bates, S. E. Targeting MDR in breast and lung cancer: Discriminating its potential importance from the failure of drug resistance reversal studies. *Drug Resist. Updat.* **15**, 50–61 (2012).

129. W. Robey, R., R. Massey, P., Amiri-Kordestani, L. & E. Bates, S. ABC Transporters: Unvalidated Therapeutic Targets in Cancer and the CNS. *Anti-Cancer Agents Med. Chem.-Anti-Cancer Agents* **10**, 625–633 (2010).

130. Assaraf, Y. G. Molecular basis of antifolate resistance. *Cancer Metastasis Rev.* **26**, 153–181 (2007).

131. Wong, S. T. & Goodin, S. Overcoming Drug Resistance in Patients with Metastatic Breast Cancer. *Pharmacother. J. Hum. Pharmacol. Drug Ther.* **29**, 954–965 (2009).

132. Hsia, T., Lin, C., Wang, J., Ho, S. & Kao, A. Relationship Between Chemotherapy Response of Small Cell Lung Cancer and P-glycoprotein or Multidrug Resistance-Related Protein Expression. *Lung* **180**, 173–179 (2002).

CHAPTER 2. OPTIMIZING THE VACCINIA VIRUS EXPRESSION SYSTEM FOR HUMAN P-GLYCOPROTEIN AND DEMONSTRATING REDUCTION OF P-GLYCOPROTEIN SURFACE EXPRESSION IS NOT CORRELATED TO INCREASED CELLULAR ACCUMULATION OF SUBSTRATE

2.1 Introduction

Expression of P-glycoprotein was achieved using the Vaccinia virus expression system in HeLa cells as previously described.[1] This system produces high expression of protein quickly in live cells and allows for modification of the expressing plasmid easily and quickly without having to create a new virus which can be a slow process as seen with baculoviruses and lentiviruses often used for protein expression.[2] Also, other expression systems including *E. coli* and yeast have not yielded significantly functional and structurally identical P-gp as observed in mammalian cells.[2] More recently, baculoviruses have been used successfully and more often for expression of P-gp in mammalian cells versus traditional use in insect cells which can be used to make membranes and purify P-gp but are not consistent with mammalian expressed P-gp in live cell assays. Transient expression of P-gp is also possible but produces low levels of protein expression not sufficient for use in large biochemical assays.

Infection of cells with Vaccinia virus, vTF7-3, produces a recombinant T7 RNA polymerase that is used to transcribe mRNA from a co-transfected plasmid.[3–5] Transfected plasmid contains the MDR1 cDNA in the pTM1 vector backbone which contains key features to achieve high levels of transient protein expression in mammalian cells. A T7 promoter region precedes the MDR1 gene allowing for T7 RNA polymerase binding and transcription of the gene. Transcription occurs in the cytoplasm as viral expression of T7 RNA polymerase and transfection with plasmid DNA does not penetrate the nucleus of eukaryotic cells.[3,5] As such, posttranscriptional modifications are not added to the produced mRNA of the MDR1 gene however the pTM1 vector contains two other key features which significantly improve the number of translations each mRNA strand goes through. First is a sequence of base pairs that follows the MDR1 gene which adds a poly-A tail to the mRNA to stabilize its structure and prevent degradation, and an internal ribosomal entry site (IRES) that immediately precedes the MDR1 gene. IRES features are RNA elements that increase translation by binding directly to the 40S subunit of ribosomes often by

recruiting eukaryotic initiation factors.[6] The IRES feature was initially discovered in poliovirus and encephalomyocarditis virus and has since been used to greatly increase translation in molecular genetics.[7,8] The transfection/ infection protocol of the Vaccinia virus expression system thus produces large quantities of protein quickly and in mammalian cells which allows us to study P-gp effectively.

Optimization of the Vaccinia virus protocol is important to produce WT and mutant P-gp reliably and with consistency. Following previously reported methods that reported 24 hours to yield cells that were expressing P-gp and could be used for flow cytometry were not consistent with early results obtained (data not shown). Infection with a recombinant Vaccinia virus will eventually lead to cell death affecting and skewing results with a large population of pre-apoptotic cells. Amounts of transfection reagent are also important to optimize as the reagent interacts directly with the cellular plasma membrane which can be solubilized, at high concentrations, making accumulation of fluorescent substrates difficult and unreliable as permeabilization of the membrane allows substrate to leak into or out of cells.

One aspect of many studies involving P-gp in live cell assays that is often not reported or usually not taken into consideration are changes in surface expression due to some alteration, often mutagenesis or deletions, of the MDR1 gene. One study mutated 15 conserved phenylalanine residues to tyrosine and reported a 50% increase in surface expression followed by transport analysis using a series of fluorescent substrates.[9] Changes in mutant P-gp transport of fluorescent substrates relative to WT P-gp was not correlated to the observed change in surface expression while both sets of cells expressing WT and mutant P-gp were directly compared. Not taking surface expression into consideration is common as there is an assumption in the field of many ABC transporters that expression above some minimum amount and longer duration of the assay is enough to confer full transport of substrate. This assumption is based on much observed biochemical data that shows mutant P-gp with varying levels of expression, both more and less than WT P-gp in the same expression system, transporting substrate at similar levels relative to WT P-gp though there are changes in kinetic data with varying levels of P-gp expression.[10] How changes in surface expression affect fluorescent substrate accumulation has not been formally studied, thus it becomes important to show that low expression of some mutants of P-gp do not necessarily correlate changes in expression to changes in substrate accumulation given sufficient time incubation time to reach equilibrium. To this end, we have shown that cells with decreased

cell surface expression of WT P-gp have similar levels of cellular accumulation of fluorescent substrate at equilibrium as cells with full expression of WT P-gp. Decoupling surface expression from cellular accumulation allows for the direct comparison of mutant P-gps that have higher or lower cell surface expression.

2.2 Materials and Methods

2.2.1 Materials

HeLa adenocarcinoma epithelial cells were purchased from ATCC (Manassas, VA). Dulbecco's Modified Eagle Medium (DMEM) with 4.5 g/L glucose and phenol red, penicillin/streptomycin, and phosphate buffer saline (PBS) were purchased from Corning Inc. (Corning, NY). Lipofectin™ transfection reagent, Opti-MEM™ reduced serum media with no phenol red, Calcein-AM, Rhodamine 123, and UIC2 monoclonal ABCB1 antibody were purchased from ThermoFisher Scientific (Waltham, MA). Fetal Bovine Serum (FBS) and Newborn Calf Serum (NCS) were purchased from R&D Systems (Minneapolis, MN). Subcloning Efficiency™ DH5α Competent Cells were purchased from Invitrogen™ (Carlsbad, CA). vTF7-3, Vaccinia Virus with the T7 RNA Polymerase reporter gene, was obtained through the NIH AIDS Reagent Program, Division of AIDS, NIAID, NIH: vTF7-3 from Dr. Tom Fuerst and Dr. Bernard Moss.[7] Basal Medium Eagle with Earle's salts and L-glutamine, and GF 120918 (Elacridar) were purchased from Sigma-Aldrich (St. Louis, MO). GlutaMAX™ supplement and TrypLE™ Express Enzyme with phenol red were purchased from Gibco™ (Grans Island, NY). C219, MRK16, and UIC2 monoclonal antibodies for (ABCB1) P-gp were a kind gift from Dr. Michael M. Gottesman (National Cancer Institute, NIH, Bethesda, MD). Mouse IgG_{2a} κ isotype control and FITC-α-mouse antibodies were purchased from BD Biosciences (San Jose, Ca). All other common chemicals and solvents were purchased from either ThermoFisher Scientific or Sigma-Aldrich.

2.2.2 HeLa Cell Culture and Expression of P-Glycoprotein using a Vaccinia Virus Expression System

HeLa cells in monolayer were maintained at 37° C in a 5% CO_2 environment and continuously cultured in DMEM containing 2 mM L-glutamine, 10 % fetal bovine serum, 50 units/mL of penicillin and 50 µg/mL streptomycin.[8]

Optimization of the Vaccinia virus expression system was carried out to determine the ideal conditions for *in vitro* assays using live cells expressing P-gp. A plasmid containing a T7 promoter followed by an internal ribosome entry site immediately before the ABCB1 gene, pTM1-MDR, is used in conjunction with a recombinant Vaccinia virus expressing a T7 RNA polymerase, vTF7-3, to express protein in cells.[7] Transfection/ infection of DNA and virus was modified from a previously described method to optimize expression of P-gp.[1] Amounts of vTF7-3, pTM1-MDR, transfection reagent, and incubation time were varied in determination of optimized conditions. HeLa cells were grown to 70 – 80% confluency in T-25 cell culture flasks before transfection/ infection. Transfection was carried out by combining 1 – 5 µg of DNA with Lipofectin™ in a 1:3 ratio yielding 5 – 25 µg of lipid added to 1 mL opti-MEM in a polystyrene conical tube and incubated at room temperature for 30 minutes. vTF7-3 at a multiplicity of infection (MOI) of 3 – 8 was added to 0.5 mL opti-MEM immediately before infection. Cells were washed once with PBS before the DNA-lipid mixture and virus were then added to T-25 flasks containing HeLa cells. Cells were incubated for 4 hours at 37° C in 5% CO2 after which 5 mL of complete media were added to the T-25 culture flasks. Cells were incubated for a total of 24 hours before trypsinization and collection for cell surface expression assays. Cells were harvested 12 hours post transfection/ infection for transport assays.

2.2.3 Surface Expression and Cellular Accumulation of Fluorescent Substrates by Flow Cytometry

P-gp expressing HeLa cells from the Vaccinia virus expression system were collected and counted. Cells were resuspended in BME (1% BME powder, 7.5% (w/v) $NaHCO_4$, 5% NCS, pH 7.4, filter sterilized (0.22 µm filter)) at a concentration of 2.5 x 10^5 cells per sample. For cell surface expression 2.5 x10^5 cells were incubated in BME with 1.5 µg of either the Mrk16 or UIC2 antibody to measure surface expression of P-gp or with 3 µg of IgG_{2a} kappa isotype antibody as a negative control. Samples were incubated at 37° C for 30 minutes before being spun at 500 xg and the supernatant removed. Pelleted cells were then incubated with 2.5 µg of FITC conjugated α-mouse antibody for an additional 30 min before being spun at 500 xg, the supernatant removed, and pellets stored on ice. Samples were then resuspended in 400 µL PBS and run on a BD Accuri™ flow cytometer with a 20 mW 488 nm solid state blue excitation laser and data was collected on the FL1 detector (530/30 nm).

For cellular accumulation of fluorescent substrates 2.5 x 10^5 cells per sample were incubated with one of the following fluorescent substrates either in the presence of absence of 1μM GF 120198 which is an inhibitor of P-gp. Samples incubated with GF 120198 are P-gp inhibited, negative controls with high levels of basal fluorescent substrate accumulation while samples incubated without GF120198 show uninhibited P-gp activity on substrate efflux and lower levels of fluorescent substrate accumulation. Calcein-AM (0.0625 μM) or rhodamine 123 (0.5 μM) were all incubated with cells in the presence or absence of GF 120198 at 0.5 μM, unless otherwise noted, for 30 minutes at 37° C except for calcein-AM which was incubated for 10 minutes at 37° C. All samples were spun at 500 xg to pellet the cells before a second incubation with BME again with or without GF 120198. Calcein-AM samples do not need a second incubation as (acetyloxy)methoxy groups are cleaved by nonspecific esterases and is no longer cell permeable. Samples are then resuspended in 400 μL PBS and data collected on a BD Accuri™ flow cytometer on the FL1 channel.

Data were gated on forward scatter (FSC) and side scatter (SSC) based on pTM1 empty vector transfected/ infected HeLa cells. Mean fluorescent intensities (MFI) were measured by the BD Accuri™ software and normalized on the IgG_{2a} isotype control or GF 120198 control for each set of samples in each of the assays. Normalized data for mutant P-gp was then compared to wild-type (WT) P-gp to get a measure of %WT.

2.3 Results and Discussion

2.3.1 Optimizing the Vaccinia Virus Expression System for P-Glycoprotein Expression in HeLa Cells

Four major factors were tested in optimizing the Vaccinia virus expression system for expressing P-gp in HeLa cells. Each factor was changed independently to determine which condition was best to achieve maximum P-gp expression while minimizing the population of cells not expressing P-gp. Multiplicity of infection measures the ratio of viral particles to cells and determines how many cells are infected with at least one viral particle which follows a Poisson distribution. MOIs of 3, 5, and 8 were tested as they confer 95%, 99.3%, and 99.9% likelihood that each cell will be infected with at least one viral particle. When comparing cell surface expression, there is no major difference between the amount of P-gp being expressed in the population of cells expressing P-gp as they all reached a similar level of fluorescence. A difference in the population

of cells expressing P-gp versus not expressing P-gp is observed though. MOIs of 3 showed an increased number of cells not expressing P-gp compared to MOIs of 5 and 8 which had similar levels of cells expressing P-gp through comparison of peaks with similar fluorescence to control IgG_{2a} labeled cells (Figure 2.1 A). It follows that the difference between an MOI of 5 and 8 is not significant as only 0.6% more cells would theoretically be infected at an MOI of 8 which is 60 cells in a count of 10,000. Next the amount of plasmid DNA was varied in each run at 1, 3, and 5 µg. While the amount of DNA does directly not impact the rate at which cells are transfected, the copies of plasmid per cell could have a potential effect on protein expression. 3 and 5 µg of DNA were similar in surface expression of P-gp while 1 µg had a larger population of cells that did not express P-gp and less overall surface expression (Figure 2.1 B).

By far the largest changes in surface expression came with the ratio of transfection reagent to DNA. Increasing the transfection reagent ratio from 1:1 to 3:1 transfection reagent to DNA significantly improved surface expression of P-gp (Figure 2.1 C). Further experiments to increase the ratio to 5:1 and greater resulted in higher expression, maximized at 5:1, but ratios of 5:1 and greater resulted in loss of accumulation of fluorescent substrates. Increasing the amount of transfection reagent in solution likely began to disrupt membranes permeability allowing for significantly increased passive diffusion across the membrane making those samples unusable for determining effects of mutations in P-gp on transport of fluorescent substrates. The incubation time after the addition of virus and transfection reagents was significant for surface expression. Initially maximal expression for flow cytometry was reported to be 24 hours post-transfection/ infection.[1] Repeating 24-hour timing yield high expression of P-gp in cells however cells were apoptotic and unable to be used in flow cytometry assays. Reducing incubation time to 12 hours yielded high levels of expression while maintaining cell viability. Taking all the data collected we determined that a MOI of 5 and a transfection reagent to lipid ratio of 3:1 with 3 µg of DNA incubated for 12 hours expressed active P-gp at high levels with good cell viability without disrupting the membrane.

2.3.2 Reduction in Surface Expression of P-Glycoprotein is Not Correlated to Changes in Cellular Accumulation of Substrates

To deconvolute the relation of total surface expression to cellular accumulation of fluorescent substrates, a direct comparison was made between cells expressing different levels of

P-gp to their ability to transport fluorescent substrates. Cell surface expression was varied by reducing the amount of incubation time. A common method to reduce protein expression in transient transfection-based systems is to reduce the amount of DNA added, however reduction in DNA amount only reduced the population of cells expressing P-gp and not total surface expression using the Vaccinia virus expression system (data not shown). This is likely due to the high number of mRNA copies produced by T7 RNA polymerase as it is constitutively active for the duration of the incubation period and the high number of translations of each mRNA molecule. Reducing incubation time in half from 10 hours to 5 hours reduced cell surface expression of P-gp to 33 ± 1.0% measured with the UIC2 antibody (Figure 2.2 B). Flow cytometry was then used to determine the ability of reduced cell surface expression cells to transport calcein-AM and rhodamine 123 relative to control cells with high cell surface expression. Cells with low cell surface expression were able to transport calcein-AM at 100.5 ± 3.4% and rhodamine 123 at 95.9 ± 1.3% (Figure 2.2 A). With no to small differences in ability to transport substrate it follows that changes in cell surface expression do not correlate significantly to changes in cellular accumulation of fluorescent substrates allowing for comparisons of control WT P-gp to P-gp mutants with different levels of surface expression.

Reduction of surface expression did not change the ability to transport fluorescent substrate is significant for analyzing mutants such as MDR Y998A. Surface expression of MDR Y998A is 10.6 ± 0.4% of WT while transport of rhodamine 123 is 98.8 ± 2.7% of WT. While surface expression is significantly different compared to relative expression of WT P-gp, the ability to transport rhodamine 123 is not. Reduction of surface expression not affecting transport in this setting confirm the significance seen in MDR Y998A as this mutant's ability to transport other fluorescent substrates is significantly different to WT P-gp. This is the first time, to our knowledge, that anyone has directly shown that surface expression of P-gp is not directly correlated to the ability to transport fluorescent substrates relative to other cells with differing cell surface expressions in cellular accumulation assays that allow for adequate incubation time to reach equilibrium. There is still the possibility that reduction of cell surface expression below some critical value may impact transport ability and substrate accumulations however, that value was not reached in this or subsequent results. Also, the ability of differing levels of P-gp surface expression may be a function of time which was not tested here. In conclusion, there is no significant correlation between accumulation of fluorescent substrate and cell surface expression

if a minimum amount of surface expression is achieved with adequate amount of time for the system to reach equilibrium.

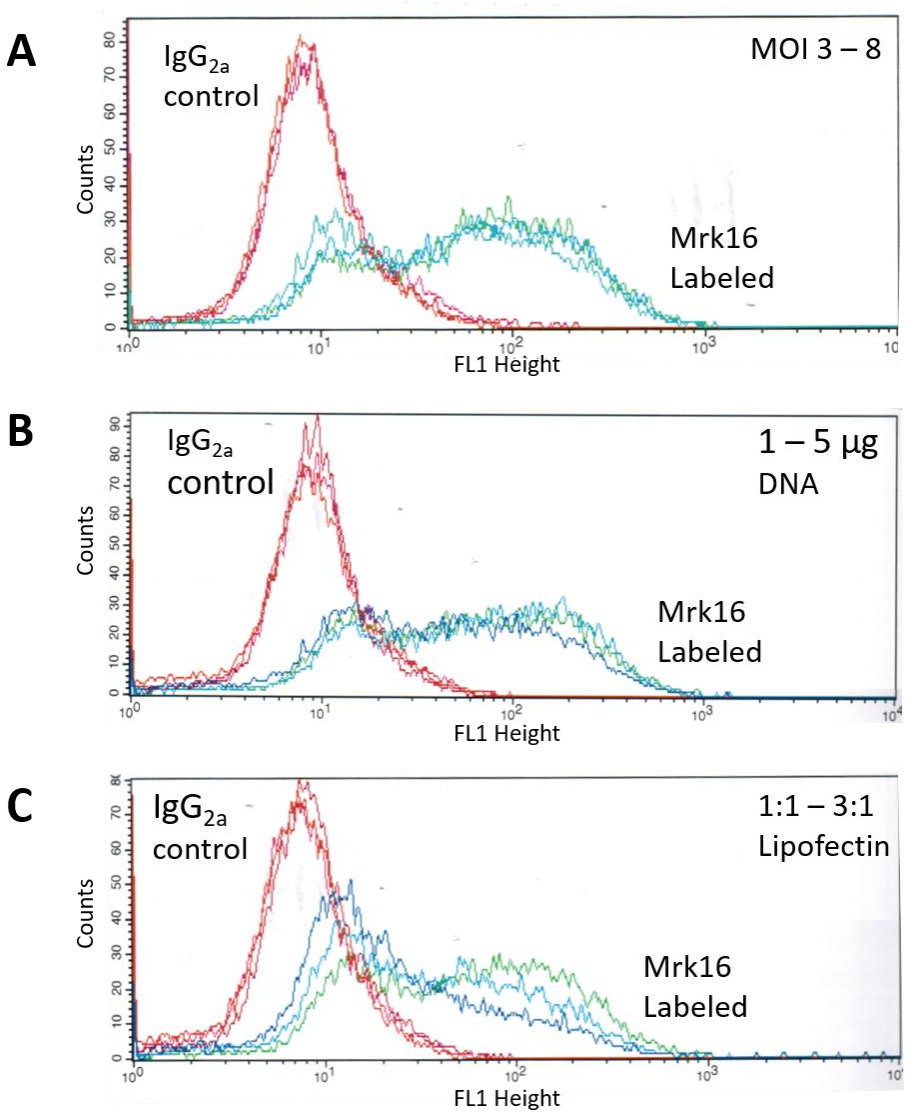

Figure 2.1: Conditions for Optimizing Expression of P-glycoprotein in HeLa Cells Using a Vaccinia Virus Expression System

Multiplicity of infection, amount of plasmid DNA, and ratio of Lipofectin™ were varied to determine optimal infection/ transfection conditions for HeLa cells at 70-80% confluency in a T-25 cell culture flask. Surface expression was measured using a monoclonal antibody, Mrk16, and maximal surface expression for each condition was determined on the maximal increase of mean fluorescence intensity compared to negative control cells labeled with IgG_{2a} antibody. (A) MOI was varied at 3 (light blue), 5 (dark blue), and 8 (green). (B) Amount of pTM1 WT MDR plasmid was varied at 1 (dark blue), 3 (light blue), and 5 (green) µg. (C) The ratio of Lipofectin™ to plasmid was varied at 1:1 (dark blue), 2:1 (light blue), and 3:1 (green). Optimized conditions for expression were determined to be a MOI of 5, 3 µg plasmid, and a 3:1 ratio of Lipofectin™ to plasmid for a 70-80% confluent T-25 cell culture flask.

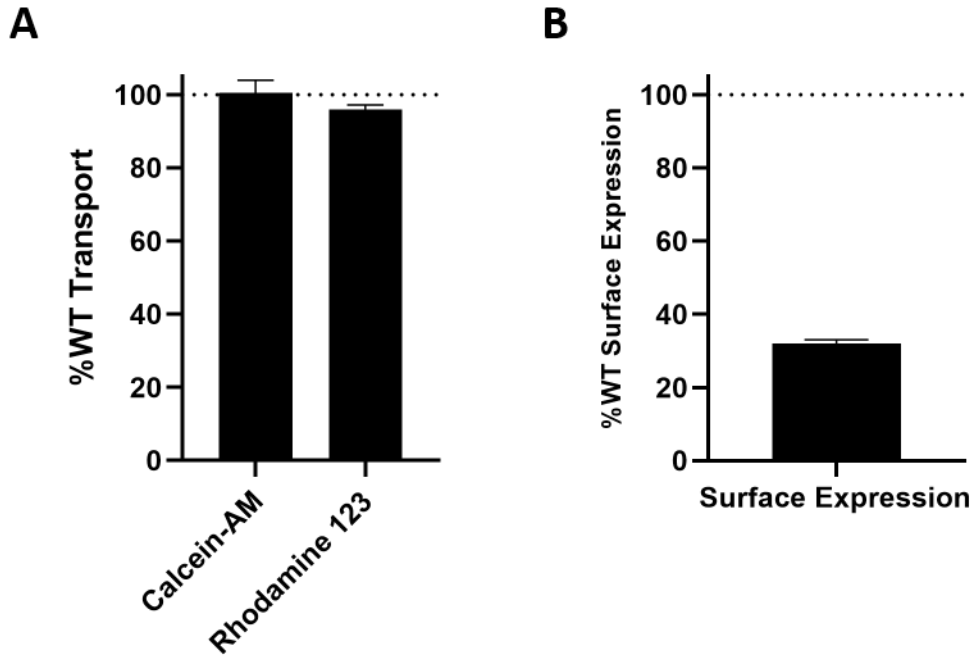

Figure 2.2: Surface Expression and Cellular Accumulation of Fluorescent Substrates in Cells with Reduced Surface Expression of P-Glycoprotein

Reduced surface expression was achieved by reducing the amount of time cells were incubated post transfection/ infection. (A) Measure of cellular accumulation of either calcein-AM or rhodamine 123 in cells with reduced surface expression of 32 ± 0.97% of P-gp in fully expressing cells. Neither substrate was shown to be effluxed less when cells were expressing lower levels of P-gp. Calcein-AM and rhodamine 123 were not significantly different from full transport by fully expressed WT P-gp. (B) Reduced surface expression of P-gp measured by UIC2. Cells were transfected/ infected and incubated afterwards for either 12 or 6 hours. Surface expression of P-gp at 6 hours was 32 ± 1.0% that of surface expression at 12 hours. Surface expression was significantly reduced ($p<0.0001$).

2.4 References

1. Hrycyna, C. A., Ramachandra, M., Pastan, I. & Gottesman, M. M. Functional Expression of Human P-Glycoprotein from Plasmids using Vaccinia Virus-Bacteriophage T7 RNA Polymerase System. *Methods Enzymol.* **292**, 456–473 (1998).

2. Evans, G. L. *et al.* Heterologous expression systems for P-glycoprotein:E. coli, yeast, and baculovirus. *J. Bioenerg. Biomembr.* **27**, 43–52 (1995).

3. Wyatt, L. S., Moss, B. & Rozenblatt, S. Replication-Deficient Vaccinia Virus Encoding Bacteriophage T7 RNA Polymerase for Transient Gene Expression in Mammalian Cells. *Virology* **210**, 202–205 (1995).

4. Fuerst, T. R., Earl, P. L. & Moss, B. Use of a hybrid vaccinia virus-T7 RNA polymerase system for expression of target genes. *Mol. Cell. Biol.* **7**, 2538–2544 (1987).

5. Elroy-Stein, O. & Moss, B. Gene expression using the vaccinia virus/T7 RNA polymerase hybrid system. *Curr. Protoc. Mol. Biol.* **Chapter 16**, Unit16.19 (2001).

6. Martínez-Salas, E. Internal ribosome entry site biology and its use in expression vectors. *Curr. Opin. Biotechnol.* **10**, 458–464 (1999).

7. Pelletier, J. & Sonenberg, N. Internal initiation of translation of eukaryotic mRNA directed by a sequence derived from poliovirus RNA. *Nature* **334**, 320–325 (1988).

8. Jackson, R. J., Howell, M. T. & Kaminski, A. The novel mechanism of initiation of picornavirus RNA translation. *Trends Biochem. Sci.* **15**, 477–483 (1990).

9. Vahedi, S., Chufan, E. E. & Ambudkar, S. V. Global alteration of the drug-binding pocket of human P-glycoprotein (ABCB1) by substitution of fifteen conserved residues reveals a negative correlation between substrate size and transport efficiency. *Biochem. Pharmacol.* **143**, 53–64 (2017).

10. Shirasaka, Y., Sakane, T. & Yamashita, S. Effect of P-Glycoprotein Expression Levels on the Concentration-Dependent Permeability of Drugs to the Cell Membrane. *J. Pharm. Sci.* **97**, 553–565 (2008).

11. Fuerst, T. R., Niles, E. G., Studier, F. W. & Moss, B. Eukaryotic transient-expression system based on recombinant vaccinia virus that synthesizes bacteriophage T7 RNA polymerase. *Proc. Natl. Acad. Sci. U. S. A.* **83**, 8122–8126 (1986).

12. Gey, G. O., Bang, F. B. & Gey, M. K. Responses of a Variety of Normal and Malignant Cells to Continuous Cultivation, and Some Practical Applications of These Responses to Problems in the Biology of Disease. *Ann. N. Y. Acad. Sci.* **58**, 976–999 (1954).

CHAPTER 3. FLEXIBILITY OF TRANSMEMBRANE HELIX 12 IN HUMAN P-GLYOPROTEIN FACILITATES SUBSTRATE TRANSPORT ACROSS MEMBRANES

3.1 Introduction

P-gp consists of two distinct types of domains, the nucleotide binding domains, and the helical transmembrane domains. The NBDs are highly conserved between all ABC transporters and fall into a larger super family of P-loop NTPases.[1,2] TMDs, however, are not nearly as conserved as the NBDs because the number and orientation of the TM helices varies greatly between ABC transporters.[3] This variability has made it difficult to compare TMDs between ABC transporters as variability includes: import versus export functionality, specific versus promiscuous substrate binding sites, number of TM helices ranging from 8 to 16, and very low sequence identity between even closely related ABC transporters.[4] Of particular interest of helices in the TMDs are helices 4 & 6 and 10 & 12, which are thought to form the two "gates" for drug entry into the large substrate binding pocket.[5] These helices are less bulky due to the presence of smaller side chain amino acids allowing for tighter packing when the TMDs undergo conformational changes for substrate transport.[6] Of these helices, it has been observed that transmembrane helix (TMH) 12 is of particular interest due to involvement in substrate transport as suggested by photocrosslinking of substrates to residues on TMH 12.

Murine P-gp and human P-gp have a high degree of sequence identity and similarity at 87% and 94%, respectively, and models of both murine and human P-gp are often used in conjunction to determine structural and functional features.[7] TM helices of P-gp are interesting since, unlike many other TM helices, they are of significant length, 36 – 59 amino acids, extending well into the cytoplasm.[4] Helices of this length tend to have breaks in their H-bonding pattern and bend slightly. Of interest is a kink caused by residues in TM helix 12 of P-gp. This kink is commonly observed as an unordered break in the TMH 12 α-helix in inward facing conformations (Figure 3.1 A). In outward facing conformations TMH 12 adopts a fully ordered helix but one that is not fully straight (Figure 3.1 B). Though TMH 12 contains a proline, P996, previous mutations of all 13 prolines in the TMDs to alanine showed no significant changes in either ATPase activity or substrate transport.[8] It is likely that P996 contributes to the observed kink in TMH 12 but is not decisive for the function of P-gp.

The large conformational change required for TMH 12 to reorder itself is observable when comparing multiple crystal structures. Crystal structures of murine P-gp were crystalized under multiple conditions including catalytically active or inactive, presence of heavy metals during crystal formation, and deletion of a linker region that resulted in similar inward facing structures of good resolution.[9] These structures, while similar, show varying degrees of NBD center of gravity separation at 46 Å and 60 Å and show significant effects on helix tilt and helix rotation on some TMHs when superimposing equivalent helices together.[9] The most significant changes occurred on TMH 12 where helix rotation and tilt varied by 24.4º and 26.5º respectively in compared structures relative to other helices which had small changes in rotation and tilt.[9] Such significant changes in orientation and conformation must be due to inherent flexibility in the TMH 12 structure.

TMH12 has also been shown to be important for conformational changes in the TMDs and NBD dimerization in substrate transport and ATPase activity stimulated by substrate binding and transport.[10] Mutations and deletions in substrate binding site residues on TMH 12, such as F978A, affected ATPase activity and transport of substrates.[11] Substrates known to bind surfaces of the substrate binding pocket and that have been shown to not directly interact with F978A are still affected by the mutation.[12] Rhodamine 123, which has a well-defined binding site not associated with F978, is not transported by mutations at that location.[12] From this and other similar biochemical work, it was concluded that TMH12 has a significant role in coupling drug binding and ATPase activity.[13–15]

TMH 12 has been shown to be flexible in undergoing large tilt and rotational movements. It is also important in TMD and NBD coupling. TMH 12 also has an unordered region in inward facing conformations become ordered in outward facing conformations. Thus, it is likely that changes in flexibility of TMH 12 will significantly affect substrate transport *in vitro*. If the helix is more rigid, then it follows that the structure would still transduce a signal to hydrolyze ATP upon substrate binding but would likely not to be able to adopt conformational flexibility required substrate binding leading to decreased transport of substrate. If the helix is made more flexible, then the ability of the helix to transduce a coupling signal to the NBDs would be compromised and substrate stimulated ATP hydrolysis would decrease leading to a decrease in substrate transport.

To test this hypothesis, sequence alignment was performed with Clustal Omega between significantly different species and it was determined that there is a conserved PDYAKA sequence

at 996-1001 which corresponded to the unordered region of TMH 12 (Table 3.1). 996-1001 were mutated to alanine or glycine to either stiffen TMH 12 or to make it more flexible based on the propensity of alanine and glycine to form α-helices.[16] Both mutations were evaluated on the ability to transport a variety of substrates in mutant P-gp expressing HeLa cells.

3.2 Materials and Methods

3.2.1 Materials

All oligonucleotides were designed in-house and purchased from Integrated DNA Technologies (Coralville, IA). In-Fusion® HD Cloning Kit was purchased from Takara Bio Inc. (Moutain View, Ca). HeLa adenocarcinoma epithelial cells were purchased from ATCC (Manassas, VA). Dulbecco's Modified Eagle Medium (DMEM) with 4.5 g/L glucose and phenol red, penicillin/streptomycin, and phosphate buffer saline (PBS) were purchased from Corning Inc. (Corning, NY). Lipofectin™ transfection reagent, Opti-MEM™ reduced serum media with no phenol red, pFastBac HTA vector, Calcein-AM, Rhodamine 123, UIC2 monoclonal ABCB1 antibody, SuperSignal™ West Pico Plus chemiluminescent substrate, DH10Bac competent cells, and LDS 751 were purchased from ThermoFisher Scientific (Waltham, MA). Nitrocellulose membrane, 0.2 µm, was purchased from Cytiva Life Sciences (Marlborough, MA). Fetal Bovine Serum (FBS) and Newborn Calf Serum (NCS) were purchased from R&D Systems (Minneapolis, MN). Q5® site-directed mutagenesis kit and restriction enzymes, NdeI and XhoI, were purchased from New England Biolabs Inc. (Ipswich, MA). Subcloning Efficiency™ DH5α Competent Cells were purchased from Invitrogen™ (Carlsbad, CA). vTF7-3, Vaccinia Virus with the T7 RNA Polymerase reporter gene, was obtained through the NIH AIDS Reagent Program, Division of AIDS, NIAID, NIH: vTF7-3 from Dr. Tom Fuerst and Dr. Bernard Moss.[9] Basal Medium Eagle with Earle's salts and L-glutamine, ammonium persulfate, and GF 120918 (Elacridar) were purchased from Sigma-Aldrich (St. Louis, MO). Bodipy(BD)-FL-Verapamil, BD-FL-Prazosin, and 3,3'-diethyloxacarbocyanine iodide ($DiOC_2$) were purchased from Setareh Biotech (Eugene, OR). *Spondoptera frugiperda* (Sf9) cells, and ESF 921 insect cell culture media were purchased from Expression Systems (Davis, CA). GlutaMAX™ supplement and TrypLE™ Express Enzyme with phenol red were purchased from Gibco™ (Grans Island, NY). Acryl/Bis 29:1, 30% solution was purchased from VWR International (Radnor, PA). N,N,N',N'-methylethylenediamine

(TEMED) was purchased from Acros Organics BVBA (Fair Lawn, NJ). C219, MRK16, and UIC2 monoclonal antibodies for (ABCB1) P-gp were a kind gift from Dr. Michael M. Gottesman (National Cancer Institute, NIH, Bethesda, MD). Mouse IgG_{2a} κ isotype control and FITC-α-mouse antibodies were purchased from BD Biosciences (San Jose, Ca). All other common chemicals and solvents were purchased from either ThermoFisher Scientific or Sigma-Aldrich.

3.2.2 Cell Culture

HeLa cells in monolayer were maintained at 37° C in a 5% CO_2 environment and continuously cultured in DMEM containing 2 mM L-glutamine, 10 % fetal bovine serum, 50 units/mL of penicillin and 50 µg/mL streptomycin.[10] Sf9 insect cells in suspension were maintained at 27° C and shaken at 230 RPM and continuously cultured in ESF 921 protein free media.[11]

3.2.3 Baculovirus Expression of P-glycoprotein in Insect Cells and Crude Membrane Preparation

cDNA encoding human P-gp was subcloned into a modified pFastBac HTA vector. Briefly, the pFastBac HTA vector was modified to remove an ATG start codon and an intrinsic sequence for a 6-histidine (His_6) tag. Both motifs were unneeded as the cDNA contained both the intrinsic start codon and a C-terminal His_6 tag. Modifications were made through deletion using inverse polymerase chain reaction (PCR) with primers designed for the Q5 mutagenesis kit. P-gp cDNA was inserted using the In-Fusion cloning system through linearization of vector by NcoI and XhoI, amplification of the gene of interest with primers that overlap with both vector and insert at the restriction sites used for linearization, and incubation with the In-Fusion protein which removes 3' nucleotides through 3'-5 exonuclease activity to allow vector and insert to anneal together. Insertion of the gene was confirmed with bidirectional dye terminating sequencing, i.e. Sanger sequencing. pFastbac constructs were transformed with DH10Bac competent cells to produce bacmid which was then subsequently transfected into Sf9 insect cells for Baculovirus construction. Protein was expressed in Sf9 insect cells infected with Baculovirus and infected cells were harvested and pelleted 40-48 hours post-infection, flash frozen, and stored at -80° C. Crude membranes were prepared from these pellets as previously described with slight modifications.[12,13] Thawed pellets were resuspended in homogenization buffer (50 mM Tris HCl pH 7.5, 50 mM

mannitol, 2.00 mM EGTA, 1% Aprotinin, 2.00 mM AEBSF) at 2 mL of homogenization buffer per 50 mL of cell culture for 30 minutes on ice before homogenization using a Dounce homogenizer with the tight fitting pestle 40x. Homogenized cells were then spun at 500 xg for 10 minutes to pellet large cellular debris and nuclei and the supernatant was further spun at 100,000 xg for 1 hour at 4° C. Membrane pellets were then resuspended in resuspension buffer (homogenization buffer, 10% glycerol) at 750 µL per 50 mL of initial insect cell culture through decreasing gauges (20, 22, and 25 gauge) of blunted syringe needles before being flash frozen at -80° C. Concentration of protein in crude membranes was determined by a modified Lowry assay using Coomassie reagent as a protein dye and bovine serum albumin as a standard (BSA).[14]

3.2.4 SDS-PAGE and Immunoblotting

Crude membranes overexpressing P-gp were loaded at 1 µg onto a 7.5% sodium dodecyl sulfate-polyacrylamide gel electrophoresis (SDS-PAGE) gel with a thickness of 0.75 mm. Gels were then western blotted through transfer to nitrocellulose membranes (0.22 µm) before immunoblotting with antibodies. Nitrocellulose membranes were blocked with 20% (w/v) non-fat dry milk in PBS (2.70 mM KCl, 137 mM NaCl, 4.00 mM Na_2HPO_4, 1.80 mM KH_2PO_4, pH 7.4) with 0.05% (v/v) Tween-20 (PBST) at 4° C overnight or room temperature for 3 hours. Membranes are then washed 3 times with PBST and then incubated with primary antibody, C219 (1:8000), prepared in 5% (w/v) non-fat dry milk in PBST at 4° C overnight or 3 hours at room temperature. Membranes were washed again 3 times with PBST and finally incubate with secondary antibody, α-mouse-HRP (1:4000), prepared in 5% (w/v) non-fat dry milk for 1 hour at room temperature before being washed with PBST 3 times for final preparation for imaging of the membrane. Enhanced chemiluminescence with SuperSignal™ West Pico Chemiluminescent substate is used to visual antibody bound protein on the gel and is visualized on a GeneGnome XRQ.

3.2.5 Expression of P-glycoprotein using a Vaccinia Virus Expression System

pTM1-MDR was obtained from a previously described preparation and this same preparation was used to clone a cys-less (CL) MDR1 gene into pTM1 to create pTM1-CLMDR.[15] Importantly, the MDR1 gene is inserted at the 3’ end of the encephalomyocarditis virus internal ribosome entry site (IRES) and is further preceded by a T7 promoter region in the pTM1 vector.

Subsequent mutations were constructed using a Q5® mutagenesis kit for site directed mutagenesis and introduction of one or many amino acid mutations (Table 3.2). P-gp was then expressed in HeLa cells using a modified Vaccinia virus expression system as previously described.[16] HeLa cells were cultured to be in mid-log phase (70 – 80% confluency) at the time of transfection/ infection. For T-75 culture flasks, HeLa cells were seeded at 1.5 x 10^6 cells 20-24 hours before the beginning of transfection/ infection to reach the desired confluency. Transfection solution was prepared 30 minutes prior to infection through the addition of 9 µg of pTM1-MDR construct with 27 µL of Lipofectin™ (1 mg/mL), a ratio of 1:3 DNA to transfection reagent, in 3mL of opti-MEM in a polystyrene conical tube. Polystyrene is desired over polypropylene as the DNA-lipid complex can interact with the plastic and reduce the amount of DNA-lipid mixture in solution. A modified Vaccinia virus expressing T7 RNA polymerase, vTF7-3, was added to 1 mL opti-MEM per T-75 flasks to the desired multiplicity of infection (MOI) of 5. Cells were washed once with PBS before the transfection solution and vTF7-3 solution were added to the culture flask and then incubated at 37° C in 5% CO_2. Complete medium was added to the flasks up to the normal working volume of 12 mL 3 hours post-transfection/ infection. Cells were incubated at 37° C in 5% CO_2 for a total of 10 hours before being washed with PBS and detached with TrypLE™ and collected with PBS.

3.2.6 Determination of Cell Surface Expression and Fluorescent Substrate Accumulation by Flow Cytometry

P-gp expressing HeLa cells from the Vaccinia virus expression system were collected and counted. Cells were resuspended in BME (1% BME powder, 7.5% (w/v) $NaHCO_4$, 5% NCS, pH 7.4, filter sterilized (0.22 µm filter)) at a concentration of 2.5 x 10^5 cells per sample. For cell surface expression 2.5 x10^5 cells were incubated in BME with 1.5 µg of either the Mrk16 or UIC2 antibody to measure surface expression of P-gp or with 3 µg of IgG_{2a} kappa isotype antibody as a negative control. Samples were incubated at 37° C for 30 minutes before being spun at 500 xg and the supernatant removed. Pelleted cells were then incubated with 2.5 µg of FITC conjugated α-mouse antibody for an additional 30 min before being spun at 500 xg, the supernatant removed, and pellets stored on ice. Samples were then resuspended in 400 µL PBS and run on a BD Accuri™ flow cytometer with a 20 mW 488 nm solid state blue excitation laser and data was collected on the FL1 detector (530/30 nm).

For cellular accumulation of fluorescent substrates 2.5 x 10^5 cells per sample were incubated with one of the following fluorescent substrates either in the presence of absence of 1µM GF 120918 which is an inhibitor of P-gp. Samples incubated with GF 120918 are P-gp inhibited, negative controls with high levels of basal fluorescent substrate accumulation while samples incubated without GF120918 show uninhibited P-gp activity on substrate efflux and lower levels of fluorescent substrate accumulation. Calcein-AM (0.0625 µM), rhodamine 123, BD-verapamil, BD-prazosin, DiOC2 (0.125 µM), and LDS751 were all incubated with cells in the presence or absence of GF 120918 at 0.5 µM, unless otherwise noted, for 30 minutes at 37° C except for calcein-AM which was incubated for 10 minutes at 37° C. All samples were spun at 500 xg to pellet the cells before a second incubation with BME again with or without GF 120918. Calcein-AM samples do not need a second incubation as (acetyloxy)methoxy groups are cleaved by nonspecific esterases and is no longer cell permeable. Samples are then resuspended in 400 µL PBS and data collected on a BD Accuri™ flow cytometer on the FL1 channel except for LDS751 which is collected on the FL3 channel (>670 nm).

Data were gated on forward scatter (FSC) and side scatter (SSC) based on pTM1 empty vector transfected/ infected HeLa cells. Mean fluorescent intensities (MFI) were measured by the BD Accuri™ software and normalized on the IgG_{2a} isotype control or GF 120918 control for each set of samples in each of the assays. Normalized data for mutant P-gp was then compared to wild-type (WT) P-gp to get a measure of %WT.

3.3 Results

To test for alterations in overall P-gp conformations due to changes in flexibility of TMH 12 near the kink region PDYAKA996-1000AAAAAA (KinkA) and PDYAKA996-1000GGGGGG (KinkG). The KinkA and KinkG mutation were made to modulate flexibility in TMH 12 as the Ala mutation will make the helix more rigid and the Gly mutation will make the helix more flexible due to the propensity of Ala and Gly to form helices. These mutations were introduced to cysteine-less P-gp (CL-P-gp) L531C/ C1074. Introduction of a cysteine in the signature motif of NBD1 at position 531 can crosslink in the presence of Cu(II) phenanthroline with an endogenous cysteine in the Walker A motif of NBD2 at position 1074 when the two NBDs dimerize.[25] Changes in dimerization can then be correlated to changes in the likelihood of mutations to change the conformational states P-gp can adopt. Crosslinked NBDs in P-gp are less

mobile in SDS-PAGE, about a 15 – 20 kDa increase in apparent size, and qualitatively can be a measure for the likelihood of P-gp NBDs to dimerize. Less dimerization of the NBDs can correlate to less sampling of conformations in the outward facing state relating decreased transport of substrate. It should also be noted that P-gp is not glycosylated in insect cell expression and the comparison of un-crosslinked to crosslinked NBDs is roughly the difference in apparent size of 145 to 160 kDa respectively.

2.5 µg of control membranes were prepared with CL-P-gp L531C/ C1074 and crosslinked and were shown to have a high degree of dimerization though not all of the protein is dimerized (Figure3.2). In comparison 5 µg of both the KinkA and KinkG mutations had a higher degree of un-crosslinked NBDs as the density of the bands around 145 kDa were darker than bands visible at around 160 kDa. Increasing the amount of protein loaded worsens streaking making evaluation of crosslinked to un-crosslinked difficult. Streaking was likely observed due to crosslinking between P-gp molecules and aggregate protein formation. Accumulation of signal near the top of gel images is likely observed from crosslinking between molecules of P-gp creating large molecular weight structures with low to no mobility and aggregates of protein due to the need to load a relatively large amount of protein for western blotting.

Next, the Vaccinia virus expression system was used to express WT P-gp, P-gp KinkA, and P-gp KinkG in HeLa cells. HeLa cells were chosen due to no detectable cell surface expression of endogenous P-gp (data not shown) meaning any observable transport is directly correlated to expression of P-gp from the Vaccinia virus expression system. Cellular accumulation of fluorescent substrates was measured with six structurally and chemically different molecules: calcein-AM, rhodamine 123, BD-verapamil, BD-prazosin, DiOC2, and LDS 751. The ability of P-gp variants to transport fluorescent substrates to reduce cellular accumulation was normalized to results from WT P-gp and reported as %WT. Normalization was carried out to determine change in MFI by subtracting MFI of uninhibited P-gp expressing cells from inhibited P-gp expressing cells. Changes in the change of MFI can then be calculated as a %WT when divided by the change in MFI of WT P-gp expressing cells.

Cells expressing P-gp were incubated with fluorescent substrate and either a P-gp inhibitor, GF 120918, to measure full accumulation of substrate or DMSO to measure possible transport of substrate. Both Kink mutations resulted in severely decreased transport with KinkA having some ability to transport substrates while KinkG had almost no ability to transport substrates. The P-gp

KinkA mutation show similar decrease in activity for all substrates. Calcein-AM, rhodamine 123, and BD-verapamil were all transported between 50 – 60% of WT while BD-prazosin, DiOC2, and LDS 751 were <25% of WT. All substrates were not transported by P-gp KinkG except DiOC2 which significantly had similar %WT transport, 16.2 ± 4.7 %WT, to P-gp KinkA, 14.9 ± 3.7 %WT (Figure 3.3).

Single mutations were made for each residue in the kink region of TMH 12 to confirm that a single mutation was not the cause of the dramatic loss of activity: P996G, D997A, Y998A, and K1000A were subcloned (Table 3.3). P996 was mutated to glycine to determine if increased flexibility at the pro position would affect activity as previous work has shown that the P996A mutation does not decrease ATPase activity or substrate transport.[8] P996G, D997A, and K1000A did not show significant decreases in transport of any of the tested substrates relative to WT transport. There were significant decreases in transport of calcein-am, BD-verapamil, BD-prazosin, DiOC2, and LDS 751 for the Y998A mutation. However, comparing the profile of decreases in substrate transport does not match the decreases observed in either KinkA or KinkG transport. This is most obvious with no decrease in transport of rhodamine 123, 98.8 ± 2.8 %WT for Y998A, showing that other factors, such as the flexibility of the helix, are the cause of decreased transport seen in the kink mutations (Figure 3.3 and Table 4.2).

Surface expression was measured for both mutations relative to maximal WT surface expression with the UIC2 monoclonal antibody. UIC2 recognizes 3 of the 4 extracellular loops of P-gp while the structure is in an outward facing conformation and is a conformationally dependent antibody. Both P-gp KinkA and P-gp KinkG had significantly decreased surface expression at 12.7 ± 3.1 %WT and 7.6 ± 4.0 %WT respectively (Figure 3.4). Even with significantly reduced surface expression in P-gp Kink mutations results can still be considered significant as data has shown that surface expression above some undetermined minimal amount is enough to convey full transport over the temporal duration of the experiment as shown with reduced surface expression of WT P-gp in reduced surface expression experiments (Chapter 2). Comparing surface of single mutations in the kink region reveals that a Y998 mutation likely causes the significant loss of expression as Y998A is expressed at 10.6 ± 0.4 %WT (Figure 3.5). Reduced expression is also observed with mutations at positions P996, D997, and K1000 though mutations at these residues did not reduce expression to the same levels as Y998A.

3.4 Discussion

Both mutations in TMH 12 were designed to alter the flexibility present in the helix as seen in comparisons between multiple x-ray structures of P-gp where the helix is observed to make substantial changes in its orientation. Mutations were placed in a conserved region of TMH 12 that potentially acts like a hinge in the reordering of the structure at it samples different conformations through its transport cycle. Introduction of a series of alanine should stiffen the helix making it more ordered which should match conformations of TMH 12 seen in outward facing structures. A more ordered helix likely helps with signal transduction between the TMDs and the NBDs that have been significantly hypothesized in the field of P-gp research.[26] Introduction of a series of glycine should be much more flexible as there are many more acceptable phi-psi angles that glycine can adopt which is why it is not often seen in α-helices. A less ordered and flexible helix likely cannot significantly be involved in signal transduction and potentially would have difficulty in being part of the process in NBD dimerization after substrate binding. Recently solved cryo-EM structures of inhibitor bound human P-gp have revealed that TMH 12 likely occupies the drug binding pocket in the outward facing conformation which signifies that the unordered to ordered structure of TMH 12 from inward to outward facing is important for substrate efflux.[11,27] Again, this emphasizes that multiple mutations to glycine would have difficulty in becoming an ordered helix capable of displacing substrate and is one explanation why no observable transport was seen with the P-gp KinkG mutation.

We observed significant decreases in transport of fluorescent substrates relative to WT in P-gp KinkA, but this decrease was interestingly not even across all substrates. Initial thoughts were that mutations in TMH 12 being part of a substrate entry gate would affect all substrates in a similar way as they would interact with TMH 12 as the moved to the substrate binding pocket, but this was not the case. One possibility is substrates interact unevenly with the drug entry gates and favor one gate over the other. Substrates that interact more with the gate formed by TMH 4 and 6 are likely to be less affected by changes in TMH 12. A second possibility is that where substrates bind in the binding pocket induces NBD dimerization differently. Potentially one region of substrate binding may induce crosstalk between the TMDs and NBDs more significantly through TMH 12 than another helix thus substrates that bind that region will be transported less.

P-gp KinkA had significant reduction in surface expression but results of reduced surface expression experiments and Y998A results showing 10.6 ± 0.4 %WT surface expression suggests

the surface expression levels measured were enough to convey full transport of substrate. While P-gp Y998A mutations did not transport all substrates comparable to WT P-gp, rhodamine 123 was still transported at near 100 %WT demonstrating the ability of a low expressing P-gp mutant to transport substrate to the same ability of WT P-gp. Other mutations in the kink region, 996-1001, did not significantly impact the ability of the protein to transport substrate. This signifies that Y998 is not solely responsible for loss in transport ability. This confirms that changes in flexibility of TMH 12 in P-gp KinkA change how substrates are transported. In comparison, P-gp KinkG had surface expression that was not significantly above P-gp non-expressing cells, negative control, leading to the possibility that there is low to no expression of P-gp KinkG. However, since UIC2 is a conformationally dependent antibody it is possible that due to the increased flexibility of the P-gp KinkG mutation the protein does not adopt the correct conformation for UIC2 binding. Some significant transport of DiOC2 was measured at 16.2 ± 4.7 %WT suggesting that reduced sampling of outward facing conformations is a likely cause of the lack of transport seen with other substrates.

As such stiffening of TMH 12 by a series of alanine mutations significantly reduced transport of substrates in an uneven amount. Conformational changes in TMH 12 have been implicated in the efflux of substrates through movement to occupy the binding pocket. BD-prazosin, DiOC2, and LDS 751 relied more heavily on the more flexible nature of TMH 12 in WT P-gp to be transported than calcein-AM, rhodamine 123, and BD-verapamil which were more readily transported by P-gp KinkA in comparison. Increased flexibility and loss of the helix to adopt a ordered helix to fill the drug binding pocket could be the cause of loss of transport seen with P-gp KinkG, however since the mutant was poorly expressed it cannot be fully confirmed that loss of rigidity in TMH 12 was the cause of loss of transport.

3.5 Future Directions

DiOC2 was transported by a similar amount in both P-gp KinkA and KinkG. Since %WT expression was low for both mutations, ~3-15 %WT, and KinkG had little to no ability to transport other substrates, there might be another transport mechanism of P-gp that is showing minimal amounts of substrate transport for both mutations. One possibility could be that the full transport cycle does not need to be complete for substrate transport of DiOC2. This would be easy to test by making a catalytically inactive form of P-gp that is unable to hydrolyze ATP. A

glutamate immediately following the Walker A motif is responsible for ATP hydrolysis. Mutating E556 and E1201 to glutamine makes P-gp unable to hydrolyze ATP and unable to transport substrate. If P-gp E556Q/ E1201Q has no transport of DiOC2 relative to WT P-gp then P-gp KinkA and KinkG do indeed have some ability to transport DiOC2 that is independent of TMH 12 structure. However, if similar levels of transport of DiOC2 is observed then a small amount of DiOC2 is being transported by P-gp in a manner independent of the transport cycle which has not been observed before.

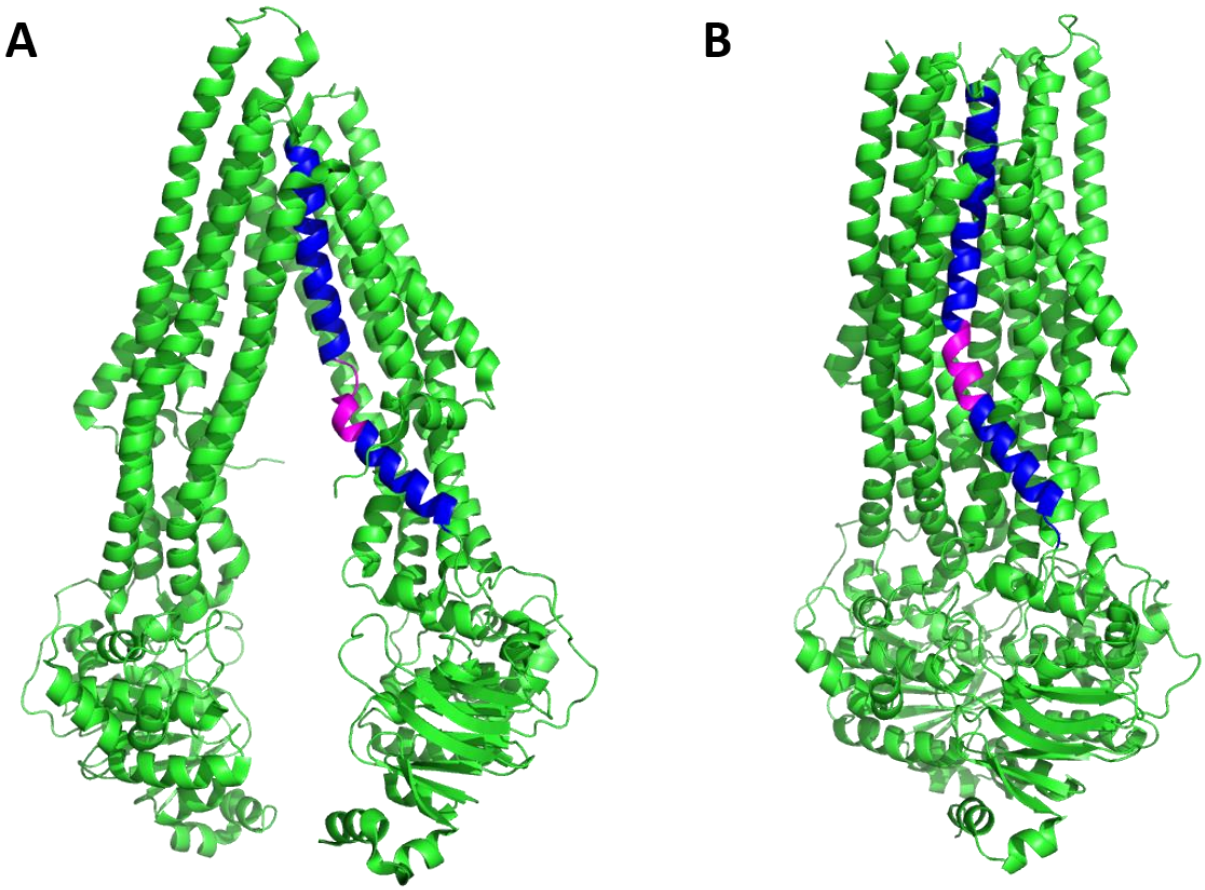

Figure 3.1: P-Glycoprotein TMH 12 is Kinked in an Open, Inward Facing Conformation and Ordered in a Closed, Outward Facing Conformation

In substrate free structures, P-gp TMH 12 contains an area that is unordered. (A) The open inward structure shows TMH 12 (blue) with a conserved sequence (magenta) that is unordered and breaks the α-helix. (B) The closed outward structure shows TMH 12 with the conserved sequence that is ordered completing the backbone H-bonding structure of the helix. PDB: 5KPI (A) and 6C0V (B)

Table 3.1: Sequence Alignment of P-Glycoprotein from Different Species to Find Conserved Sequences in TMH 12.

Species		Sequence Alignment	
H. sapien	968	LM--SFEDVLLVFSAVVFGAMAVGQVSSFAPDYAKAKISAAHIIMIIEKTPLIDSYSTEG	1025
M. mulatta	971	LM--SFEDVLLVFSAVVFGAMAVGQVSSFAPDYAKAKVSAAHIIMIIEKTPLIDSYSTEG	1028
M. fascicularis	971	LM--SFEDVLLVFSAVVFGAMAVGQVSSFAPDYAKAKVSAAHIIMIIEKTPLIDSYSTEG	1028
M. musculus	964	LM--TFENVLLVFSAIVFGAMAVGQVSSFAPDYAKATVSASHIIRIIEKTPEIDSYSTQG	1021
R. norvegicus	960	LM--TFENVLLVFSAIVFGAMAVGQVSSFAPDYAKAKVSASHIIRIIEKIPEIDSYSTEG	1017
C. griseus	961	LM--TFENVLLVFSAIVFGAMAVGQVSSFAPDYAKAKVSASHIIMIIEKVPSIDSYSTGG	1022
G. gallus	976	HI--EYKTVFLVFSAVVFGAMALGQTSSFAPDYAKAKISAAHLFVLFNRVPPIDSYREDG	1033
C. elegans	1009	PPTMQPMRVLRVMYAITISTSTLGFATSYFPEYAKATFAGGIIFGMLRKISKIDSLSLAG	1068

Eight species were aligned using Clustal Omega to determine conserved sequences in the TMDs of P-gp: *H. sapien* (Human), *M. mulata* (Rhesus macaque), *M. fascicularis* (Crab-eating macaque), *M. musculus* (House mouse), *R. norvegicus* (Brown rat), *C. griseus* (Chinese hamster), *G. gallus* (Red junglefowl), and *C. elegans* (Roundworm). While the sequences were similar among closely related species, only a single motif in TMH 12 was conserved in all eight. A PDYAKA motif was observed with the only synonymous difference occurring between Asp and Glu in the *C. elegans* sequence.

Table 3.2: Mutagenesis Primers for Crosslinking and Kink Mutations

Name	**Primer**
MDR L531C	5'-AGGGGCCCAGTGCAGTGGTGGGC-3'
MDR L531C R	5'-CTCTCTCCAACCAGGGTGTCAAATTTATGAG-3'
MDR A1074C	5'-CAGCAGTGGCTGTGGGAAGAGCACAGTGG-3'
MDR A1074C R	5'-CCCACCAGAGCCAGCGTC-3'
MDR 996-1001A	5'-TGCCGCAGCCAAAATATCAGCAGCC-3'
MDR 996-1001A R	5'-GCGGCAGCAGCAAATGAACTGACTTGC-3'
MDR 996-1001G	5'-GGCGGAGGCAAAATATCAGCAGCCCAC-3'
MDR 996-1001G R	5'-ACCGCCACCAGCAAATGAACTGACTTG-3'
MDR P996A	5'-TTCATTTGCTGCTGACTATGCCAAAGC-3'
MDR P996G	5'-TTCATTTGCTGGTGACTATGCCAAAGCCAAAATATCAGCAG-3'
MDR P996A or G R	5'-CTGACTTGCCCCACGGCC-3'
MDR D997A	5'-ATTTGCTCCTGCCTATGCCAAAG-3'
MDR D997A R	5'-GAACTGACTTGCCCCACG-3'
MDR Y998A	5'-TGCTCCTGACGCTGCCAAAGCCAAAATATC-3'
MDR Y998A R	5'-AATGAACTGACTTGCCCC-3'
MDR K1000A	5'-TGACTATGCCGCAGCCAAAATATC-3'
MDR K1000A R	5'-GGAGCAAATGAACTGACTTG-3'

Primers were designed as end to end primers for use in a Q5® mutagenesis kit. Sequences align with cDNA for the WT MDR gene.

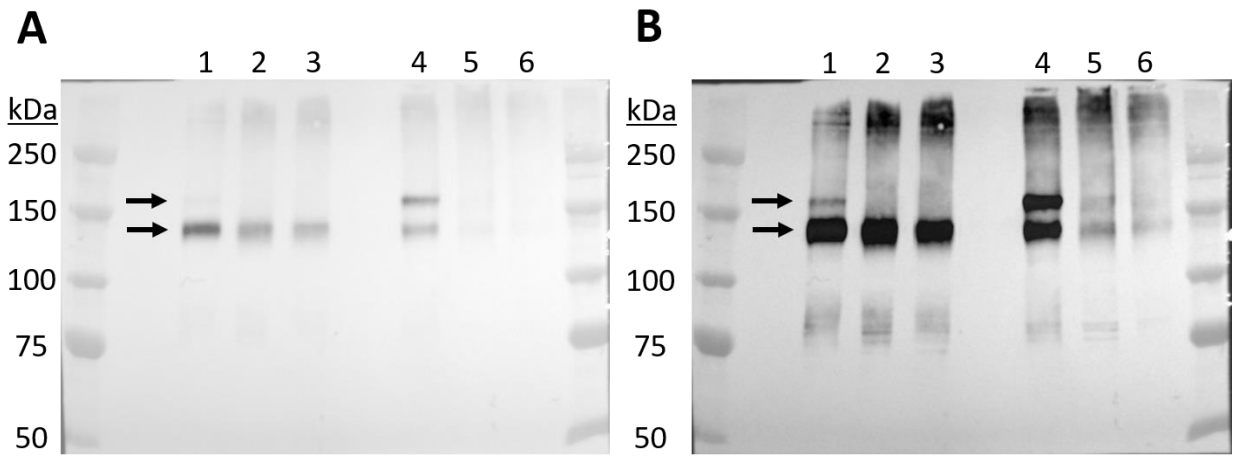

Figure 3.2: Immunoblot of Crosslinked NBDs of P-gp Show P-gp Kink Mutations Have Less Dimerization of their NBDs

Crosslinking was performed in mutant CL P-gp containing opposing L531C and 1074C cysteines that can be crosslinked with copper phenanthroline when NBDs dimerize which will migrate slower in SDS-PAGE and is indicated with the top arrow. The bottom arrow corresponds to un-crosslinked P-gp. Lane 1-3 are un-crosslinked, and Lane 1 contains 2.5 µg CL P-gp L531C/1074C (control), Lane 2 contains 2.5 µg CL P-gp L531C/1074C KinkA, and Lane 3 contains 2.5 µg CL P-gp L531C/1074C KinkG. Lane 4-6 are crosslinked, and Lane 4 contains 2.5 µg CL P-gp L531C/1074C, Lane 5 contains 5 µg CL P-gp L531C/1074C KinkA, and Lane 6 contains 5 µg CL P-gp L531C/1074C KinkG. More total protein is loaded for the kink mutations as the crosslinked bands tend to be very faint. 1:4000 C219 was used to label P-gp and 1:8000 α-mouse-HRP was used for detection with chemiluminescence. A is normally exposed and an increased amount of crosslinked P-gp is observed for the control lane 4. (B) Overexposure is required to observe crosslinking in Lanes 5 and 6 where is can be seen that for both Kink mutations less crosslinking is observed relative to the Lane 4 control.

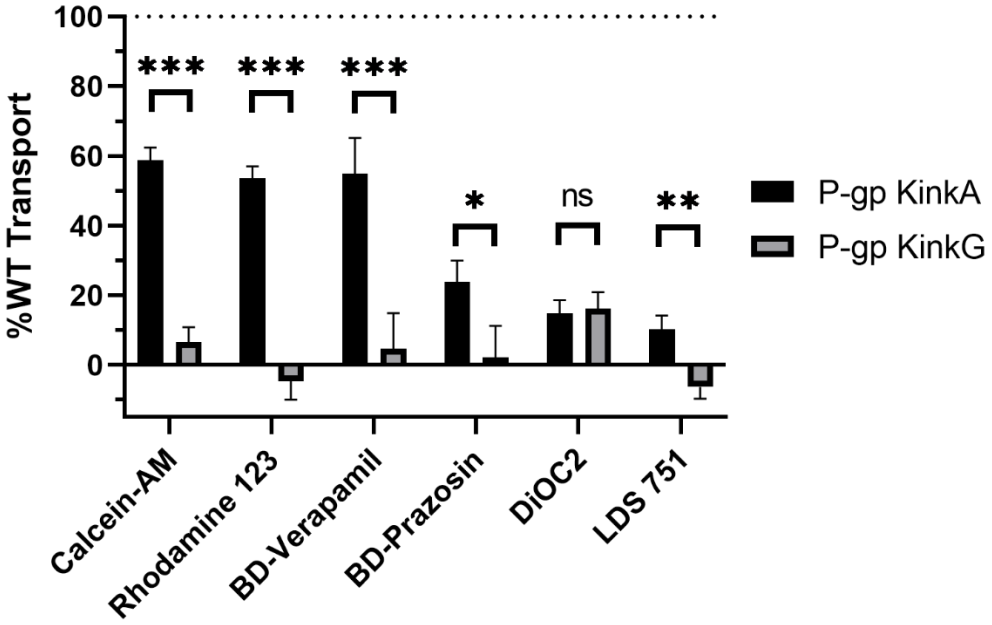

Figure 3.3: %WT Transport of Fluorescent Substrates by P-Glycoprotein KinkA and KinkG

Transport of fluorescent substrate by P-gp KinkA and P-gp KinkG was measured against transport by WT P-gp. Substrates were incubated with P-gp expressing cells at 0.5 µM (rhodamine 123, BD-verapamil, BD-prazosin, LDS 751) except for calcein-AM (0.0625 µM) and DiOC2 (0.125 µM) in the presence or absence of P-gp inhibitor GF120918. MFI data was collected and normalized before comparison with WT P-gp to determine %WT transport. P-gp KinkA transported calcein-AM at 58.7 ± 3.7 %WT, rhodamine 123 at 53.6 ± 3.4 %WT, BD-Verapamil at 54.9 ± 10.3 %WT, BD-prazosin at 23.9 ± 6.1 %WT, DiOC2 at 14.9 ± 3.7 %WT, and LDS 751 at 10.2 ± 4.0 %WT. P-gp KinkG transported calcein-AM at 6.6 ± 4.2 %WT, rhodamine 123 at -4.7 ± 5.3 %WT, BD-Verapamil at 4.6 ± 10.3 %WT, BD-prazosin at 2.2 ± 9.0 %WT, DiOC2 at 16.2 ± 4.7 %WT, and LDS 751 at -6.3 ± 3.4 %WT. *** $p < 0.0001$, ** $p < 0.005$, * $p < 0.05$, ns not significant.

Table 3.3: Transport of Fluorescent Substrates by Single Mutations in the Kink Region of Transmembrane Helix 12

Substrate	**%WT P-gp Transport Normalized**				
	F994A	**P996G**	**D997A**	**Y998A**	**K1000A**
Calcein-AM	98.4 ± 0.7	100.8 ± 1.3	92.6 ± 3.3	72.5 ± 1.7	100.3 ± 7.7
Rhodamine 123	98.0 ± 1.1	96.6 ± 3.1	98.1 ± 1.2	98.8 ± 2.7	99.4 ± 3.5
BD-Verapamil	70.4 ± 6.8	100.3 ± 4.2	102.7 ± 0.7	83.1 ± 2.7	92.5 ± 7.2
BD-Prazsosin	90.0 ± 4.0	102.2 ± 7.1	99.3 ± 7.2	45.8 ± 5.0	106.7 ± 11.2
DiOC2	99.6 ± 2.0	97.2 ± 2.8	99.9 ± 7.2	84.9 ± 3.9	104.8 ± 6.2
LDS 751	87.9 ± 1.9	103.2 ± 2.1	107.5 ± 4.5	74.1 ± 5.0	101.5 ± 9.2

Transport of fluorescent substrate by single mutations in the kink region was measured against transport by WT P-gp. Substrates were incubated with P-gp expressing cells at 0.5 µM (rhodamine 123, BD-verapamil, BD-prazosin, LDS 751) except for calcein-AM (0.0625 µM) and DiOC2 (0.125 µM) in the presence or absence of P-gp inhibitor GF120918. MFI data was collected and normalized before comparison with WT P-gp to determine %WT transport. Error is reported as standard deviations.

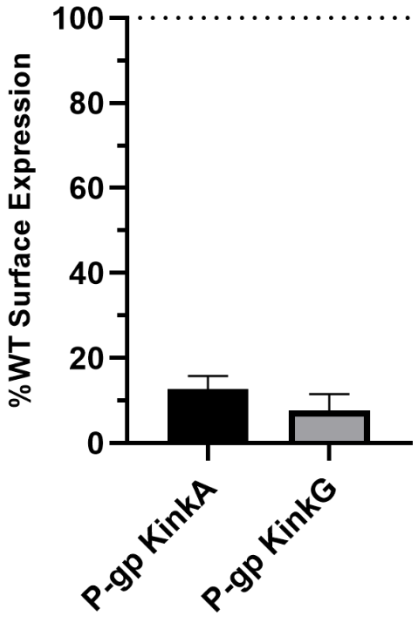

Figure 3.4: Surface Expression of KinkA and KinkG Variants are Significantly Reduced from WT P-Glycoprotein Expression

Surface expression of KinkA and KinkG mutations are significantly reduced from WT P-gp expression Surface expression was measured using UIC2 monoclonal antibody and a secondary FITC antibody. Expression for P-gp KinkA was reduced to 12.7 ± 3.1 %WT and P-gp KinkG was reduced to 7.6 ± 4.0 %WT. Though both mutants had significant decreases in expression it has been shown that low levels of expression do not significantly reduce transport ability at these levels which has been confirmed with reduced expression of WT P-gp experiments as well as cellular accumulation experiments performed with P-gp Y998A which has similar levels of expression to the KinkA mutation but has similar levels of transport of rhodamine 123 compared to WT P-gp with high levels of relative expression.

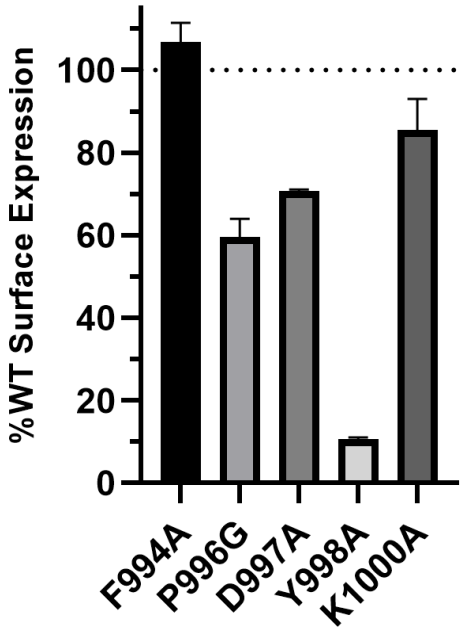

Figure 3.5: UIC2 Labeled Cell Surface Expression of TMH 12 Kink Single Mutations

Single mutations of the mutated kink residues were expressed, and their cell surface expression was measured relative to control WT expression to determine effects of single mutations on changes in surface expression of the TMH 12 kink mutations. F994A was measured at 106.7 ± 4.7 %WT, P996G at 59.6 ± 4.4 %WT, D997A at 70.7 ± 0.4 %WT, Y998A at 10.6 ± 0.4 %WT, and K1000A at 85.4 ± 7.6 %WT.

3.6 References

1. Dean, M., Hamon, Y. & Chimini, G. The human ATP-binding cassette (ABC) transporter superfamily. *J. Lipid Res.* **42**, 1007–1017 (2001).

2. Leipe, D. D., Koonin, E. V. & Aravind, L. Evolution and classification of P-loop kinases and related proteins. *J. Mol. Biol.* **333**, 781–815 (2003).

3. Chang, G. Multidrug resistance ABC transporters. *FEBS Lett.* **555**, 102–105 (2003).

4. Linton, K. J. Structure and Function of ABC Transporters. *Physiology* **22**, 122–130 (2007).

5. Loo, T. W. & Clarke, D. M. Do drug substrates enter the common drug-binding pocket of P-glycoprotein through "gates"? *Biochem. Biophys. Res. Commun.* **329**, 419–422 (2005).

6. Li, J., Jaimes, K. F. & Aller, S. G. Refined structures of mouse P-glycoprotein. *Protein Sci.* **23**, 34–46 (2014).

7. Chufan, E. E. *et al.* Multiple Transport-Active Binding Sites Are Available for a Single Substrate on Human P-Glycoprotein (ABCB1). *PLOS ONE* **8**, e82463 (2013).

8. Loo, T. W. & Clarke, D. M. Functional consequences of proline mutations in the predicted transmembrane domain of P-glycoprotein. *J. Biol. Chem.* **268**, 3143–3149 (1993).

9. Esser, L. *et al.* Structures of the Multidrug Transporter P-glycoprotein Reveal Asymmetric ATP Binding and the Mechanism of Polyspecificity. *J. Biol. Chem.* **292**, 446–461 (2017).

10. Loo, T. W. & Clarke, D. M. Drug-stimulated ATPase Activity of Human P-glycoprotein Requires Movement between Transmembrane Segments 6 and 12. *J. Biol. Chem.* **272**, 20986–20989 (1997).

11. Bonito, C. A. *et al.* Theoretical insights on helix repacking as the origin of P-glycoprotein promiscuity. *Sci. Rep.* **10**, 9823 (2020).

12. Mittra, R. *et al.* Location of contact residues in pharmacologically distinct drug binding sites on P-glycoprotein. *Biochem. Pharmacol.* **123**, 19–28 (2017).

13. Shapiro, A. B., Fox, K., Lam, P. & Ling, V. Stimulation of P-glycoprotein-mediated drug transport by prazosin and progesterone. *Eur. J. Biochem.* **259**, 841–850 (1999).

14. Martin, C. *et al.* Communication between Multiple Drug Binding Sites on P-glycoprotein. *Mol. Pharmacol.* **58**, 624–632 (2000).

15. Shapiro, A. B. & Ling, V. Effect of quercetin on hoechst 33342 transport by purified and reconstituted p-glycoprotein. *Biochem. Pharmacol.* **53**, 587–596 (1997).

16. Pace, C. N. & Scholtz, J. M. A helix propensity scale based on experimental studies of peptides and proteins. *Biophys. J.* **75**, 422–427 (1998).

17. Fuerst, T. R., Niles, E. G., Studier, F. W. & Moss, B. Eukaryotic transient-expression system based on recombinant vaccinia virus that synthesizes bacteriophage T7 RNA polymerase. *Proc. Natl. Acad. Sci. U. S. A.* **83**, 8122–8126 (1986).

18. Gey, G. O., Bang, F. B. & Gey, M. K. Responses of a Variety of Normal and Malignant Cells to Continuous Cultivation, and Some Practical Applications of These Responses to Problems in the Biology of Disease. *Ann. N. Y. Acad. Sci.* **58**, 976–999 (1954).

19. Drews, M., Paalme, T. & Vilu, R. The growth and nutrient utilization of the insect cell line Spodoptera frugiperda Sf9 in batch and continuous culture. *J. Biotechnol.* **40**, 187–198 (1995).

20. Mao, Q. & Scarborough, G. A. Purification of functional human P-glycoprotein expressed in Saccharomyces cerevisiae. *Biochim. Biophys. Acta BBA - Biomembr.* **1327**, 107–118 (1997).

21. Emmert, D. *et al.* Reversible Dimers of the Atypical Antipsychotic Quetiapine Inhibit P-Glycoprotein-Mediated Efflux in Vitro with Increased Binding Affinity and in Situ at the Blood-Brain Barrier. *ACS Chem. Neurosci.* **5**, 305–317 (2014).

22. Bradford, M. M. A rapid and sensitive method for the quantitation of microgram quantities of protein utilizing the principle of protein-dye binding. *Anal. Biochem.* **72**, 248–254 (1976).

23. Ramachandra, M., Ambudkar, S. V., Gottesman, M. M., Pastan, I. & Hrycyna, C. A. Functional characterization of a glycine 185-to-valine substitution in human P-glycoprotein by using a vaccinia-based transient expression system. *Mol. Biol. Cell* **7**, 1485–1498 (1996).

24. Hrycyna, C. A., Ramachandra, M., Pastan, I. & Gottesman, M. M. Functional Expression of Human P-Glycoprotein from Plasmids using Vaccinia Virus-Bacteriophage T7 RNA Polymerase System. *Methods Enzymol.* **292**, 456–473 (1998).

25. Loo, T. W., Bartlett, M. C. & Clarke, D. M. The "LSGGQ" Motif in Each Nucleotide-binding Domain of Human P-glycoprotein Is Adjacent to the Opposing Walker A Sequence. *J. Biol. Chem.* **277**, 41303–41306 (2002).

26. Verhalen, B. *et al.* Energy transduction and alternating access of the mammalian ABC transporter P-glycoprotein. *Nature* **543**, 738–741 (2017).

27. Nosol, K. *et al.* Cryo-EM structures reveal distinct mechanisms of inhibition of the human multidrug transporter ABCB1. *Proc. Natl. Acad. Sci.* **117**, 26245–26253 (2020).

CHAPTER 4. AROMATIC RESIDUES ON AND NEAR TRANSMEMBRANE HELIX 12 OF HUMAN P-GLYCOPROTEIN INTERACT WITH SUBSTRATES AT A PRE-BINDING SITE AT THE PROTEIN LIPID INTERFACE

4.1 Introduction

Crystallographic data have identified portals on either side of P-glycoprotein in the inward facing conformation that are proposed to allow for substrate and inhibitor entry to the drug binding pocket from the plasma membrane of cells.[1,2] TM helices 4 and 6 and TM helices 10 and 12 make up these drug entry portals as observed in various crystal structures of P-gp from *C. elegans*, mouse, and human homologues.[3] Many residues have been identified as part of the drug binding pocket, which has expanded from canonical R and H binding sites to a large hydrophobic pocket that spans roughly 6000 Å^3.[4–7] Many crystal structures and biochemical data have investigated which residues in P-gp interact with various structurally and chemically different molecules that have been identified as substrates of P-gp and have identified the drug binding pocket primarily composing of residues near the apex of the two TMDs.[3,8] NMR studies with lipids and substrates has shown that many substrates have a high affinity for the interface region of lipids and lipid membranes.[9] Drug entry portals in the inward facing structure of P-gp confirm that substrates can enter from the inner leaflet, but there is no space for substrate entry at the outer leaflet.[1] The exact transduction pathway for how substrates enter the drug binding pocket from the inner leaflet and which residues substrates interact with along that pathway has not been fully elucidated as little research has been done in pre-binding events that occur before substrate binding.

Prebinding events would be consistent with substrates interacting with residues and secondary structures on P-gp before directly binding to the drug binding site. Recent cryo-EM structures of ATP occluded human P-gp shows an access tunnel extending from the drug binding pocket to an area adjacent and formed partially by TMH 12 near the inner leaflet interface region of the plasma membrane (Figure 4.1 B).[10] While the portal to the tunnel is too small for substrates to enter in the occluded state, it gives insight to a potential pathway substrate may follow when moving to the binding pocket. P-gp samples many conformational states during drug binding as seen in multiple various NBD separated structures of *m*P-gp and other human homologues.[11] As pre-occluded states are sampled, the access tunnel may begin to be formed providing a pathway

for substrates to be transposed from the inner leaflet to the substrate binding pocket before large conformational changes expose substrate to extracellular space at which point substrate becomes solvent exposed and has a reduced affinity for P-gp in the new conformation.[12]

Recently a crystal structure of P-gp has been solved that shows QZ-Val, a cyclic peptide, bound to the exterior of P-gp at the inner leaflet-protein interface (Figure 4.1 A).[13] This cyclic peptide was shown to make significant contact with residues on TMH 12 and elbow helix (EH) 2. There are two elbow helices that are present on the C-terminal side of each homologous half that sit directly at the cytosolic interface region of the plasma membrane. Bound cyclic peptide observed on the exterior of P-gp was shown to interact with TMHs 9 and 12 and EH 2 which formed a surface facing away from P-gp with which substrates could potentially bind. Residues F994 and Y998 (TMH 12) and W698 (EH 2) were identified to be within close contact with the cyclic peptide. This observation is in conjunction with observed lower affinity vs higher affinity "On-sites" within a bacterial P-gp homolog using electron paramagnetic resonance where the lower affinity on-site potentially correlates to a prebinding or recognition site for substrates of P-gp.[14,15]

Aromatic residues in the binding site of P-gp have been shown to be significant in substrate binding through mutagenesis.[16] Many substrates of P-gp tend to be relatively hydrophobic or have regions of high hydrophobicity for drugability purposes leading to the importance of hydrophobic interactions with the drug binding pocket.[17] Residues facing the substrate binding pocket in inward facing crystal structures tend to be more hydrophobic and aromatic, and are shown to interact with substrates in substrate bound crystal structures.[1,18] The propensity of substrates and inhibitors to interact with hydrophobic and aromatic residues in crystallographic data suggest that hydrophobic and aromatic residues are good candidates for study. Thus, particular interest was put towards studying F994 and Y998 on TMH 12 and W698 and the adjacent phenylalanine, F697, on EH 2. Adjacent TMH 9 that also forms this surface was not investigated here as residues on this helix are primarily small and hydrophobic only lending dispersion forces for substrate interactions. Mutagenesis of these residues to alanine was performed and the resulting proteins were utilized in cellular accumulation assays of fluorescent substrates to elucidate the importance of exterior residues as a potential prebinding or pre-recognition site for substrates and inhibitors at the protein-lipid interface region of P-gp. Mutagenesis revealed significant changes in transport relative to WT at position Y998 with smaller changes in transport for some substrates at F994 and F697.

Interestingly not all substrates were affected similarly by mutagenesis leading to the possibility of some substrates requiring interaction with certain residues to achieve full WT transport.

4.2 Materials and Methods

4.2.1 Materials

All oligonucleotides were designed in-house and purchased from Integrated DNA Technologies (Coralville, IA). HeLa adenocarcinoma epithelial cells were purchased from ATCC (Manassas, VA). Dulbecco's Modified Eagle Medium (DMEM) with 4.5 g/L glucose and phenol red, penicillin/streptomycin, and phosphate buffer saline (PBS) were purchased from Corning Inc. (Corning, NY). Lipofectin™ transfection reagent, Opti-MEM™ reduced serum media with no phenol red, Calcein-AM, Rhodamine 123, UIC2 monoclonal ABCB1 antibody, and LDS 751 were purchased from ThermoFisher Scientific (Waltham, MA). Fetal Bovine Serum (FBS) and Newborn Calf Serum (NCS) were purchased from R&D Systems (Minneapolis, MN). Q5® site-directed mutagenesis kit was purchased from New England Biolabs Inc. (Ipswich, MA). Subcloning Efficiency™ DH5α Competent Cells were purchased from Invitrogen™ (Carlsbad, CA). vTF7-3, Vaccinia Virus with the T7 RNA Polymerase reporter gene, was obtained through the NIH AIDS Reagent Program, Division of AIDS, NIAID, NIH: vTF7-3 from Dr. Tom Fuerst and Dr. Bernard Moss.[9] Basal Medium Eagle with Earle's salts and L-glutamine, ammonium persulfate, and GF 120918 (Elacridar) were purchased from Sigma-Aldrich (St. Louis, MO). Bodipy(BD)-FL-Verapamil, BD-FL-Prazosin, and 3,3'-diethyloxacarbocyanine iodide ($DiOC_2$) were purchased from Setareh Biotech (Eugene, OR). GlutaMAX™ supplement and TrypLE™ Express Enzyme with phenol red were purchased from Gibco™ (Grans Island, NY). MRK16 was a kind gift from Dr. Michael M. Gottesman (National Cancer Institute, NIH, Bethesda, MD). Mouse IgG_{2a} κ isotype control and FITC-α-mouse antibodies were purchased from BD Biosciences (San Jose, Ca). All other common chemicals and solvents were purchased from either ThermoFisher Scientific or Sigma-Aldrich.

4.2.2 HeLa Cell Culture and Expression of P-Glycoprotein using a Vaccinia Virus Expression System

HeLa cells in monolayer were maintained at 37° C in a 5% CO_2 environment and continuously cultured in DMEM containing 2 mM L-glutamine, 10 % fetal bovine serum, 50 units/mL of penicillin and 50 µg/mL streptomycin.[20]

pTM1-MDR was obtained from a previously described preparation.[21] Importantly, the MDR1 gene is inserted at the 3' end of the encephalomyocarditis virus internal ribosome entry site (IRES) and is further preceded by a T7 promoter region in the pTM1 vector. Subsequent mutations were constructed using a Q5® mutagenesis kit for site directed mutagenesis and introduction of one or many amino acid mutations. P-gp was then expressed in HeLa cells using a modified Vaccinia virus expression system as previously described.[22] HeLa cells were cultured to be in mid-log phase (70 – 80% confluency) at the time of transfection/ infection. For T-75 culture flasks, HeLa cells were seeded at 1.5 x 10^6 cells 20-24 hours before the beginning of transfection/ infection to reach the desired confluency. Transfection solution was prepared 30 minutes prior to infection through the addition of 9 µg of pTM1-MDR construct with 27 µL of Lipofectin™ (1 mg/mL), a ratio of 1:3 DNA to transfection reagent, in 3mL of opti-MEM in a polystyrene conical tube. Polystyrene is desired over polypropylene as the DNA-lipid complex can interact with the plastic and reduce the amount of DNA-lipid mixture in solution. A modified Vaccinia virus expressing T7 RNA polymerase, vTF7-3, was added to 1 mL opti-MEM per T-75 flasks to the desired multiplicity of infection (MOI) of 5. Cells were washed once with PBS before the transfection solution and vTF7-3 solution were added to the culture flask and then incubated at 37° C in 5% CO_2. Complete medium was added to the flasks up to the normal working volume of 12 mL 3 hours post-transfection/ infection. Cells were incubated at 37° C in 5% CO_2 for a total of 10 hours before being washed with PBS and detached with TrypLE™ and collected with PBS. Cells were then used for P-gp surface expression or cellular accumulation assays.

4.2.3 Surface Expression and Cellular Accumulation of Fluorescent Substrates by Flow Cytometry

P-gp expressing HeLa cells from the Vaccinia virus expression system were collected and counted. Cells were resuspended in BME (1% BME powder, 7.5% (w/v) $NaHCO_4$, 5% NCS, pH 7.4, filter sterilized (0.22 µm filter)) at a concentration of 2.5 x 10^5 cells per sample. For cell

surface expression 2.5 x10^5 cells were incubated in BME with 1.5 µg of either the Mrk16 or UIC2 antibody to measure surface expression of P-gp or with 3 µg of IgG_{2a} kappa isotype antibody as a negative control. Samples were incubated at 37° C for 30 minutes before being spun at 500 xg and the supernatant removed. Pelleted cells were then incubated with 2.5 µg of FITC conjugated α-mouse antibody for an additional 30 min before being spun at 500 xg, the supernatant removed, and pellets stored on ice. Samples were then resuspended in 400 µL PBS and run on a BD Accuri™ flow cytometer with a 20 mW 488 nm solid state blue excitation laser and data was collected on the FL1 detector (530/30 nm).

For cellular accumulation of fluorescent substrates 2.5 x 10^5 cells per sample were incubated with one of the following fluorescent substrates either in the presence of absence of 1µM GF 120198 which is an inhibitor of P-gp. Samples incubated with GF 120198 are P-gp inhibited, negative controls with high levels of basal fluorescent substrate accumulation while samples incubated without GF120198 show uninhibited P-gp activity on substrate efflux and lower levels of fluorescent substrate accumulation. Calcein-AM (0.0625 µM), rhodamine 123, BD-verapamil, BD-prazosin, DiOC2 (0.125 µM), and LDS751 were all incubated with cells in the presence or absence of GF 120198 at 0.5 µM, unless otherwise noted, for 30 minutes at 37° C except for calcein-AM which was incubated for 10 minutes at 37° C. All samples were spun at 500 xg to pellet the cells before a second incubation with BME again with or without GF 120198. Calcein-AM samples do not need a second incubation as (acetyloxy)methoxy groups are cleaved by nonspecific esterases and is no longer cell permeable. Samples are then resuspended in 400 µL PBS and data collected on a BD Accuri™ flow cytometer on the FL1 channel except for LDS751 which is collected on the FL3 channel (>670 nm).

Data were gated on forward scatter (FSC) and side scatter (SSC) based on pTM1 empty vector transfected/ infected HeLa cells. Mean fluorescent intensities (MFI) were measured by the BD Accuri™ software and normalized on the IgG_{2a} isotype control or GF 120198 control for each set of samples in each of the assays. Normalized data for mutant P-gp was then compared to wild-type (WT) P-gp to get a measure of %WT.

4.3 Results

To test for prebinding events near the substrate portal adjacent to TMH 12, WT P-gp was mutated to substitute aromatic residues known to interact with a cyclic peptide that bound the

exterior of the protein. These aromatic residues were mutated to alanine including F994 (TMH 12), Y998 (TMH12), and W698 (EH 2) along with the adjacent phenylalanine adjacent to W698 at position 697 that likely could also make prebinding interactions with substrates with slightly altered rotational conformation of EH 2. These mutations were made in pTM1 WT MDR for use in expression with the Vaccinia virus expression system in HeLa cells. Cellular accumulation of fluorescent substrates was measured with six structurally and chemically different molecules: calcein-AM, rhodamine 123, BD-verapamil, BD-prazosin, DiOC2, and LDS 751. The ability of P-gp variants to transport fluorescent substrates to reduce cellular accumulation was normalized to results from WT P-gp and reported as % WT. Cells expressing P-gp were incubated with fluorescent substrate and either a P-gp inhibitor, GF 120918, to measure full accumulation of substrate or DMSO to measure transport of fluorescent substrate.

The two EH 2 mutants, W698A and F697A, were tested for their ability to transport substrates (Table 4.2). While QZ-Val had potential interactions with W698 in a crystal structure W698A did not significantly affect transport of the tested substrates relative to WT P-gp. The greatest decrease in transport was seen with calcein-AM at 94.3 ± 0.4% which is not significantly reduced from full transport. Interestingly there was a slight increase in transport of BD-prazosin to 107.8 ± 1.8% relative to WT P-gp transport of the same substrate. F697A had a greater impact on transport than W698A. The largest decreases in activity with F697A were with BD-Verapamil and BD-prazosin which were decreased to 89.9± 4.4% and 89.3 ± 1.7% of WT transport. While the slight variances in transport could yield to the importance of substrate interactions in prebinding events with EH 2, changes in transport were not significant enough to conclude that aromatic residues play a large role in substrate prebinding events.

Mutation of aromatic residues on TMH 12 proved to be more significant in affecting transport of substrate (Table 4.2). There were moderate decreases in transport of BD-prazosin and LDS 751 at 90.0 ± 4.0% and 87.9 ± 1.9% of WT transport respectively in the F994A mutation. A more significant decrease in F994A transport was seen with BD-verapamil which decreased to 70.4 ± 6.8% of WT transport. The largest effects in transport for the most substrates came with the Y998A mutation. Transport was significantly decreased to 72.5 ± 1.7% for calcein-AM, 83.1 ± 2.7% for BD-verapamil, 45.8 ± 5.0% for BD-prazosin, 84.9 ± 3.9% for DiOC2, and 74.1 ± 5.0% for LDS 751 with the Y998A mutation. While Y998A had the greatest effect on most of the substrates there was no significant decrease in transport of rhodamine 123 relative to WT as

transport remained at 98.8 ± 2.7% which is not significantly different from cells expressing WT P-gp.

Finally, surface expression was measured for each of the mutants to determine if there were any significant changes relative to WT P-gp surface expression (Figure 4.2). UIC2 is a monoclonal antibody used to determine functional cell surface expression as it binds three extracellular loops of P-gp in a conformationally dependent manner.[23,24] F697A and W698A had reduced surface expression at 87.8 ± 2.3% and 74.6 ± 8.5% of WT P-gp surface expression. In contrast, F994A increased surface expression to 106.7 ± 4.7% WT P-gp surface expression. Y998A had significantly reduced surface expression of 10.6 ± 0.4% of WT surface expression. However, reduction in surface expression is not directly correlated to reduction of transport of fluorescent substrates as previously shown with reduced surface expression of WT P-gp (Chapter 2). Surface expression of WT P-gp was reduced to roughly 32% of full surface expression with no significant change in transport of either calcein-AM or rhodamine 123. Reduction in surface expression not resulting in reduction of transport ability can also be seen in the Y998A mutation as its surface expression is severely reduced relative to WT but was still able to transport rhodamine 123 at the same levels of WT P-gp.

4.4 Discussion

The substrate binding site of P-gp sits at the vertex of the TMDs towards the outer leaflet in the open inward conformation and studies have shown that substrate enters the substrate binding pocket from the inner leaflet of the plasma membrane. It follows that there must be some pathway that substrates follow in the process of substrate transport. Recently described crystal structures of P-gp in different conformations give some insight as to a possible pathway. First, a crystal structure of P-gp in an open conformation has shown that a cyclic peptide can interact with TMH 12 and EH 2 at the lipid-protein interface and provides insight to a potential pre binding site.[13] To study potential pre binding events, mutations of aromatic residues on TMH 12 and EH 2 were made and it was observed that some of these residues have a role in substrate prebinding events especially Y998. Mutating Y998 significantly reduced transport of several substrates signaling the importance of Y998 in interacting with these substrates at the protein lipid interface. Y998 is positioned facing outward in all solved structures of human P-gp near the interface region of the inner leaflet and has not been previously associated with substrate binding. This region forms a

potential surface for substrate prebinding with TMH 11, TMH 12, and EH 2. Interestingly not all substrates had reduced transport as rhodamine 123 was transported at similar levels to WT P-gp. This indicates that either substrates can bind this potential prebinding surface in many orientations and do not need to contact Y998 or that substrates could potentially have a preference for which portal they enter the substrate binding pocket through as the there is also a portal on the other homologous half of P-gp formed by TMHs 4 and 6.

There is further support that residues on TMH 12 and EH 2 are important in pre-binding events as there is an access tunnel to the binding pocket adjacent to TMH 12 and EH 2 that is formed in an occluded conformation of P-gp where the NBDs become dimerized and the binding pocket is occluded from further substrate binding.[10] The occluded structure of P-gp has been shown to bind substrate in the substrate binding pocket but has also shown inhibitors of P-gp binding into the access tunnel. Thus, we propose that pre-binding events help recognize substrate to increase interaction with the protein before following the access tunnel as P-gp undergoes conformational changes from an inward facing to occluded state. Though mutating residues on TMH 12 and EH 2 can reduce substrate recognition, transport remains relatively high either through random interactions of substrate with the protein or potential interaction of substrate with the other substrate entry portal. It is possible that pre-binding events at the lipid-protein interface mostly increase the rate of substrate transport but are likely not necessary for some minimal amount of transport due to random interactions of substrate with the protein which would eventually lead to a substrate bound state.

It is also interesting to note the severe decrease in surface expression of Y998 which was reduced to near 10% of WT P-gp while the other mutants were expressed much closer to WT P-gp surface expression. It has been shown that this decrease in surface expression is not correlated to a decrease in transport as seen with cellular accumulation assays with WT P-gp that is being fully expressed. Some evidence points to phosphorylation being an important factor in maturation and cell trafficking of P-gp specifically with Pim-1 kinase.[25] There is the possibility that Y998 may also be a potential site for phosphorylation though there is no current evidence that shows that Y998 is phosphorylated during maturation of the protein.

Y998A also had full transport of rhodamine 123 at its reduced surface expression. This can be interpreted as rhodamine 123 having no interaction with TMH 12 and EH 2 in its transport cycle with P-gp leading to either interaction with the other substrate portal between TMHs 4 and 6 or

altered binding near TMH 12 and EH 2. Substrates of P-gp have been shown to be able to bind the substrate binding pocket in multiple orientations, interacting with multiple different residues. A similar occurrence could be happening at these pre-binding sites as that would help with the promiscuity of the protein allowing for transport of many chemically and structurally different molecules.

In conclusion, reduction of transport observed with residues on TMH 12 and EH 2 supports the hypothesis that this region is important for pre-binding substrate recognition events at the lipid-protein interface of P-gp. Analysis of recent crystal structures supports substrates interacting with TMH 12 and EH 2 as seen with cyclic peptide bound P-gp.[13] An observed access tunnel in occluded structures of P-gp adjacent to TMH 12 also suggest a potential pathway that substrates can follow to access the drug binding pocket from a pre-binding pocket on TMH 12 and EH 2 during conformational changes in the transport cycle.[10] Finally, large conformational changes rearrange the TMDs so that the substrate binding pocket becomes solvent exposed and substrate is effluxed.[12] The significance of the data shown suggests substrate interaction at the lipid-protein interface of TMH 12 and EH 2. An inward facing conformation of P-gp, PDB: 5KPI, show F994 and F697 turned away from Y998 while an outward facing conformation, PDB: 6C0V, shows F994 and F697 oriented towards Y998 allowing for potential increased aromatic interactions with substrate. Thus, it is possible that there exists a pre-binding site in the outward facing conformation that stages substrate for the next catalytic transport cycle and changes in conformation towards inward facing, with the rearrangement of F994 and F697, facilitate substrate transduction towards the substrate binding pocket in a revised transport cycle (Figure 4.3). The data shown here brings new potential to understanding substrate interactions with P-gp at the lipid-protein interface and how substrate enters the substrate binding pocket from the inner leaflet of the plasma membrane which has yet to be investigated thoroughly within the field of P-gp.

4.5 Future Directions

P-gp has been shown to be phosphorylated at S661, S667, S671, and S683 but the function of this phosphorylation has not been elucidated.[26] Deletion mutations of these residues, which are in the linker region between NBD1 and TMD2, had no effect on surface expression and activity in cells transiently expressing deletion mutants of P-gp.[27] However, another kinase, Pim-1, that also phosphorylates at S683 decreases cell surface expression, glycosylation, and increase degradation

when inhibited in cells that are endogenously expressing P-gp.[25] Since there is some indication that phosphorylation is tied to P-gp maturation for cell surface expression then there is a possibility that Y998 may also be a residue important in phosphorylation and further posttranslational modifications. Structural significance versus posttranslational modification could be ruled out through mutagenesis of Y998F to determine if mutagenesis away from an aromatic residue was the cause for reduced surface expression. If Y998F is still observed to have reduced surface expression, then further studies into posttranslational modifications could be carried out to determine the significance of Y998 in P-gp maturation.

Additionally, the significance of prebinding sites near the portal formed by TMH 10 and 12 could also hold for the portal formed by TMH 4 and 6. There are several aromatic residues on TMH 6 and EH 1 that are in similar spatial positions to their counterparts studied here on TMH 12 and EH 2. F355 is positioned on TMH 6 at the same position Y998 is on TMH 12 and thus may have similar effects on substrate transport. Additionally, F193 and F194 on TMH 3 and F40 and Y42 on EH 1 may make significant contacts with substrates at a prebinding site formed by TMH 3 and 6 and EH 1 at the interface region of the inner leaflet. Determination of the significance of these residues near the portal formed by TMHs 4 and 6 would expand understanding of how substrates first interact and are recognized by P-gp. By extension, double and higher ordered mutations of aromatic residues can yield greater understanding of the cumulative effects of these residues and such high ordered mutations of aforementioned single mutations should be considered for future study. Photocrosslinking or other chemical methods of covalently modifying Y998 can also help directly elucidate the significance of Y998 in substrate pre-binding.

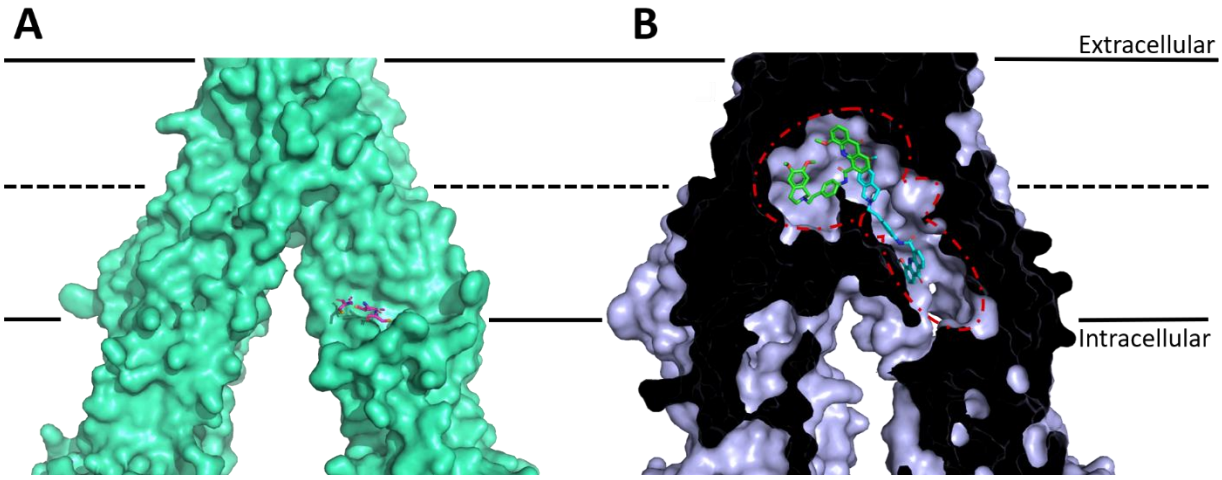

Figure 4.1: QZ-Val Bound P-Glycoprotein at the Lipid-Protein Interface and Elacridar Bound P-Glycoprotein at the Substrate Binding Pocket and Access Tunnel

Substrate bound structures of P-gp in the inward facing and occluded states show substrate pre-binding interactions and substrate interactions in the access tunnel to the substrate binding pocket. (A) A cyclic valine peptide (magenta) is shown bound to the lipid-protein interface of an inward facing structure of P-gp. The peptide is making significant contacts with residues on TMH 12 and EH 2. (B) Elacridar is shown to bind the substrate binding pocket (green) as well as an access tunnel (cyan) running from near TMH 12 to the substrate binding pocket simultaneously in an occluded conformation of P-gp. These structures suggest that there may be a transduction pathway from pre-binding with TMH 12 to the substrate binding pocket as P-gp undergoes conformational sampling during substrate binding. PDB: 4Q9J (A) and 7A6C (B)

Table 4.1: Mutagenesis Primers for alteration of Aromatic Residues on EH2 and TMH 12

Name	**Primer**
MDR F697	5'-TCCAGTTTCCGCTTGGAGGATTATG-3'
MDR F697 R	5'-GGTATACTTTCATCCAGAG-3'
MDR W698A	5'-AGTTTCCTTTGCGAGGATTATGAAGC-3'
MDR W698A R	5'-GGAGGTATACTTTCATCC-3'
MDR F994A	5'-AGTCAGTTCAGCTGCTCCTGACTATGCCAAAGCCAAAATATCAGC-3'
MDR F994A R	5'-TGCCCCACGGCCATGGCA-3'
MDR Y998A	5'-TGCTCCTGACGCTGCCAAAGCCAAAATATC-3'
MDR Y998A R	5'-AATGAACTGACTTGCCCC-3'

Primers were designed as end to end primers for use in a Q5® mutagenesis kit. Sequences align with cDNA for the WT MDR gene.

Table 4.2: Cellular Accumulation of Fluorescent Substrates with Various Aromatic Mutations in P-Glycoprotein TMH 12 and EH 2

Substrate	**%WT P-gp Transport Normalized**			
	F697A	**W698A**	**F994A**	**Y998A**
Calcein-AM	93.8 ± 2.3	94.3 ± 0.4	98.4 ± 0.7	72.5 ± 1.7
Rhodamine 123	95.0 ± 1.8	95.0 ± 2.1	98.0 ± 1.1	98.8 ± 2.7
BD-Verapamil	89.9 ± 4.4	95.5 ± 0.3	70.4 ± 6.8	83.1 ± 2.7
BD-Prazsosin	89.3 ± 1.7	107.8 ± 1.8	90.0 ± 4.0	45.8 ± 5.0
DiOC2	101.3 ± 3.2	98.9 ± 0.9	99.6 ± 2.0	84.9 ± 3.9
LDS 751	95.1 ± 1.3	99.6 ± 10.3	87.9 ± 1.9	74.1 ± 5.0

Cellular accumulation assays were performed to determine percent transport of WT P-gp with mutations on EH 2 of F697A and W698A and on TMH 12 at positions F994A and Y998A. Mutations were selected based on previously solved crystal structures were a cyclic peptide was shown to interact directly with these residues. Data was collected in triplicate using flow cytometry measuring mean fluorescence intensity on the FL1 or FL3 detectors. Data was then normalized and calculated as a percent of WT transport. Most significant changes occurred with the Y998A and F994A. Significant transport was determined to be a 10% decrease or more of WT transport.

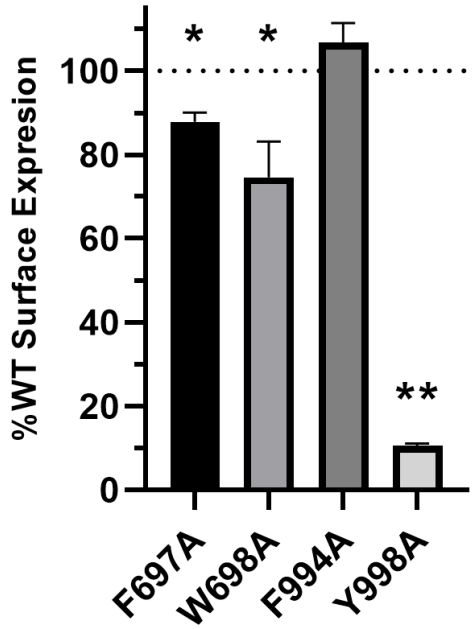

Figure 4.2: UIC2 Labeled Surface Expression of P-glycoprotein TMH 12 and EH 2 Aromatic Residues

Surface expression for aromatic mutants of P-gp were measured using the monoclonal antibody UIC2. UIC2 is a conformational antibody that recognizes three extracellular loops of P-gp in an outward facing conformation. Surface expression was normalized to expression of WT P-gp expressed simultaneously with aromatic mutants. F697A was expressed at 87.8 ± 2.3 %WT, W698A at 74.6 ± 8.5 %WT, F994A at 106.7 ± 4.7 %WT, and Y998A at 10.6 ± 0.4 %WT. F994A is not significantly different from 100 %WT expression while F697A, W698A, and Y998A are significantly different. * $p<0.01$ ** $p<0.0001$

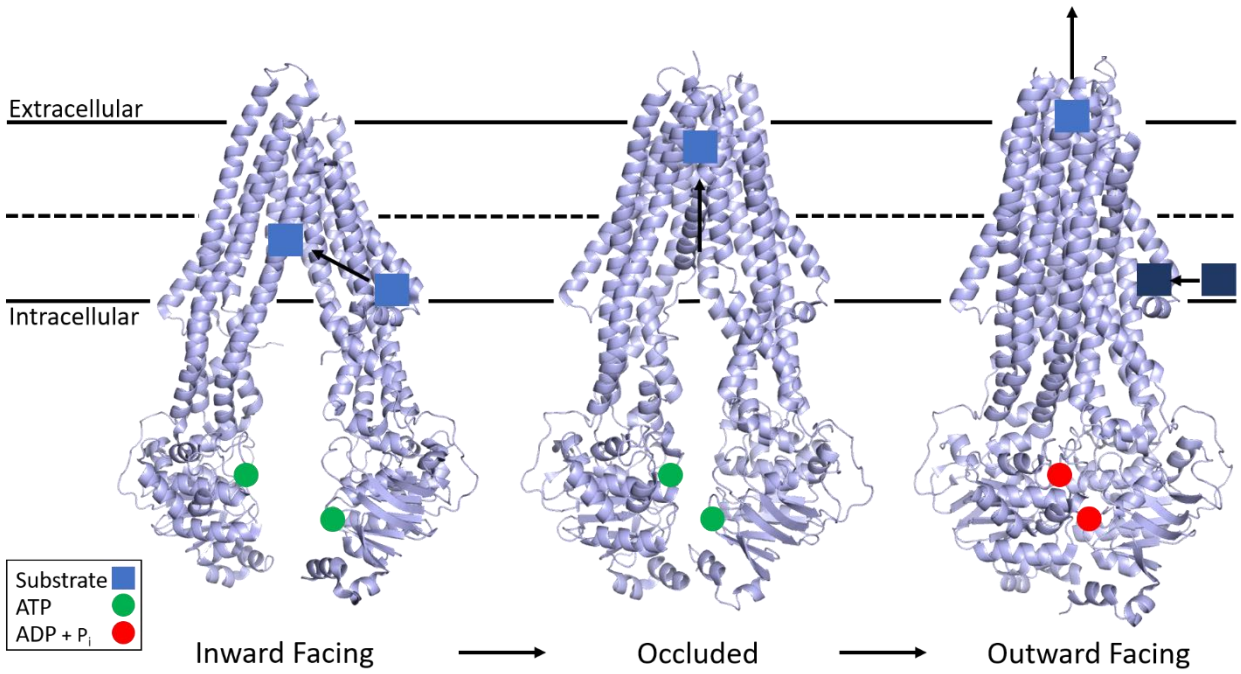

Figure 4.3: Revised Substrate Transduction Pathway Showing Staging of Second Substrate at the Protein-Lipid Interface of the Outward Facing Conformation

Substrate from the inner leaflet interacts with TMH 12 and EH 2 at the lipid-protein interface. Substrate can then occupy the substrate binding pocket at the apex of the IF structure. Large conformational changes by TMHs 4 and 10 then occlude the substrate binding pocket in an intermediate step. ATP hydrolysis drives large conformational changes in TMHs 4, 10, and 9 while TMH 12 reorders to occupy the substrate binding pocket to expose and efflux substrate into extracellular space. The orientation of residues at the protein-lipid interface then potentially allow for new substrate (navy) to be staged for the next catalytic transport cycle. PDB: 5KPI (inward), 7A6C (occluded), and 6C0V (outward)

4.6 References

1. Aller, S. G. *et al.* Structure of P-glycoprotein reveals a molecular basis for poly-specific drug binding. *Science* **323**, 1718–1722 (2009).

2. Li, J., Jaimes, K. F. & Aller, S. G. Refined structures of mouse P-glycoprotein. *Protein Sci.* **23**, 34–46 (2014).

3. Jin, M. S., Oldham, M. L., Zhang, Q. & Chen, J. Crystal structure of the multidrug transporter P-glycoprotein from Caenorhabditis elegans. *Nature* **490**, 566–569 (2012).

4. Loo, T. W. & Clarke, D. M. Defining the Drug-binding Site in the Human Multidrug Resistance P-glycoprotein Using a Methanethiosulfonate Analog of Verapamil, MTS-verapamil. *J. Biol. Chem.* **276**, 14972–14979 (2001).

5. Loo, T. W. & Clarke, D. M. Location of the Rhodamine-binding Site in the Human Multidrug Resistance P-glycoprotein. *J. Biol. Chem.* **277**, 44332–44338 (2002).

6. Loo, T. W. & Clarke, D. M. Identification of Residues in the Drug-binding Domain of Human P-glycoprotein ANALYSIS OF TRANSMEMBRANE SEGMENT 11 BY CYSTEINE-SCANNING MUTAGENESIS AND INHIBITION BY DIBROMOBIMANE. *J. Biol. Chem.* **274**, 35388–35392 (1999).

7. Pleban, K. P-Glycoprotein Substrate Binding Domains Are Located at the Transmembrane Domain/Transmembrane Domain Interfaces: A Combined Photoaffinity Labeling-Protein Homology Modeling Approach. *Mol. Pharmacol.* **67**, 365–374 (2004).

8. Frank, G. A. *et al.* Cryo-EM Analysis of the Conformational Landscape of Human P-glycoprotein (ABCB1) During its Catalytic Cycle. *Mol. Pharmacol.* **90**, 35–41 (2016).

9. Siarheyeva, A., Lopez, J. J. & Glaubitz, C. Localization of Multidrug Transporter Substrates within Model Membranes. *Biochemistry* **45**, 6203–6211 (2006).

10. Nosol, K. *et al.* Cryo-EM structures reveal distinct mechanisms of inhibition of the human multidrug transporter ABCB1. *Proc. Natl. Acad. Sci.* **117**, 26245–26253 (2020).

11. Li, M. J., Guttman, M. & Atkins, W. M. Conformational dynamics of P-glycoprotein in lipid nanodiscs and detergent micelles reveal complex motions on a wide time scale. *J. Biol. Chem.* **293**, 6297–6307 (2018).

12. Kim, Y. & Chen, J. Molecular structure of human P-glycoprotein in the ATP-bound, outward-facing conformation. *Science* 73–89 (2018).

13. Szewczyk, P. *et al.* Snapshots of ligand entry, malleable binding and induced helical movement in P-glycoprotein. *Acta Crystallogr. D Biol. Crystallogr.* **71**, 732–741 (2015).

14. Al-Shawi, M. K. & Omote, H. The Remarkable Transport Mechanism of P-glycoprotein; a Multidrug Transporter. *J. Bioenerg. Biomembr.* **37**, 489–496 (2005).

15. Dey, S., Ramachandra, M., Pastan, I., Gottesman, M. M. & Ambudkar, S. V. Evidence for two nonidentical drug-interaction sites in the human P-glycoprotein. *Proc. Natl. Acad. Sci. U. S. A.* **94**, 10594–10599 (1997).

16. Vahedi, S., Chufan, E. E. & Ambudkar, S. V. Global alteration of the drug-binding pocket of human P-glycoprotein (ABCB1) by substitution of fifteen conserved residues reveals a negative correlation between substrate size and transport efficiency. *Biochem. Pharmacol.* **143**, 53–64 (2017).

17. Alam, A., Kowal, J., Broude, E., Roninson, I. & Locher, K. P. Structural insight into substrate and inhibitor discrimination by human P-glycoprotein. *Science* **363**, 753–756 (2019).

18. Sharom, F. J. The P-glycoprotein multidrug transporter. *Essays Biochem.* **50**, 161–178 (2011).

19. Fuerst, T. R., Niles, E. G., Studier, F. W. & Moss, B. Eukaryotic transient-expression system based on recombinant vaccinia virus that synthesizes bacteriophage T7 RNA polymerase. *Proc. Natl. Acad. Sci. U. S. A.* **83**, 8122–8126 (1986).

20. Gey, G. O., Bang, F. B. & Gey, M. K. Responses of a Variety of Normal and Malignant Cells to Continuous Cultivation, and Some Practical Applications of These Responses to Problems in the Biology of Disease. *Ann. N. Y. Acad. Sci.* **58**, 976–999 (1954).

21. Ramachandra, M., Ambudkar, S. V., Gottesman, M. M., Pastan, I. & Hrycyna, C. A. Functional characterization of a glycine 185-to-valine substitution in human P-glycoprotein by using a vaccinia-based transient expression system. *Mol. Biol. Cell* **7**, 1485–1498 (1996).

22. Hrycyna, C. A., Ramachandra, M., Pastan, I. & Gottesman, M. M. Functional Expression of Human P-Glycoprotein from Plasmids using Vaccinia Virus-Bacteriophage T7 RNA Polymerase System. *Methods Enzymol.* **292**, 456–473 (1998).

23. Alam, A. *et al.* Structure of a zosuquidar and UIC2-bound human-mouse chimeric ABCB1. *Proc. Natl. Acad. Sci. U. S. A.* **115**, E1973–E1982 (2018).

24. Mechetner, E. B. & Roninson, I. B. Efficient inhibition of P-glycoprotein-mediated multidrug resistance with a monoclonal antibody. *Proc. Natl. Acad. Sci. U. S. A.* **89**, 5824–5828 (1992).

25. Xie, Y., Burcu, M., Linn, D. E., Qiu, Y. & Baer, M. R. Pim-1 Kinase Protects P-Glycoprotein from Degradation and Enables Its Glycosylation and Cell Surface Expression. *Mol. Pharmacol.* **78**, 310–318 (2010).

26. Chambers, T. C., Pohl, J., Glass, D. B. & Kuo, J. F. Phosphorylation by protein kinase C and cyclic AMP-dependent protein kinase of synthetic peptides derived from the linker region of human P-glycoprotein. *Biochem. J.* **299**, 309–315 (1994).

27. Goodfellow, H. R. *et al.* Protein Kinase C-mediated Phosphorylation Does Not Regulate Drug Transport by the Human Multidrug Resistance P-glycoprotein. *J. Biol. Chem.* **271**, 13668–13674 (1996).

APPENDIX A. OVERCOMING P-GLYCOPROTEIN-ASSOCIATED RESISTANCE IN A MODEL OF CHRONIC MYELOGENOUS LEUKEMIA WITH DIMERIC DASATINIB-BASED PRODRUGS

Overcoming P-glycoprotein-Associated Resistance in a Model of Chronic Myelogenous Leukemia with Dimeric Dasatinib-Based Prodrugs

Allison Lange, Jason Goebel, Jean A. Chmielewski, and Christine A. Hrycyna

Introduction

Acquired multidrug resistance (MDR) is a major obstacle to successfully treating human malignancies. MDR describes the ability of a malignant cell to develop resistance to multiple chemotherapy drugs that are structurally and mechanistically unrelated [1]. One of the most well-established routes of MDR in the laboratory is through the action of the ATP binding (ABC) transporter P-glycoprotein (P-gp), which uses the energy from ATP hydrolysis to move substrates across the lipid bilayer [1-3]. In the case of MDR, P-gp transports anti-neoplastic agents outside the cell for excretion, decreasing the accumulation of anti-cancer compounds inside cells and ultimately limiting their effectiveness [2]. To date, there are no P-gp inhibitors available clinically to increase drug efficacy and it remains controversial whether or not P-gp contributes to MDR in this setting [3]. However, this association of P-gp with MDR may prove to be a fruitful area of investigation with chronic myelogenous leukemia (CML).

CML is a cancer of the myelogenous blood cell lineage that can become resistant to treatment through up-regulation of P-gp [3, 4]. Approximately 95% of CML patients share a unique genetic abnormality known as the Philadelphia Chromosome, where a reciprocal translocation of chromosomes 9 and 22 and subsequent protein expression results in expression of the Bcr-Abl fusion protein [3-5]. When fused with Bcr, Abl lacks auto-inhibition, resulting in constitutive activity and survival and propagation of myeloid blast cells, initiating CML [5-7]. The Philadelphia Chromosome is also known to be causative for 25% of acute lymphoblastic leukemia (ALL) cases, making Bcr-Abl a significant drug target [6].

The introduction of tyrosine kinase inhibitors (TKIs) have transformed the treatment for CML and have significantly improved disease-free survival rates for patients [6]. TKIs compete with ATP for the ATP-binding site of Abl, preventing phosphorylation of downstream targets [6-8]. Before its discovery in 2001, the five-year survival rate for CML was a dismal 42% [3]. However, patients in the chronic phase of CML receiving the TKI therapy Imatinib (Gleevec®) can now expect a survival probability of >95% after 5 years [3, 9]. The TKI Imatinib is an ATP-competitive inhibitor of Bcr-Abl that binds to the catalytic site of Abl kinase and prevents Abl auto-phosphorylation, preventing phosphorylation of downstream proteins associated with enhanced proliferation [5]. Despite the promising clinical results presented by Imatinib treatment, approximately 20-30% of patients in the chronic phase will develop resistance to Imatinib, notably through point mutations in the kinase domain of Abl [7]. For patients in advanced stages of CML, nearly 80% of patients experience Imatinib resistance [3, 9].

Acquired Imatinib resistance led to the discovery and clinical establishment of second-generation Abl kinase inhibitors. Dasatinib (Sprycel®) is a second-generation TKI that inhibits multiple tyrosine kinases at low nanomolar concentrations, and notably Abl and Src family kinases [7, 12]. Dasatinib's ability to bind to Abl in both the active and inactive conformations have enhanced its potency, and dasatinib can overcome many of the clinically-relevant mutations in the Abl kinase domain that lead to Imatinib resistance [2, 7, 9, 10]. As is common with cancer therapeutics, resistance also develops against Dasatinib [10]. Besides additional point mutations

in the kinase domain, especially the T315I mutation, up-regulation of Bcr-Abl expression, or over-expression P-gp can contribute to Dasatinib resistance [9, 12].

P-gp can be expressed in all stages of CML, but is up-regulated in the accelerated and blast crisis phases of CML and is clinically indicative of a poor response to Imatinib therapy [8, 10, 11]. Of TKIs used clinically, Imatinib, Dasatinib, and Nilotinib are known to be exported by P-gp at clinically relevant concentrations [2, 10, 12]. In fact, patient samples of Imatinib-resistant CML patient samples show higher expression of P-gp [13]. Because of its supposed contribution to CML progression, inhibiting P-gp for the subset of CML cases that express P-gp should be investigated.

Our lab has ongoing projects involving the development and characterization of novel inhibitors of P-gp. For our inhibitors, FDA-approved pharmaceutical compounds are linked via a biodegradable spacer [16, 18-20]. Importantly, these dimers should retain stability to interact with P-gp and subsequently degrade in the cell [16, 18-20]. The regenerated molecule will have pharmacokinetic properties of the parent compound that are well-established [18]. Inhibitor synthesis is facilitated with secondary or primary hydroxyl groups on the substrate that can be easily esterified in a single-step reaction. The ester bond allows for release of the monomeric compound in the cytosol by cellular esterases. Additionally, incorporation of a disulfide linker within the tether region similarly allows for reduction in the intracellular compartment and reversion to the original monomeric compound via intramolecular addition and elimination reactions [18]. Generating a library of molecules with increasing tether lengths allows for optimizing the length of the dimeric molecule for maximum P-gp inhibition.

P-gp and ABCG2 are thought to possess multiple, distinct binding sites that allows both transporters to recognize a vast library of substrates [1, 17]. We and others have previously demonstrated that bivalent molecules may serve as potent inhibitors of P-gp [14-18]. Specifically, the bivalent nature will occupy the multiple binding sites with greater affinity than the monomeric compound alone, corresponding to a slower rate of dissociation from the transporter and thus act as an inhibitor. In this study, we report the synthesis, characterization, and biological activity of a novel class of inhibitors of Dasatinib for P-gp and ABCG2 that retain potency against Abl kinase in P-gp-expressing, drug resistant, CML cells.

Materials and Methods

Dasatinib was purchased from MedChemExpress (Monmouth Junction, NJ), Quinine was purchased from TCI (Portland, OR); GF120918 was synthesized in our laboratory as described previously [19, 20]. MX was purchased from LKT Laboratories, Inc (St. Paul, MN); R123, Calcein-AM, Sf9 cells, and antibiotic-antimycotic were purchased from Invitrogen (Carlsbad, CA). FBS was purchased from Atlanta Biologicals (Lawrencewill, GA). L-Glutamine, penicillin-streptomycin, trypsin, and RPMI were purchased from Corning. Basal Medium Eagle was purchased from Mediatech (Herdon, VA). EDC was purchased from AK Scientific (Union City, CA). The C219 and MRK16 antibodies were a generous gift from Dr. Michael M. Gottesman (National Cancer Institute, NIH, Bethesda, MD). The BXP21 and 5D3 antibodies were obtained from Novus Biologicals (Littleton, CO). All other reagents were purchased from Sigma-Aldrich (St. Louis, MO) or Invitrogen (Carlsbad, CA).

General Synthesis of Dasatinib Heterodimers

To a solution of commercially available diacid tether (1.54 mmol) in dry dimethylformamide (DMF) at 0°C was added N-(3-dimethylaminopropyl)-N-ethylcarbodiimide (EDC) (0.462 mmol), 4-dimethylaminopyridine (DMAP) (0.462 mmol), Quinine (0.154 mmol), and N,N-diisopropylethylamine (DIEA) (0.462 mmol). The solution was stirred for 5 hours at 0°C and then brought back to room temperature and allowed to react for an additional 20 hours. Solvent was removed *in vacuo* and compounds were separated by reverse-phase HPLC using a C8 column (Phenomenex, Torrance, CA) with an eluent consisting of solvent A (water and 0.1% trifluoroacetic acid (TFA)) and solvent B (acetonitrile and 0.1% TFA) with a gradient of 10-80% solvent B over 60 minutes, a flow rate of 10 ml/min, and a UV detection at 214 and 254 nm. Recovered monomer-tether was reacted with Dasatinib (0.076 mmol), EDC (0.084 mmol), DIEA (0.304 mmol), and DMAP (0.114 mmol) in dry DMF at 0°C. Solution stirred at 0°C for 5 hours and was then moved to ambient temperature where reaction proceeded for an additional 20 hours. Solvent was removed *in vacuo* and compounds were separated as described above. Pure compounds (>95% by analytical HPLC) were characterized by ESI mass spectroscopy. DasC4Q $[M + H]^+$: 922.5 calculated, 922.8 observed; DasC6Q $[M + H]^+$: 950.6 calculated, 950.7 observed; DasC8Q $[M + H]^+$: 978.7 calculated, 978.8 observed; DasC10Q $[M + H]^+$: 1006.7 calculated, 1007.0 observed; Das6SSQ $[M + H]^+$: 986.7 calculated, 986.8 observed; Das8SSQ $[M + H]^+$: 1014.7 calculated, 1015.1 observed; Das10SSQ $[M + H]^+$: 1042.8 calculated, 1043.0 observed.

Cell Culture

MCF-7/DX1, 12D7MDR, and K562 cells were cultured at 37°C in 5% CO_2 in RPMI containing 50 units/ml of penicillin, 50 µg/ml of streptomycin, 2 mM L-glutamine, 10% fetal bovine serum, and 1 µM doxorubicin. Sf9 cells were maintained at 27°C in SF-900 II SFM medium supplemented with 0.5X antibiotic/antimycotic. K562-Imatinib Resistant (K562-IR) were a kind gift from Dr. Zhe-Sheng Chen (St. John's University). K562 IR cells were maintained in 30 µM imatinib until 72 hours prior to each experiment.

Generation of K562 Dox Cells

K562 cells expressing P-gp as a mechanism of resistance were generated as described previously [21]. Briefly, K562 wild type cells were incubated tolerated, low-doses of doxorubicin (dox) in increasing concentrations from 0.1 µM to 1 µM dox over four months, increasing in 0.1 µM increments. Once cells reached a density of $1x10^6$ cells/ml, cells were passaged, approximately two or three times weekly. Dead cells were removed by centrifugation at 200 x g for 1 minute and pellet was resuspended in fresh culture medium containing a higher concentration of dox at a density of $0.1x10^6$ cells/ml. Dox concentration was increased only when the proliferation rate was comparable to the parental K562 cells maintained simultaneously. K562 dox cells were maintained in 1 µM dox until 72 hours prior to each experiment.

Expression of P-gp and ABCG2 in Insect Cells

Sf9 cells (9.3 x 10^6 cells) in 75-cm^2 flasks were infected with *Baculovirus (BV)-MDR1* or *BV-ABCG2* at a multiplicity of infection of 5 in 2.5 ml of culture media. After 3 hours of incubation in a light-protected 27°C incubator, 10 ml of media was added and incubated an additional 72 hours as described previously [22, 23].

Preparation of Crude Insect Cell Membranes

P-gp or ABCG2 over-expressing crude membrane isolates were prepared as described previously [22]. Briefly, BV-MDR1 or BV-ABCG2 infected Sf9 cells were harvested 75 hours after infection and centrifuged at 3000 x g for 10 minutes at 4°C. The pellet was re-suspended in homogenization buffer (50 mM Tris-HCl pH=7.5; 50 mM Mannitol; 1 mM 4-(2-aminoethyl) benzenesulfonyl fluoride hydrochloride (AEBSF); 2 mM ethylene glycol tetraacetic acid (EGTA); and 1% Aprotinin). The resuspension was incubated on ice for 30 minutes and homogenized using 30 strokes with each pestle A and B in a Dounce homogenizer. Nuclear debris was pelleted and removed by centrifugation at 3000 x g for 10 minutes at 4°C. The supernatant containing the crude membrane portion was collected following centrifugation at 100,000 x g for 60 minutes at 4°C. The pellet was re-suspended using blunt-ended 18-, 20-, 22-, and 25- gauge needles sequentially in resuspension buffer (50 mM Tris-HCl pH 7.5; 200 mM Mannitol; 1 mM EGTA; 1 mM AEBSF; 1% Aprotinin; 10% glycerol). Crude membranes were flash-frozen on dry ice as 30 µl aliquots and stored at -80C. Expression of P-gp or ABCG2 was confirmed through immunoblotting using C219 or BXP21 primary antibody (1:4000 in 4% milk) and HRP-conjugated goat anti-mouse secondary (1:4000 in 4% milk).

Flow Cytometry Assays

Flow cytometry assays were performed as described previously with minor modifications [24]. All flow cytometry assays were performed with 125,000 cells. Briefly, MCF7/DX1 cells were incubated in 1 ml of Basal Medium Eagle (BME) supplemented with 5% FBS (pH 7.4). BME contained either calcein-AM (0.5 µM) or rhodamine-123 (0.5 µg/ml) as a fluorescent substrate. MCF7/FLV1000 cells were incubated in mitoxantrone (MX, 20 µM). 12D7MDR cells were incubated in 0.25 µM calcein-AM. Cells were incubated with fluorescent molecule and increasing concentrations of inhibitor. GF120918 (1 µM) was used as a positive control and all samples had a final concentration of 1% DMSO. Cells were incubated in light-resistant 37ºC water bath for 10 minutes (MCF7/DX1 + Calcein-AM) or 30 minutes (MCF7/DX1 + R123, 12D7MDR, and MCF7/FLV1000). Media was aspirated following centrifugation at 300 x g at 4ºC for 5 minutes. Cells incubated in MX or R123 were re-suspended in 1 mL substrate-free BME containing corresponding inhibitors at increasing concentrations and incubated in light-resistant 37 ºC for an additional 30 minutes. Centrifugation and aspiration were repeated and cells were stored on ice. Cells were re-suspended in 400 µl PBS (pH 7.4) immediately before analysis on a FACS Calibur Flow Cytometer with a 488 nm argon laser. Calcein-AM and R123 were analyzed using a 585/542 nm band pass filter (FL1) while MX was analyzed at 670 nm band pass filter (FL3). The average fluorescence for 10,000 cells was collected for each sample and the mean fluorescence was input in GraphPad Prism 4.0 to calculate at IC_{50}.

Flow Cytometry-Based Surface Expression of Transporters

P-gp and ABCG2 expression in live cells was conducted using 250,000 cells diluted in 50 µl of BME and incubated with MRK16 (P-gp), IgG2a (MRK16 isotype control), 5D3 (ABCG2), or IgG2b (5D3 isotype control) antibodies in a 1:25 ratio. Samples incubated in a covered water bath for 30 minutes at 37C and washed in excess media, centrifuged (300 x g for 5 minutes) and aspirated. Samples were resuspended in the appropriate secondary antibody (α-IgG2a-FITC for P-gp and α-IgG2b-FITC for ABCG2) at a 1:50 dilution and incubated and aspirated as described above. Immediately before analysis, cells were re-suspended in 400 µl PBS (pH 7.4) and analyzed on a FACS Calibur Flow Cytometer with a 488 nm argon laser using a 585/542 nm band pass filter (FL1) and reading the average fluorescence for 10,000 cells.

ATPase Activity Assay in Crude Membranes Expressing P-gp

Vanadate-sensitive ATP hydrolysis in P-gp-expressing crude membranes was quantified in the presence or absence of increasing concentrations of Das, quinine, Das8SSQ, or DasCarbQ as described previously [18]. Briefly, crude membranes (10 µg) were incubated with either DMSO or test compounds in assay buffer (45 mM Tris-HCl, pH 7.5, 5 mM sodium azide, 10 mM $MgCl_2$, 2 mM EGTA, 1 mM ouabaine, and 2 mM DTT) in the presence or absence of 300 µM sodium orthovanadate. The reaction was started by the addition of ATP (5 mM final) in a final volume of 100 µl and incubated at 37°C for 20 minutes. The reaction was terminated with the addition of 100 µl 5% (w/v) SDS. ATPase activity was measured by the colorimetric determination of inorganic phosphate released (λ 880 nm). A minimum of two assays were performed in duplicate.

To detect the vanadate-sensitive attenuation of P-gp in the presence of test compound, Verapamil (30 µM) was added to P-gp expressing membranes as described previously [18]. Replicates were prepared as in the stimulation assay in the presence of increasing concentrations of Das, Das8SSQ, DasCarbQ, or quinine as inhibitors of substrate stimulated ATPase activity. A minimum of two assays were performed in duplicate.

MTT Assays for Cell Viability

Viability of K562 cells was determined as described previously with minor modifications [25]. Briefly, cells (K562, K562 IR, or K562 Dox) were diluted to 4000 cells/100 µl and plated in 96-well plate with increasing concentrations of drug (<1% DMSO) and incubated for 72 hours in media containing no phenol red. MTT reagent (5 mg/ml in PBS) was added and incubated 3 hours at 37 C protected from light. Plates were centrifuged at 300 x g for 5 minutes and wells were carefully aspirated. Crystals were re-suspended in DMSO, incubated for 1 hour covered at ambient temperature, and read on Tecan plate reader at λ=590 nm. Absorbance values from each trial were normalized to 100% viability in the 0 nM (DMSO) sample. Normalized values from three independent trials (a total of 21 replicates) were averaged and an IC_{50} corresponding to the dose of half-maximal viability was calculated using GraphPad Prism 4.0. 10 µM taxol was used as a qualitative positive control to estimate background from minimal cell viability.

In Vitro Abl Kinase Activity Assay

The ability of test compounds to inhibit Abl kinase *in vitro* was measured by using a Universal Kinase Assay Kit (R&D Systems, Minneapolis, MN). WT Abl (Calbiochem, San Diego, CA) was diluted to 0.12 ng/µl in storage buffer (100 mM NaCl, 50 mM HEPES pH=7.2, 1 mM DTT, 50% glycerol, and 0.01% Brij 35) and stored at -80ºC. To test activity, 1.5 ng of purified Abl was incubated with 1 mM ATP, 2% test compound (DMSO, Dasatinib, Das8SS, or DasCarbQ), 10 ng/µl coupling phosphatase 4, 0.75 mM peptide substrate, and brought to a final volume of 40 µl with assay buffer. 1 mM ATP was added every 10 seconds to each sample and samples incubated for 15 minutes at room temperature. Reactions were terminated by adding 30 µl of Reagent A, 100 µl of water, and 30 µl of Reagent B. Color was allowed to stabilize at room temperature for 20 minutes. Samples were added to 96-well plate and the absorbance was read at 620 nm. Specific activity was calculated from the stock phosphate standard curve and using the efficiency correction of the coupling enzyme. Data were normalized to 100% Abl kinase activity in the DMSO sample and values represent at least two independent trials performed in duplicate.

DTT Assay for Compound Stability

DTT stability studies were performed as described previously with minor modifications [18]. Briefly, Dasatinib dimers (150 µM) were incubated with 10 mM DTT in PBS (pH 7.4) containing the internal standard, benzophenone (25 µM) at 37°C. DMSO concentrations were kept at 0.75%. At varying time points, aliquots from the reaction were collected and frozen immediately on dry ice. Samples were stored at -80°C until the time of HPLC analysis. For HPLC analysis, samples were thawed and then immediately analyzed by reverse-phase HPLC equipped with a C18 analytical column (Phenomenex, Torrance, CA). Eluent contained solvent A (acetonitrile and 0.1% TFA) and solvent B (water and 0.1% TFA). The linear gradient increased from 10-75% solvent A over 30 minutes at a flow rate of 1.2 ml/min and peaks were detected at 280 nm. The peak area corresponding to the released monomeric Dasatinib was quantified and half-lives were obtained by fitting data using GraphPad Prism 4.0. Assays were performed in triplicate.

Detecting p-Crkl in K562 and K562-Derived Cells

Inhibition of Crkl phosphorylation in K562 cells was performed as described previously with minor modifications [12]. Briefly, K562, K562-IR, or K562-Dox cells ($5x10^5$ cells/well) were plated in a 6-well dish and incubated at 37ºC. Increasing concentrations of either Dasatinib or DasCarbQ (0.5% DMSO final concentration) was added and cells incubated for 12 hours at 37ºC. After 12 hours, cells were collected and washed twice with PBS and lysed in 50 µl RIPA buffer containing phosphatase and protease inhibitors. Lysates were diluted in 5X SDS loading buffer to a final concentration of 2X, sonicated for 2 minutes, and incubated at room temperature for 30 minutes. 40 µl of lysate was loaded onto 1.5 mm, 10% acrylamide gel. Lyste was separated by SDS-PAGE and transferred to 0.2 µm nitrocellulose membrane for 3 hours at 100V. Membrane incubated overnight at 4ºC with gentle shaking in primary antibody (1:1000 α-p-Crkl, Cell Signaling Technology, Danvers, MA) in 5% BSA in PBS + 0.5% tween. Following washing, membrane was incubated in HRP-conjugated α-rabbit (1:4000) for one hour at room temperature and washed. Levels of p-Crkl were detected by autoradiography.

To detect total levels of Crkl, membrane was stripped (0.2 M glycine, 1% Tween 20, pH 2.2) and blocked for hour in 20% w/v nonfat milk in PBS + 0.5% tween at room temperature. Following three washes, membrane was incubated in α-Crkl in 5% w/v nonfat milk in PBS + 0.5% tween overnight at at 4ºC with gentle shaking (1:1000, Cell Signaling Technology, Danvers, MA). Following three washes in PBS + Tween, membrane was incubated with HRP-conjugated α-mouse (1:4000) for one hour at room temperature and washed. Levels of Crkl were detected by autoradiography.

Results

The association between P-gp and drug-resistance in CML is observed both in the laboratory and the clinic [8, 10, 12, 26]. These data suggest that inhibiting P-gp may have the potential to reverse P-gp-associated MDR and improve patient prognosis in a subset of cases where P-gp appears to be a major mechanism of resistance. Furthermore, TKI treatments for CMLs are substrates of P-gp, and the action of P-gp may contribute to the decreased penetration of TKIs in resistant CML cells. Therefore, we applied our prodrug dimer approach to the treatments for CML. Dasatinib was selected as a candidate for a dimeric inhibitor because it is known to be a substrate of P-gp at clinically relevant concentrations [12, 27]. Furthermore, Dasatinib contains a primary alcohol that can be functionalized into an ester linkage in a straightforward, single-step reaction [16, 18-20]. Besides being reactive and unhindered, this primary alcohol appears to be unnecessary for the high affinity binding of Dasatinib to Abl. The crystal structure of Dasatinib bound in the kinase domain of Abl reveals that this alcohol is solvent-exposed (PBD file 2GQG) [28]. Together, these qualities make Dasatinib an ideal candidate for our inhibitor efforts.

Dasatinib Homodimers are not Potent Inhibitors of P-gp

P-gp has been shown to have spatially distinct substrate binding sites, and we and others have previously described the advantages of synthesizing P-gp inhibitors using bivalency and degradable tethers [16, 18-20]. Candidate P-gp inhibitors were synthesized using the free primary alcohol on Dasatinib to generate ester bonds [16, 18-20]. The library of Dasatinib homodimers consisted of compounds with four to eight methylene units between ester bonds (DasC4, DasC6, DasC8) (Figure 1, panel A). A compound with a symmetrical disulfide linker within the tether replacing the two central methylene units in DasC8 was also synthesized.

Fluorescence activated cell sorting was used to screen compounds for P-gp efflux inhibition in MCF-7/DX1 cells overexpressing P-gp. Increasing concentrations of test compounds were incubated with cells and the substrate calcein-AM. Increased intracellular fluorescence is linked to the capacity of a compound to inhibit P-gp efflux and can be quantified using flow cytometry to generate an inhibition curve.

This assay failed to identify any homodimer that possessed potent P-gp inhibition, either in MCF-7/DX1 (Figure 3.2) or 12D7MDR cells (data not shown). We defined P-gp inhibition as the capacity to inhibit calcein-AM efflux by at least 50% of the level that the control P-gp inhibitor GF120918 can achieve. Likewise, these homodimers did not exhibit potent inhibition of MX transport in MCF-7/FLV1000 cells (data not shown). We suggest that the Dasatinib homodimers may be incapable of crossing the cellular membrane because of their large molecular weight and thus never interact with P-gp and ABCG2. Solubility of test compounds was not observed to be a factor.

Dasatinib-Quinine Heterodimers are Potent Inhibitors of P-gp

Quinine is a well-characterized substrate of P-gp [29]. It has been previously demonstrated by our labs that quinine homodimers are potent inhibitors of P-gp efflux [20]. Furthermore, quinine is an inexpensive starting material that is well-tolerated in most humans and thus has an advantage over other P-gp-modulating molecules. As an MDR-reversing agent, quinine may also compete with Dasatinib for the binding site of P-gp to improve Dasatinib's toxicity [31]. Additionally, *in vitro* data has indicated that quinine is capable of inhibiting P-gp to limit doxorubicin efflux in the K562 human leukemia cell line [29, 30]. Clinical experiments report a similar ability of quinine to increase plasma levels of the anti-cancer agent mitoxantrone in patients with acute leukemia that exhibit MDR through P-gp expression [31]. Finally, quinine has well-established and predictable pharmacokinetic properties in humans, as well as a low incidence of toxicity or side effects. Quinine toxicity is possible in patients with abnormal cardiac conductance profiles, corresponding to cardiotoxicity [41]. Specifically, quinine is capable of inhibiting sodium channels in cardiomyocytes, prolonging the Q-T interval [41]. Besides this population, coupling Dasatinib with quinine may produce a compound that has a high binding affinity for P-gp in patients not at risk for this cardiotoxic event. Following the same EDC-coupling strategy, a library of heterodimeric Dasatinib-quinine compounds was synthesized. Excess dicarboxylic acid was reacted with quinine and the resulting 'quinine-tether' produced was purified and collected by reverse-phase HPLC as described in Materials and Methods. In a second step, the Quinine-tether was reacted with Dasatinib to generate various heterodimers (Figure 1 panels B-C).

The heterodimers were screened for P-gp inhibition in MCF-7/DX1 cells using the flow cytometry assay described above. Importantly, all the Dasatinib-quinine dimers, except for DasC10Q and Das10SSQ, were more potent inhibitors of P-gp efflux than either the Das or quinine monomers ($p<0.001$, Table 1). Heterodimers that were considered inhibitors had IC_{50} values ranging from 2.2-5.5 μM, compared with IC_{50} values of 54.6 μM for Dasatinib and 120.7 μM for quinine (Table 1). DasC10Q and Das10SSQ both displayed low solubility in assay media, but besides this observation, tether length does not appear to affect inhibition for compound with 4, 6, or 8 atoms in the tether backbone.

To confirm the transport inhibition properties of each molecule, rhodamine (R123) was also used in addition to calcein-AM. Both Dasatinib and quinine are capable of inhibiting fluorescent molecule transport, but the Dasatinib-quinine compounds show more potent inhibition as indicated by the lower micromolar IC_{50} values, ranging between 2.2 and 8.6 μM ($p<0.001$, Table 1). Similar to the calcein-AM trials, both DasC10Q and Das10SSQ displayed low solubility in incubation media, even in higher concentrations of DMSO, and no IC_{50} value was calculated for these compounds (Table 1). Together, these data suggest that the dimeric approach to P-gp inhibition is viable with Dasatinib-based heterodimers.

DasCarbQ Inhibits P-gp in 12D7MDR Human T-Cells

To better understand the behavior of the dimeric compounds, we also synthesized a carbamate-linked heterodimer (Figure 1 panel D). Carbamate linkages are exceptionally stable in biological conditions, and this uncleavable molecule (DasCarbQ) provides a model of heterodimer behavior without the risk of the SS tether reduction or hydrolysis of the ester bonds [18]. While DasCarbQ failed to inhibit P-gp-mediated fluorescent substrate transport in MCF-7/DX1 cells, this molecule did provide inhibition in P-gp-overexpressing 12D7MDR human T-cells, indicating the potential for P-gp inhibition (Table 2). The 12D7MDR cells provide a more relevant model for P-gp inhibition compared to MCF7/DX1 cells because of their immunological origin. Like the MCF-

7/DX1 cells, heterodimers inhibit calcein-AM efflux more potently than either Dasatinib (IC_{50} ~8.4 μM) or quinine (IC_{50} ~5.0 μM) alone (Table 1).

Dasatinib-based Heterodimers Display ABCG2 Inhibition

While P-gp appears to be the major ABC transporter that contributes to the MDR phenotype in CML cells, ABCG2 is capable of transporting Dasatinib *in vitro*, although clinical data is much less conclusive [2, 3, 8, 10]. Furthermore, Dasatinib can compete with the prazosin analog [^{125}I]-IAAP for the ABCG2 binding site in crude membrane preparations [12]. ABCC1 is not known to contribute to MDR in clinical cases of CML [32]. Because of its suspected role in conferring resistance to CML, ABCG2 inhibition was subsequently studied. Like P-gp, the binding site of ABCG2 recognizes hundreds of structurally and functionally unrelated compounds, and is also reported to contain multiple drug binding sites [33]. The flow cytometry assay for substrate transport inhibition was performed in MCF-7/FLV1000 cells that overexpress the ABCG2 transporter with the fluorescent substrate mitoxantrone (MX, 20 μM). Importantly, each heterodimer that we tested was capable of inhibiting MX transport more potently than Dasatinib (IC_{50} ~35.2 μM). Heterodimer IC_{50} values ranged from 0.8-1.8 μM (Table 1). Quinine did not demonstrate ABCG2 inhibition at any concentration tested and no IC_{50} value was calculated. Like P-gp inhibition, ABCG2 inhibition does not appear to be tether length-dependent.

Das8SSQ Releases Dasatinib in Reducing Conditions

The Das8SSQ compound was chosen to further characterize because of its ability to rapidly revert to Dasatinib through reduction of the disulfide bond. Das8SSQ is designed to break down in intracellular reducing conditions, a process which will release Dasatinib, quinine, and the re-cyclized tether. Appearance of Dasatinib was monitored and quantified by analytical HPLC following incubation in dithiothreitol (DTT) and has half-maximal release at 1.8 hours (Figure S.1).

Heterodimers are Potent Inhibitors of P-gp ATP Hydrolysis

Many P-gp substrates are capable of stimulating basal ATP activity, indicative of a physical interaction with P-gp or ABCG2 [16]. Both P-gp and ABCG2 activity can be quantified colorimetrically by measuring the amount of phosphate released following ATP hydrolysis [18]. Quinine, Dasatinib, Das8SSQ, and DasCarbQ were evaluated for the ability to stimulate ATP turnover in crude membrane preparations of both transporters. Consistent with previous results, Dasatinib stimulates P-gp ATP hydrolysis approximately 2.7-fold over basal [12]. Das8SSQ and DasCarbQ are weak stimulators of ATP hydrolysis at low concentrations, possibly indicating that these compounds are substrates of P-gp at low concentrations (Figure 2). Indeed, we have observed previously that dimeric inhibitors stimulate ATPase activity at low concentrations and exhibit inhibition at higher concentrations [16, 18]. Quinine also displays a concentration-dependent increase in P-gp ATP hydrolysis (Figure 2).

Crude transporter-expressing membranes can likewise be used to evaluate the inhibition of ATP hydrolysis. To test for ATP inhibition, crude membranes expressing P-gp or ABCG2 are maximally stimulated with 30 μM verapamil (P-gp) or 40 μM prazosin (ABCG2). Increasing concentrations of Dasatinib, quinine, Das8SSQ, or DasCarbQ are also added to observe the concentration-dependent attenuation of ATP turnover. Both Dasatinib and quinine were capable

of inhibiting verapamil-stimulated ATP turnover, but Das8SSQ and DasCarbQ both exhibit statistically more potent inhibition than either monomer ($p<0.05$, Table 2, Figure 3). These results indicate that both Das8SSQ and DasCarbQ can potently inhibit ATP hydrolysis and thus likely interrupt substrate efflux for both transporters and inhibit the substrate-stimulated ATPase activity.

Das8SSQ and DasCarbQ Retain Sub-nanomolar Potency for Abl

In conjunction with an ability to inhibit P-gp and ABCG2, our compounds must also have the capacity to inhibit Abl kinase. *In vitro* assays with purified Abl kinase have been used extensively to screen for molecules that inhibit kinase ability [7, 9, 21, 35]. We used a Universal Kinase Activity kit to measure Abl kinase activity colormetrically. Briefly, Abl was incubated with ATP and increasing concentrations of test compound and a short peptide containing a tyrosine. Specific activity was calculated and values were normalized to 100% kinase activity in 0 nM inhibitor. Unsurprisingly, as reported previously by other research groups, Dasatinib has a low-nanomolar potency against Abl kinase (Table 3) [35]. Interestingly, both Das8SSQ and DasCarbQ retain the sub-nanomolar inhibition that is seen with Dasatinib, and IC_{50} values corresponding to Abl inhibition were not statistically different between the three test compounds (Table 3). These results indicate that the primary alcohol on Dasatinib is likely non-essential for Abl binding, making this an ideal site for ester bond formation. Additionally, these data suggest that it may not be necessary for this molecule to break down intracellularly for efficacy against Abl kinase. Previously, our dimers were designed to break down intracellularly to revert to monomer, but these molecules do not require this property in the *in vitro* model. The stability of the Das8SSQ molecule was tested in reaction buffer and did not to revert to Dasatinib in a time frame that was relevant for this assay (data not shown).

K562 Cells Cultured in Imatinib or Doxorubicin are Resistant to Dasatinib Through P-gp Expression

K562 cells have become the standard for studying CML in the laboratory [3]. K562 cells are a line of immortalized human CML cells with stable expression of the Philadelphia Chromosome and wild-type Bcr-Abl [3]. K562 can display the MDR phenotype through step-wise selection in Imatinib or doxorubicin [34]. For our studies, we used two different P-gp-expressing K562 cell lines. K562-Imatinib resistant (K562-IR) cells are >9000-fold more resistant to imatinib compared to WT cells (Table 4). Resistance in these cells was established through step-wise selection in Imatinib [34]. We generated a line of P-gp-expressing K562 cells through selection and passaging in increasing concentrations of doxorubicin (K562-dox) as described above in Materials and Methods. K562-dox cells also display ~14-fold higher resistance to Dasatinib, confirming the cross-resistance quality of MDR.

To verify P-gp expression, a flow cytometry-based surface expression analysis was utilized. Using the P-gp-reactive MRK16 antibody, we confirmed P-gp expression in both the K562-IR and K562-dox cell lines, but importantly failed to visualize any P-gp expression in the parental cells (Figure 4). This result was confirmed through immunoblotting (Supp. Figure S.2). Furthermore, we were unable to confirm any ABCG2 surface expression, either by flow cytometry or Western blotting, indicating that P-gp is likely the major transporter responsible for drug efflux. Finally,

we observed a shift in calcein-AM accumulation using flow cytometry with and without GF120918, indicating that the overexpressed P-gp is functional (data not shown).

Test Compounds are Toxic to Human Leukemia Cells

Abl kinase was inhibited potently *in vitro* and we next sought to show a similar quality in cells. K562 cells are immortalized human CML cells that express wild-type BCR-Abl. These cells were isolated from a patient suffering from terminal blast crisis and have become the standard for studying CML in the laboratory [3]. Using an MTT assay to estimate cell viability, we determined that Dasatinib, Das8SSQ, and DasCarbQ possess a similar toxicity in wild-type K562 cells ($p>0.05$, Table 4). This further supports the observation that tether degradation and reversion back to Dasatinib are not necessary for biological activity against Bcr-Abl in the laboratory.

K562 cells can be selected in doxorubicin to establish resistance via P-gp efflux. We generated a line of K562 cells that over-express P-gp as indicated by flow cytometry and P-gp-specific antibodies and established that the major MDR transporter was P-gp and not ABCG2 (Supp. Figure S.2). To estimate the contribution of P-gp to resistance, we incubated 5 μM GF120918 with increasing concentrations of Dasatinib (Table 4). With maximal P-gp inhibition, we were able to restore sensitivity back to wild-type levels. Interestingly, our compounds were also able to restore a sub-nanomolar toxicity to the K562-dox cells, indicating that P-gp inhibition allows accumulation of the therapeutic, and that the P-gp-inhibiting dimeric compound also possesses a cytotoxic quality with its ability to inhibit Bcr-Abl (Table 4).

K562 cells can also be selected for TKI resistance by culturing in increasing concentrations of Imatinib. Our lab secured a line of resistant K562 cells that are resistant to Imatinib as well as a variety of other drugs traditionally exported by P-gp, thus demonstrating the MDR phenotype. Importantly, expression of P-gp was shown to contribute to the multidrug resistance phenotype of these K562 Imatinib-resistant (IR) cells [34]. Furthermore, ABCG2 is not detected in these cells and thus is unlikely to be a source of resistance (Supp Figure S.2). Because of these qualities, they are another important cellular model for our drug discovery efforts. The MTT assay was again employed to estimate cytotoxicity. K562-IR cells are approximately 9000-fold more resistant to Dasatinib than wild-type cells (Table 4). We then incubated K562-IR cells with the dual P-gp/ABCG2 inhibitor GF120918 to quantify the contribution of ABC transporters to Dasatinib resistance. Incubation with GF120918 restored the sensitivity approximately ten-fold, giving us an estimation of P-gp-related resistance in this cell line. Incubation with Das8SSQ produced a similar toxicity as incubation with Dasatinib and GF120918 (Table 4). This indicates that our dimer can enter cells, inhibit P-gp, and elicit its cytotoxic effects through Abl inhibition.

Because toxicity was not restored to wild-type levels, other mechanisms of resistance must be present in this cell line. The most well-established route of Dasatinib resistance is through point mutations in Abl, most notably the T315I mutation in the ATP binding site. Other point mutations, both in the ATP binding site and elsewhere on the protein are also known to decrease sensitivity to Dasatinib. In these cases, we would not expect our dimer to be efficacious. Other sources show that up-regulation of BCR-Abl also confers resistance. Pathways implicated in malignant transformation are also known to contribute to Dasatinib resistance, including the JAK/STAT, Wnt-β-catenin, PI3K/AKT, and the Ras-Raf-MEK-ERK pathways [2, 26, 36]. Other routes of MDR observed in cell models include enhanced DNA repair mechanisms and resistance to apoptotic mechanisms [3]. Taken together, data show that our prodrug has a dual capacity to inhibit P-gp and confer toxicity to P-gp-expressing cells.

3.3.9 P-gp, but not ABCG2, Contributes to the MDR Phenotype in Resistant K562 Cells

ABCG2 can contribute to MDR in the laboratory but clinical data is much less convincing and P-gp appears to be the major ABC protein that contributes to MDR in CML [8]. Interestingly, several reports have indicated that TKIs are substrates of ABCG2 in cell models, leading to the possibility that this transporter can contribute to the resistant phenotype [12, 37, 38]. Specifically, Dohse and colleagues showed that ABCG2 expression in K562 cells confers a higher IC_{50} in a cell viability assay, as well as a higher concentration necessary for inhibiting phosphorylation of the Bcr-Abl adapter protein, Crkl [12]. For these reasons, we next investigated the contribution of ABCG2 expression in our K562-IR and K562-Dox cells. Both Western blotting and surface probing using flow cytometry (Figure 4) failed to reveal ABCG2 expression. Regardless of previous reports, our compounds are dual inhibitors of ABCG2 and P-gp, so ABCG2 activity can be potently inhibited by our compounds.

DasCarbQ Inhibits Crkl Phosphorylation More Potently than Dasatinib in Resistant K562 Cells

Monitoring Abl kinase activity in live cells is essential for establishing the clinical relevance of our compounds. Specifically, our compounds must inhibit Bcr-Abl at concentration where P-gp inhibition occurs. The 39-kDa Bcr-Abl adapter protein Crkl is a well-established cellular marker for Abl kinase activity in cells [39,40]. Crkl is the major tyrosine-phosphorylated protein in CML patient blood samples and the specificity of Crkl to Bcr-Abl phosphorylation has led to its acceptance as a robust and accurate method to quantify Bcr-Abl status [40].

We detected phosphorylation of Crkl at Y207 at increasing concentrations of either Dasatinib or DasCarbQ in K562 WT, K562 IR, or K562 Dox cells using immunoblotting. K562 cells expressing P-gp (K562 IR and K562 Dox) exhibited higher levels of p-Crkl compared to the parental cells at the same concentrations of dasatinib (figure 5), adding further support to the status of Dasatinib as P-gp substrate. DasCarbQ has properties of both a P-gp and Bcr-Abl inhibitor, and inhibition Crkl phosphorylation would support this claim. Indeed, resistant K562 cells incubated with DasCarbQ exhibit lower levels of p-Crkl compared to dasatinib-treated samples at the same concentration. Furthermore, DasCarbQ was able to restore p-Crkl levels to WT levels in K562 Dox cells, indicating that our compound has an ability to inhibit P-gp as well as Bcr-Abl.

Conclusion

Herein we describe the synthesis and characterization of a novel class of therapeutic compounds that have the capacity to inhibit P-gp as well as the oncogenic protein Bcr-Abl. Clinically, P-gp may be correlated with poorer prognosis for CML, and is up-regulated in later stages of CML [8, 10, 12]. P-gp is capable of effluxing the TKIs Imatinib, Nilotinib, and Dasatinib, possibly contributing to the selection of resistant leukemic blast cells in the laboratory and a subset of CML cases.

Our lead compounds, Das8SSQ and DasCarbQ, have shown a dual capacity for inhibition of P-gp and Bcr-Abl both *in vitro* and relevant cellular models. Importantly, it appears that reversion to monomeric Dasatinib is not necessary for cytotoxic activity. The carbamate-linked DasCarbQ, which is resistant to cellular enzymatic cleavage, maintains potency *in vitro* and in cell viability assays.

Dasatinib inhibits Abl and Src kinases, so our Dasatinib-Quinine prodrugs can also be applied to cancers employ Src as a major route of malignant transformation. Furthermore, the use of

Dasatinib for cancers of the head and neck has been thwarted by the blood-brain barrier. Specifically, P-gp expressed in the BBB is shown to be a major limiting factor in Dasatinib accumulation in gliomas [26]. Indeed, administration of Dasatinib with GF120918 allows Dasatinib accumulation in the brain. The Dasatinib-quinine prodrugs may have application for brain tumors and can be tested for their capacity to cross the BBB by inhibiting P-gp [2].

Cancer may become drug-resistant through a malignant clone, so treating multiple pathways of malignancies has some benefit. In the future, another anti-neoplastic agent may be coupled with Dasatinib to address other routes of malignant transformation. For example, coupling Dasatinib with a nucleoside analog could target cells with a high replication rate. This could be a beneficial advancement in the study of multidrug resistance. Furthermore, data indicate that combination therapy for cancer treatment is a useful mechanism to combat multidrug resistance. Dharmapuri *et. al*. showed that imatinib-resistant cells can be re-sensitized to imatinib by targeting multiple pathways, namely the PGE2-cAMP-PKC-NFkB pathway and the Ras-Raf pathway which contribute to oncogenesis [36]. This strategy should be applied to future multidrug resistance research.

While clinical inhibition of P-gp has failed to extend patient survival, we present a novel approach for re-addressing this therapeutic potential. A subset of leukemia cases that express P-gp may benefit from a dual P-gp/ABCG2 inhibitor. Here we present a compound that retains the potency of Dasatinib against Bcr-Abl but has the added feature of P-gp inhibition, which has never been reported. While inhibiting P-gp to restore sensitivity to malignant cells has been vastly unsuccessful in the clinic, identifying patients who will benefit from this therapy and targeting multiple mechanisms of resistance may revive this area of research.

Table 1: Flow Cytometry Assays in MCF-7 Cell Lines
Flow cytometry was used to evaluate the ability of test compounds to inhibit fluorescent substrate efflux in cells expressing P-gp (MCF-7/DX1 or 12D7MDR) or ABCG2 (MCF-7/FLV1000). For P-gp expressing cells, either calcein-AM or R123 was used as a substrate. Mitoxantrone (MX) was used as a transport substrate for ABCG2. Data represent the concentration at half-maximal intracellular fluorescence (IC_{50}) ± SEM from at least two independent trials performed in duplicate. For each concentration of test compound, the mean fluorescence from 10,000 cells was used to generate a dose response curve.

	P-gp-Overexpressing Cells			**ABCG2-Overexpressing Cells**
Compound	**0.5 µM calcein-AM MCF7/DX1 IC_{50} (µM)**	**0.5 µg/ml R123 MCF7/DX1 IC_{50} (µM)**	**0.25 µM calcein-AM 12D7MDR IC_{50} (µM)**	**20 µM MX MCF7/FLV1000 IC_{50} (µM)**
Dasatinib	54.6 ± 2.2	70.3 ± 1.3	8.4 ± 0.8	35.2 ± 4.0
Quinine	120.7 ± 13.8	105.5 ± 7.7	5.0 ± 1.0	ND
DasC2Q	20.2 ± 4.8	30.3 ± 7.6	4.4 ± 0.9	4.5 ± 0.9
DasC4Q	2.9 ± 0.3	2.7 ± 0.3	0.3 ± 0.04	1.4 ± 0.5
DasC6Q	2.2 ± 0.3	2.2 ± 0.2	0.5 ± 0.1	1.8 ± 0.4
DasC8Q	2.4 ± 0.3	3.2 ± 0.3	1.9 ± 0.2	1.0 ± 0.4
DasC10Q	ND	ND	ND	ND
Das6SSQ	5.5 ± 0.6	8.6 ± 1.1	0.3 ± 0.05	1.0 ± 0.2
Das8SSQ	4.3 ± 0.4	7.7 ± 1.0	2.0 ± 0.2	1.8 ± 0.5
Das10SSQ	ND	ND	ND	ND
DasCarbQ	ND	ND	1.9 ± 0.6	0.8 ± 0.2

Table 2: Inhibition of ATP Hydrolysis in P-gp Crude Membranes
Das8SSQ and DasCarbQ Potently Inhibit ATP Hydrolysis in P-gp-expressing crude membranes. Crude membranes (10 µg) were incubated with verapamil (30 µM) and increasing concentrations of test compounds for 20 minutes at 37ºC. ATPase activity was determined colorimetrically by quantifying the amount of inorganic phosphate released. IC_{50} values calculated represent the concentration at which 50% of maximal attenuation of verapamil-stimulated phosphate release is achieved after two independent trials peformed in duplicate.

Compound	**P-gp IC_{50} (µM)**
Dasatinib	21.9 ± 4.0
Quinine	178 ± 40.1
Das8SSQ	2.5 ± 0.9
DasCarbQ	1.1 ± 0.3

Table 3: Inhibition of Abl Kinase *In Vitro*
Dasatinib, Das8SSQ, and DasCarbQ have a similar sub-nanomolar ability to inhibit Abl kinase *in vitro*. Purified Abl kinase was incubated with a tyrosine-containing peptide substrate, a coupling phosphatase, ATP, and increasing concentrations of test compounds. The phosphatase cleavage of phosphorylated peptide substrate released inorganic phosphate, which was quantified colorimetrically and normalized against the 0 nM samples. IC_{50} values represent the concentration of half-maximal Abl inhibition after two independent trials performed in duplicate ± SEM.

Compound	**IC_{50} (nM)**
Dasatinib	0.3 ± 0.1
Quinine	Not Determined
Das8SSQ	0.5 ± 0.1
DasCarbQ	0.4 ± 0.1

Table 4: MTT Assay for Cell Viability
Dasatinib, Das8SSQ, and DasCarbQ have sub-nanomolar potencies in wild-type K562 cells. MTT assays were used to estimate cell viability in K562, K562 IR, and K562 Dox cells after 72 hours of incubation in increasing drug concentrations. IC_{50} values represent the concentration of 50% viability following normalizing data within each trial. Each value includes at least three independent trials performed with seven replicates.

Cell Line	**Treatment**	**IC_{50} (nM)**
K562 WT	Dasatinib	0.5 ± 0.1
K562 WT	Das8SSQ	0.3 ± 0.1
K562 WT	DasCarbQ	0.5 ± 0.1
K562 IR	Dasatinib	4900 ± 800
K562 IR	Das8SSQ	500 ± 100
K562 IR	DasCarbQ	500 ± 100
K562 IR	Dasatinib + 5 µM GF	400 ± 100
K562 Dox	Dasatinib	7.0 ± 0.4
K562 Dox	Das8SSQ	0.5 ± 0.1
K562 Dox	DasCarbQ	0.9 ± 0.1
K562 Dox	Dasatinib + 5 µM GF	0.5 ± 0.1

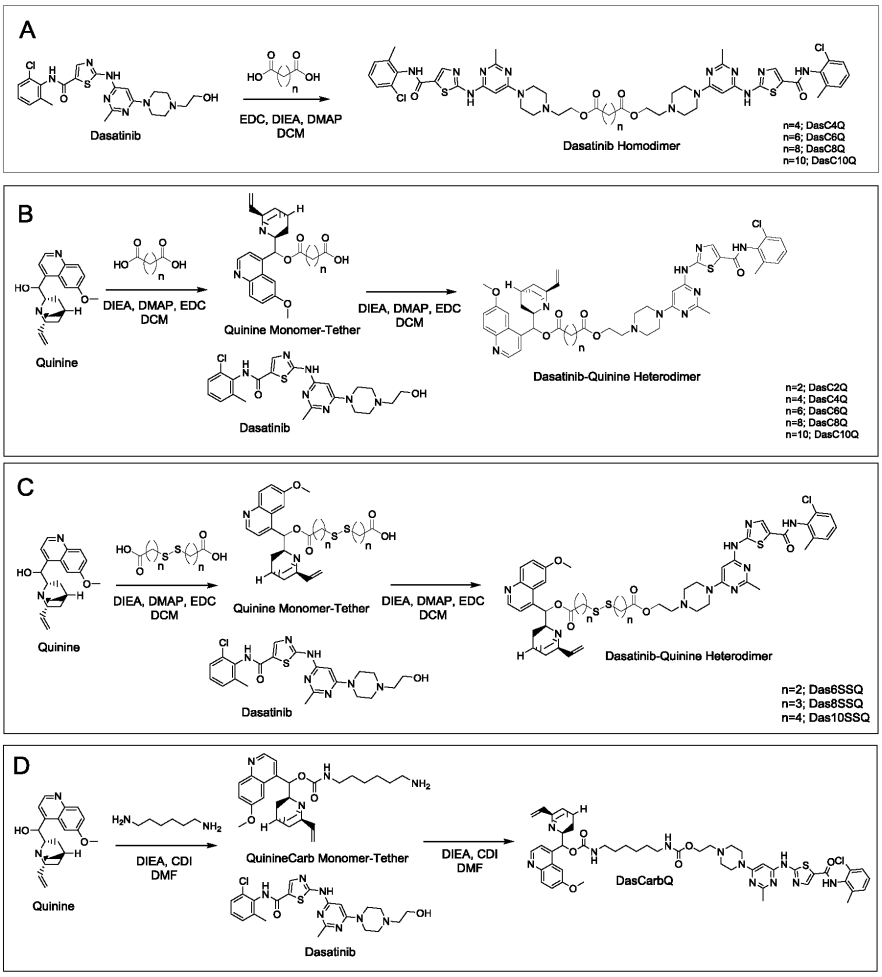

Figure 1: General Scheme of Dasatinib-based Dimers

Dasatinib dimers were synthesized in either EDC-coupling mechanisms (ester-linked) or CDI-coupling reactions (carbamate-linked). Dimers were named corresponding to the number of methylene units and/or sulfur atoms between ester bonds. For Dasatinib-Quinine dimers, Quinine was reacted either a carboxylic acid or a diamine to obtain 'Quinine-tether.' Quinine-tether was subsequently reacted with Dasatinib and coupling reagents to synthesize the heterodimers. All dimers were purified to >95% purity by semi-preparative HPLC and characterized by ESI mass spectroscopy and analytical HPLC.

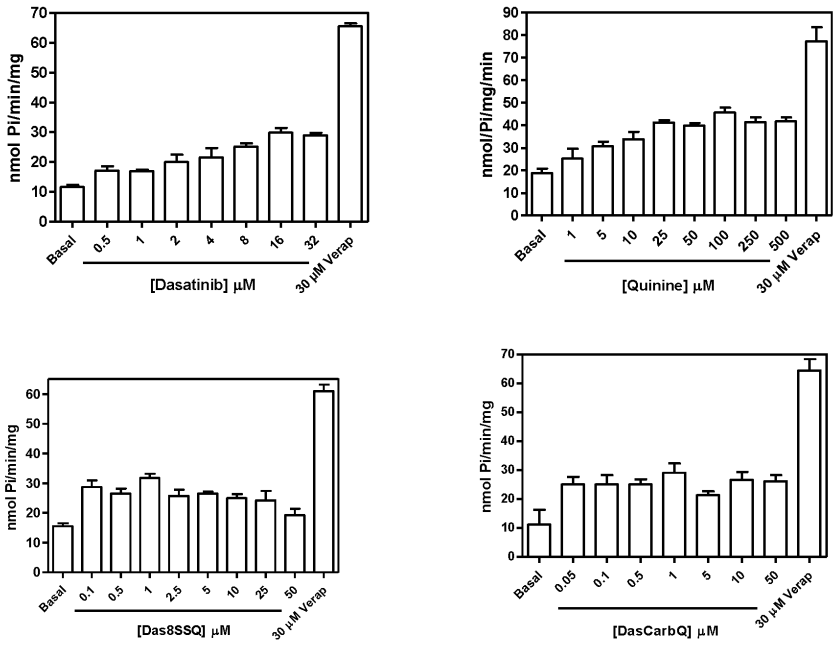

Figure 2: Test Compounds are Weak Stimulators of P-gp ATP Hydrolysis
Test compounds were incubated with crude Sf9 membranes expressing P-gp. ATP hydrolysis was approximated by the colorimetric detection of inorganic phosphate at each concentration by subtracting out the vanadate-insensitive portion as described previously [18]. Data represent at least two independent trials performed in duplicate ± standard error of the mean.

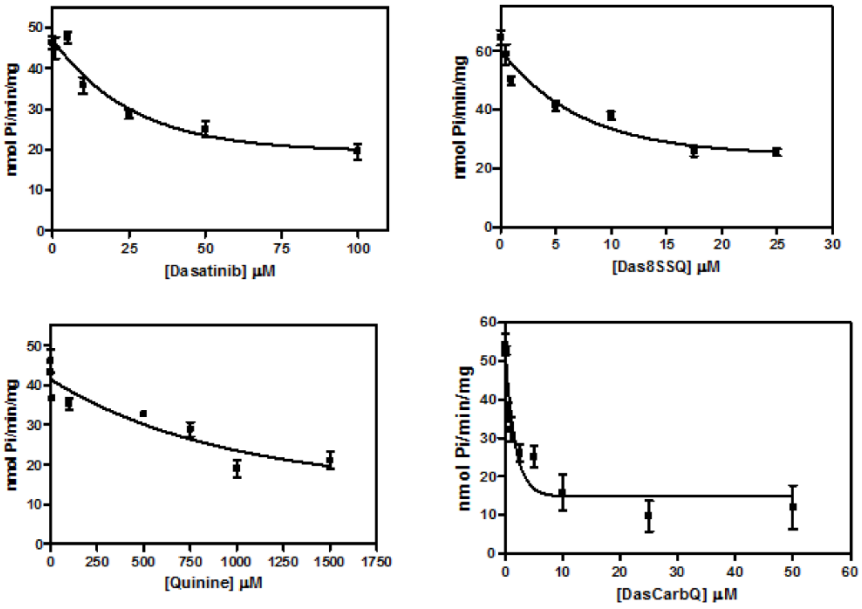

Figure 3: Test Compounds Inhibit Verapamil-Stimulated ATP Hydrolysis
Test compounds were incubated in increasing concentrations with verapamil (30 µM), ATP, and crude P-gp-expressing crude membranes derived from Sf9 cells. ATP hydrolysis is quantified colorimetrically by detecting inorganic phosphate release. Both Dasatinib and Quinine are capable of inhibiting verapamil-stimulated ATP hydrolysis, but Das8SSQ and DasCarbQ have a statistically significant more potent attenuation. These results indicate that our heterodimers are potent inhibitors of the P-gp catalytic cycle. Data represent two independent trials performed in duplicate. Activity is represented as nmol inorganic phosphate/min/mg.

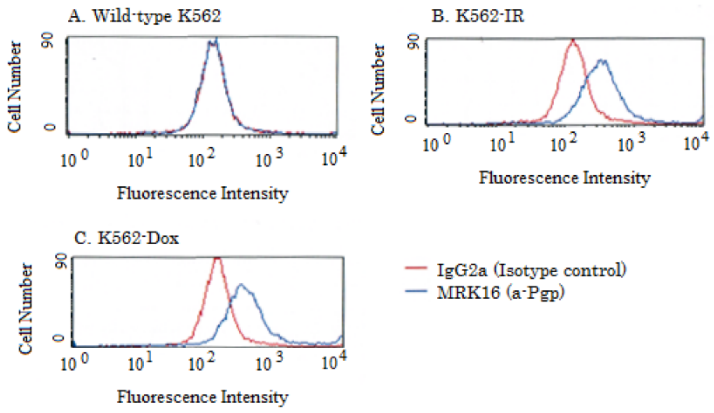

Figure 4: K562 Cell Surface Expression of P-gp
Flow cytometry was used to detect surface expression of P-gp in K562 and K562-derived cell lines. K562 WT cells do not express P-gp, while K562-IR and K562-Dox both express P-gp. MRK16 (α-P-gp) or IgG2a (isotype control) was incubated with K562 cells, followed by incubation with α-IgG2a-FITC antibody. Activity of P-gp in both cell lines was confirmed with the Calcein-AM inhibition assay with K562-IR or K562-Dox cells.

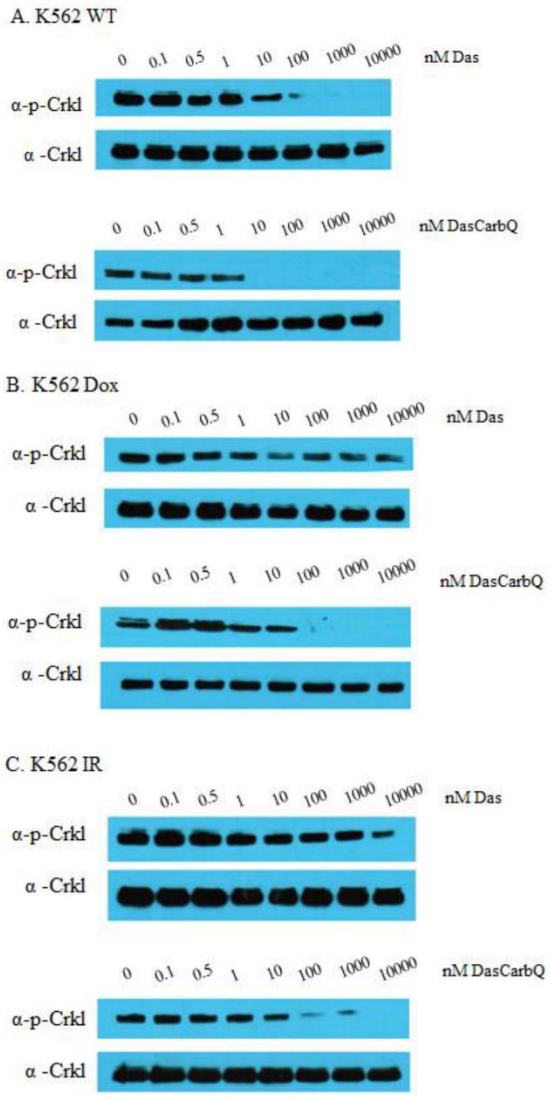

Figure 5: DasCarbQ has a more potent ability to inhibit Crkl phosphorylation than Das
K562 cells (WT, Dox, or IR) were incubated in increasing concentrations of either Dasatinib (Das) or DasCarbQ for 12 hours. Cells were harvested and lysates were probed for p-Crkl (Y207) using immunoblotting. Following p-Crkl detection, blots were stripped and probed for Crkl expression. Data are representative results for each condition. Two independent experiments were performed for each condition.

References

1. Gottesman, M.M., T. Fojo, and S.E. Bates, *Multidrug resistance in cancer: role of ATP-dependent transporters.* Nat Rev Cancer, 2002. **2**(1): p. 48-58.

2. Shukla, S., Z.S. Chen, and S.V. Ambudkar, *Tyrosine kinase inhibitors as modulators of ABC transporter-mediated drug resistance.* Drug Resist Updat. 10 2012. **15**(1-2): p. 70-80.

3. Rumjanek, V.M., R.S. Vidal, and R.C. Maia, *Multidrug resistance in chronic myeloid leukaemia: how much can we learn from MDR-CML cell lines?* Biosci Rep. 2013. **33**(6).

4. Stavrovskaya, A., et al., *Prognostic value of P-glycoprotein and leukocyte differentiation antigens in chronic myeloid leukemia.* Leuk Lymphoma, 1998. **28**(5-6): p. 469-82.

5. Hantschel, O. and G. Superti-Furga, *Regulation of the c-Abl and Bcr-Abl tyrosine kinases.* Nat Rev Mol Cell Biol, 2004. **5**(1): p. 33-44.

6. Pinilla-Ibarz, J., et al., *Role of tyrosine-kinase inhibitors in myeloproliferative neoplasms: comparative lessons learned.* Onco Targets Ther. 2016. **9**: p. 4937-57.

7. Yang, K. and L.W. Fu, *Mechanisms of resistance to BCR-ABL TKIs and the therapeutic strategies: A review.* Crit Rev Oncol Hematol. 2015. **93**(3): p. 277-92.

8. Eadie, L.N., et al., *The clinical significance of ABCB1 overexpression in predicting outcome of CML patients undergoing first-line imatinib treatment.* Leukemia. 2016. **31**(1): p. 75-82.

9. Daflon-Yunes, N., et al., *Characterization of a multidrug-resistant chronic myeloid leukemia cell line presenting multiple resistance mechanisms.* Mol Cell Biochem. 2013. **383**(1-2): p. 123-35.

10. Eadie, L.N., T.P. Hughes, and D.L. White, *Interaction of the efflux transporters ABCB1 and ABCG2 with imatinib, nilotinib, and dasatinib.* Clin Pharmacol Ther. 2014. **95**(3): p. 294-306.

11. Giles, F.J., et al., *Multidrug resistance protein expression in chronic myeloid leukemia: associations and significance.* Cancer, 1999. **86**(5): p. 805-13.

12. Dohse, M., et al., *Comparison of ATP-binding cassette transporter interactions with the tyrosine kinase inhibitors imatinib, nilotinib, and dasatinib.* Drug Metab Dispos. 2010. **38**(8): p. 1371-80.

13. Vasconcelos, F.C., et al., *Variation of MDR proteins expression and activity levels according to clinical status and evolution of CML patients.* Cytometry B Clin Cytom. 2011. **80**(3): p. 158-66.

14. Chan, K.F., et al., *Amine linked flavonoid dimers as modulators for P-glycoprotein-based multidrug resistance: structure-activity relationship and mechanism of modulation.* J Med Chem. 2012. **55**(5): p. 1999-2014.

15. Chan, K.F., et al., *Flavonoid dimers as bivalent modulators for P-glycoprotein-based multidrug resistance: synthetic apigenin homodimers linked with defined-length poly(ethylene glycol) spacers increase drug retention and enhance chemosensitivity in resistant cancer cells.* J Med Chem, 2006. **49**(23): p. 6742-59.

16. Namanja, H.A., et al., *Inhibition of human P-glycoprotein transport and substrate binding using a galantamine dimer.* Biochem Biophys Res Commun, 2009. **388**(4): p. 672-6.

17. Sauna, Z.E., et al., *Biochemical basis of polyvalency as a strategy for enhancing the efficacy of P-glycoprotein (ABCB1) modulators: stipiamide homodimers separated with defined-length spacers reverse drug efflux with greater efficacy.* Biochemistry, 2004. **43**(8): p. 2262-71.

18. Bohn, K., et al., *Dual Modulation of Human P-glycoprotein and ABCG2 with Prodrug Dimers of the Atypical Antipsychotic Agent Paliperidone in a Model of the Blood-Brain Barrier.* Mol Pharm. 2017. 14(4): 1107-1119.

19. Pires, M.M., C.A. Hrycyna, and J. Chmielewski, *Bivalent probes of the human multidrug transporter P-glycoprotein.* Biochemistry, 2006. **45**(38): p. 11695-702.

20. Pires, M.M., et al., *Inhibition of P-glycoprotein-mediated paclitaxel resistance by reversibly linked quinine homodimers.* Mol Pharmacol, 2009. **75**(1): p. 92-100.

21. Ouellette, S.B., B.M. Noel, and L.L. Parker, *A Cell-Based Assay for Measuring Endogenous BcrAbl Kinase Activity and Inhibitor Resistance.* PLoS One, 2016. **11**(9): p. e0161748.

22. Germann, U.A., et al., *Expression of the human multidrug transporter in insect cells by a recombinant baculovirus.* Biochemistry, 1990. **29**(9): p. 2295-303.

23. Ozvegy, C., et al., *Functional characterization of the human multidrug transporter, ABCG2, expressed in insect cells.* Biochem Biophys Res Commun, 2001. **285**(1): p. 111-7.

24. Hrycyna, C.A., et al., *Functional expression of human P-glycoprotein from plasmids using vaccinia virus-bacteriophage T7 RNA polymerase system.* Methods Enzymol, 1998. **292**: p. 456-73.

25. Assef, Y., et al., *Imatinib resistance in multidrug-resistant K562 human leukemic cells.* Leuk Res, 2009. **33**(5): p. 710-6.

26. Lagas, J.S., et al., *Brain accumulation of dasatinib is restricted by P-glycoprotein (ABCB1) and breast cancer resistance protein (ABCG2) and can be enhanced by elacridar treatment.* Clin Cancer Res, 2009. **15**(7): p. 2344-51.

27. Eck, M.J. and P.W. Manley, *The interplay of structural information and functional studies in kinase drug design: insights from BCR-Abl.* Curr Opin Cell Biol, 2009. **21**(2): p. 288-95.

28. Tokarski, J.S., et al., *The structure of Dasatinib (BMS-354825) bound to activated ABL kinase domain elucidates its inhibitory activity against imatinib-resistant ABL mutants.* Cancer Res, 2006. **66**(11): p. 5790-7.

29. Solary, E., et al., *Quinine circumvents the doxorubicin resistance of a multidrug resistant human leukemic cell-line, K562/DXR.* Nouv Rev Fr Hematol, 1990. **32**(5): p. 361-3.

30. Solary, E., et al., *Combination of quinine as a potential reversing agent with mitoxantrone and cytarabine for the treatment of acute leukemias: a randomized multicenter study.* Blood, 1996. **88**(4): p. 1198-205.

31. Solary, E., et al., *Feasibility of using quinine, a potential multidrug resistance-reversing agent, in combination with mitoxantrone and cytarabine for the treatment of acute leukemia.* J Clin Oncol, 1992. **10**(11): p. 1730-6.

32. Heaney, N.B. and T.L. Holyoake, *Therapeutic targets in chronic myeloid leukaemia.* Hematol Oncol, 2007. **25**(2): p. 66-75.

33. Giri, N., et al., *Substrate-dependent breast cancer resistance protein (Bcrp1/Abcg2)-mediated interactions: consideration of multiple binding sites in in vitro assay design.* Drug Metab Dispos, 2009. **37**(3): p. 560-70.

34. Peng, X.X., et al., *Overexpression of P-glycoprotein induces acquired resistance to imatinib in chronic myelogenous leukemia cells.* Chin J Cancer. 2012. **31**(2): p. 110-8.

35. O'Hare, T., et al., *In vitro activity of Bcr-Abl inhibitors AMN107 and BMS-354825 against clinically relevant imatinib-resistant Abl kinase domain mutants.* Cancer Res, 2005. **65**(11): p. 4500-5.

36. Dharmapuri, G., et al., *Celecoxib sensitizes imatinib-resistant K562 cells to imatinib by inhibiting MRP1-5, ABCA2 and ABCG2 transporters via Wnt and Ras signaling pathways.* Leuk Res. 2015. **39**(7): p. 696-701.

37. Ozvegy-Laczka, C., et al., *Tyrosine kinase inhibitor resistance in cancer: role of ABC multidrug transporters.* Drug Resist Updat, 2005. **8**(1-2): p. 15-26.

38. Hegedus, C., et al., *Interaction of nilotinib, dasatinib and bosutinib with ABCB1 and ABCG2: implications for altered anti-cancer effects and pharmacological properties.* Br J Pharmacol, 2009. **158**(4): p. 1153-64.

39. Hamilton, A., et al., *Optimization of methods for the detection of BCR-ABL activity in Philadelphia-positive cells.* Exp Hematol, 2009. **37**(3): p. 395-401.

40. Hamilton, A., et al., *BCR-ABL activity and its response to drugs can be determined in CD34+ CML stem cells by CrkL phosphorylation status using flow cytometry.* Leukemia, 2006. **20**(6): p. 1035-9.

41. Bateman DN, et. al. *Pharmacokinetics and clinical toxicity of quinine overdosage: lack of efficacy of techniques intended to enhance elimination*. Q J Med: 1985 ; 54 (214):125-31.

42. Cowan-Jacob SW, et. al. *Structural biology contributions to the discovery of drugs to treat chronic myelogenous leukaemia*. Acta Crystallogr D Biol Crystallogr. 2007. 63: 80-93.

43. Tang, C., et. al. *Tyrosine kinase inhibitor resistance in chronic myelogenous leukemia cell lines: investigating resistance pathways.* Leukemia & Lymphoma. 2011. 52(11): 2139-2147.

PUBLICATION

Manuscript under review with the journal Cancer Drug Resistance Dec. 2020

Current methodologies in defeating ATP-binding cassette transporter mediated multidrug resistance in cancer

Jason Goebel[1], Jean Chmielewski[1], and Christine Hrycyna[1]
[1]Department of Chemistry, Purdue University West Lafayette, IN 47907, USA
Correspondence Address: Christine Hrycyna, Department of Chemistry, Purdue University, 560 Oval Drive, West Lafayette, IN 47907-2084, USA Email: hrycyna@purdue.edu

Abstract

Many patients in terminal states of cancer have acquired a disseminated disease often becoming resistant to a variety of chemotherapeutics. Evidence acquired over the past 60 years suggests that the expression of ATP-binding cassette (ABC) transporters confer resistance to a wide variety of chemically and structurally unrelated anti-cancer agents. Most notably, ABC subfamily B member 1, known as P-glycoprotein (P-gp), and ABC subfamily G member 2 (ABCG2), also known as the breast cancer resistance protein, have been shown to have significant expression and thus function in the efflux of chemotherapeutics in the multidrug resistance phenotype observed in many cancers. Much effort has been dedicated to developing potent inhibitors to these proteins that have been effective *in vitro* however, no such inhibitor has yet to be FDA approved for the purpose of inhibiting an ABC transporter in multidrug resistant cancer. Recent developments in cryo-electron microscopy have allowed for the best crystal structures of human P-gp and ABCG2 in inhibited conformations to date helping to derive mechanisms of inhibition. Discovery of new classes of inhibitors is currently driving the discovery of new ABC transporter modulators. Other methods such as targeting signaling pathways controlling ABC transporter expression, use of microRNAs and small interfering RNAs, and drug and RNA conjugated nanoparticles are currently being researched in defeating multidrug resistance in cancer.

Keywords: P-glycoprotein, ABCG2, ABC Transporters, Multidrug Resistance

Introduction

A major and unfortunate outcome of long-term chemotherapy is accrued multidrug resistance (MDR) to a large range of structurally and chemically unrelated compounds.[1] It should be noted that the multidrug resistance phenotype is separate from drug resistance in certain cancers towards direct modulators of specific enzymes such as the observable Gleevec resistance in

chronic myelogenous leukemia due to mutations in the target oncogene enzyme, BCR-Abl.[2] Despite major efforts in combating multidrug resistance many patients with metastatic cancer will be overcome by the disease due to the lack in response to traditional chemotherapeutics. Many studies and reviews have been carried out describing the history of the discovery of multidrug resistance and the difficulty in developing new methodologies in treating patients who have developed multidrug resistance cancer at the end of a long regimen of chemotherapy.[3–5]

The basic mechanism of multidrug resistance has been extensively studied for 60 years. The phenotype was initially described in a subculture of HeLa cells that had been grown in selective media containing actinomycin D.[6] Later several cell lines of Chinese hamster cells were cultured with increasing concentrations of actinomycin D and then were shown to be resistant to a number of other drugs including daunomycin, vincristine, and vinblastine.[7] Further study of developed resistance was correlated to a transmembrane transporter which was later identified in Chinese hamster ovary (CHO) cells that were grown in media containing increasing concentrations of colchicine and shown to be resistant to a number of unrelated drugs.[8,9] The transporter was later purified from colchicine resistant CHO cells and identified as a 170 kDa glycoprotein.[10] Because of its observed glycosylation and effects in reducing permeability of many unrelated drugs in resistant cell lines, the transporter was given the name permeability glycoprotein or as it is more commonly referred, P-glycoprotein (P-gp). The gene encoding P-gp was identified and cloned from colchicine resistant CHO cells and the human homolog was soon discovered in carcinoma cells and soon thereafter given the gene name *mdr* for multidrug resistance gene.[11–13] Since the discovery of P-gp, an entire superfamily of transporters has been discovered and continues to be studied.[14,15] P-gp is a member of this family of ATP-binding cassette (ABC) transporters and has been given the gene classification of ABC subfamily B member 1, ABCB1, and the protein name modified from MDR1 to P-gp, though the two are often interchanged in literature, as MDR1 is a misnomer for the protein's endogenous function. Further study of the ABC transporter superfamily has revealed 48 human membrane transporters with diverse functions and many other ABC transporters in all domains of life.[16]

Another member of the ABC superfamily contributed to multidrug resistance in cancer is the breast cancer resistance protein (BCRP) often referred to as ABCG2 after its gene name. ABCG2 was reported on by a number of studies that discovered the protein in Adriamycin resistant MCF-7 breast cancer cells and mitoxantrone resistant S1-M1-80 colon carcinoma cells.[17–19]

Discovery of more ABC transporters associated with a multidrug resistance phenotype in drug resistant cells increased the interest in studying and developing methodologies to combat acquired multidrug resistance in cancer. Although the presence of ABC transporters in cancer has been attributed to multidrug resistance the extent of the multidrug resistance phenotype in cancer has not been fully elucidated. Also of interest, and something to be mindful of, is endogenous expression of ABC transporters at blood-tissue barriers such as the blood brain barrier leading to reduced uptake of therapeutics across these barriers.[20] P-gp and ABCG2 are expressed on the apical surface of endothelial cells and affect drug penetration to specific tissues and is of importance when developing small molecules that will need to pass these barriers.[21] Many inhibitors and modulators of P-gp and ABCG2 that have been successful *in vitro* have not been successful in reversing multidrug resistance *in vivo* though continued evidence marks that expression of ABC transporters remain important in multidrug resistance in some settings and thus motivates the need for continued development of ABC transporter inhibitors and modulators.

Evidence for the importance of ABC transporters in cancer

Many studies have examined the importance of ABC transporter expression in cancer with poor outcomes due to multidrug resistance.[22,23] Overexpression of these transporters have been reported in many cancers including but not limited to leukemias, kidney, colon, breast, carcinoid tumors, adrenal, pancreas, and lung cancers.[24–28] P-gp overexpression confers multidrug resistance to a variety of unrelated neutral and cationic hydrophobic anticancer agents including anthracyclines, camptothecins, epipodophyllotoxins, taxanes, tyrosine kinase inhibitors, and vinca alkaloids.[29–32] Substrate recognition by ABCG2 has some overlap with P-gp and some notable differences as ABCG2 transports the anticancer drugs flavopiridol, irinotecan, methotrexate, and mitoxantrone.[33]

P-gp and ABCG2 expression have been correlated to several low response rates to chemotherapeutics in many cases. Poor outcomes in patients with higher expression levels of P-gp have been described in non-small-cell and small-cell lung carcinomas in treatment with paclitaxel and cyclophosphamide, cis-platin, doxorubicin, and vincristine, respectively.[34] CML patients with high expression of ABCG2 were shown to have a two-fold higher risk of relapse than patients with lower expression of the transporter suggesting enhanced efflux of tyrosine kinase inhibitors and diminished efficacy of chemotherapeutic treatment.[35] Numerous more studies

indicate the presence of ABC transporter mRNA and protein in clinical samples and indicate poor responses to chemotherapy.[24–26] Drug interactions with ABC transporters must be taken into consideration as small molecule anticancer treatments continue to be developed.

Mechanisms of Multidrug Resistance and Implications for clinical drug resistance

ABC transporters present in cell membranes of multidrug resistant cancer are responsible for significant alterations in pharmacokinetics of many chemotherapeutics in absorption, distribution, secretion of drugs in cells.[36] The major mode of multidrug resistance observed in cancer due to the expression of ABC transporters, specifically P-gp and ABCG2, is their ability to confer enhanced efflux of drugs from cell plasma membranes thereby reducing drug permeability into cancer cells reducing intracellular concentrations of those chemotherapeutics. Structurally, ABC transporters consist of 4 domains. Two cytoplasmic nucleotide binding domains (NBDs) that hydrolyze ATP for substrate transport and two transmembrane domains (TMDs) that bind substrates. These domains can be encoded by a single gene to produce a full-transporter, as with P-gp, or a gene or pair of genes can encode one NBD and one TMD to produce a half-transporter that can homodimerize, as with ABCG2, or heterodimerize to produce the full-transporter structure.[37]

The NBDs are highly conserved and fall into the P-loop NTPase superfamily with a RecA-type binding core along with a unique ABC signature motif, LSGGQ.[38] TMDs are more heterogenous allowing for a range of substrate recognition and differences in function.[14] While energy from ATP hydrolysis primarily drives substrate transport, high levels of basal ATP hydrolysis, seen in multidrug resistance related transporters, suggests that these transporters sample a range of conformations that may facilitate transport of a wide range of substrates.[39] Figure 1 highlights the basic scheme of ATP hydrolyzed substrate transport in P-gp demonstrating the highly dynamic nature of ABC transporter substrate efflux. High resolution cryo-electron microscopy structures, as well as many other x-ray crystallography structures, of P-gp and ABCG2 have been solved and have been useful in determining substrate binding but it must be remembered that these structures are only snapshots of highly dynamic proteins.[40,41] Even with numerous structures of related P-gp and ABCG2 homologues, the exact translocation mechanism remains unresolved though recent breakthroughs with single molecule cryo-EM are substantially improving the understanding of the structure function relationship in both P-gp and ABCG2.[42]

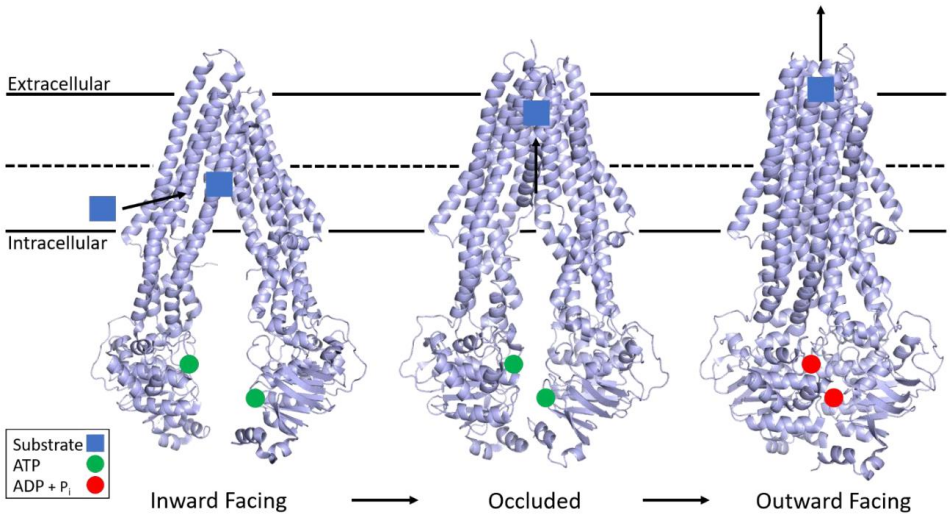

Figure 1: Structure of P-gp and basic mechanism of ATP hydrolysis and transport. P-gp undergoes large conformational changes in its transport mechanism. Substrate from the inner leaflet first interacts with an inward facing conformation of P-gp while two ATP molecules bind the free NBDs. The structure then adopts an occluded state with substrate bound at the apex of the TMDs while TM helices 4 and 10 significantly kink inwards occluding the binding pocket. The outward facing conformation is correlated with asymmetric ATP hydrolysis and solvent exposed substrate diffusion into extracellular space before ADP release and the mechanism resetting. PDB: 5KPI (inward), 7A6C (occluded), and 6C0V (outward)

Many techniques have been used to elucidate the drug binding site of P-gp. Initially cysteine scanning mutagenesis with thiol-reactive substrates and photoaffinity labeling were used to describe initial substrate binding pockets.[43,44] Further attempts documented separate rhodamine 123, Hoeschst 33342, and prazosin binding sites and their complex interplay of competitive binding or positively cooperative transport.[45–47] However, mutagenesis of previously determined binding site residues revealed alternate binding sites within the P-gp binding pocket.[48,49] Continued study and analysis of residues in the binding pocket reveal a mostly hydrophobic region of aromatic residues that are capable of binding a large variety of substrates and able to bind multiple substrates simultaneously.[50,51] Similarly, ABCG2 has the ability to recognize a multitude of substrates as it has a similar function as P-gp as a transporter of xenobiotics. Both P-gp and ABCG2 recognize many anticancer agents and as such overexpression of these transporters can lead to ABC transporter multidrug resistance observed cancer.

Mechanisms of Inhibition through Stabilization of Intermediate Conformations

P-gp contains two homologous halves of 6 transmembrane helices and an NBD each forming a Type I exporter. Recent cryo-EM structures have shown P-gp in an inhibitor bound, occluded state which gives insight into how some inhibitors of P-gp may function. In the occluded state, either paclitaxel or zosuquidar bound, transmembrane helices 4 and 10 are significantly kinked inward towards each other in the structure occluding the binding site from the plasma membrane.[52] Further investigation of occluded structures with bound substrates and inhibitors revealed the known, large hydrophobic binding pocket of P-gp, with bound paclitaxel and vincristine, and also a vestibule and access tunnel formed by transmembrane helices 7, 8, 9, and 12 occupied by elacridar, tariquidar, and zosuquidar.[53] These structures also reveal that two inhibitor molecules bind simultaneously with one molecule occupying the drug binding pocket while the other binds the drug binding pocket but extends into the vestibule (zosuquidar) or further into the access tunnel (elacridar and tariquidar) [Figure 2A]. Rearrangement of transmembrane helices 9 and 12 are hindered by occupation of the access tunnel and to a lesser extent the vestibule region which further inhibits dimerization of the NBDs and ATP hydrolysis that drive transport.[53]

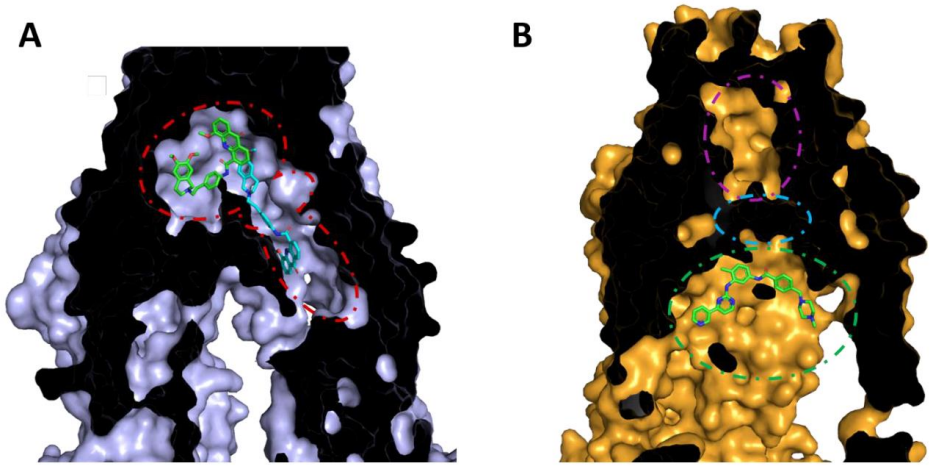

Figure 2: Cross sections of cryo-EM structures of P-gp and ABCG2 with bound inhibitors in inward facing conformations. Extracellular space is towards the top of the image and intracellular space is towards the bottom. A: Cryo-EM structure of P-gp bound with two molecules of the inhibitor elacridar. One molecule (green) is bound to the drug binding pocket while the other (cyan) passes through a smaller binding region, vestibule, before extending into an access tunnel. It is thought that the presence of inhibitor in the vestibule and to a greater extent the access tunnel inhibits conformational changes of TM helices 9 and 12 inhibiting transport of substrates. B: Cryo-EM structure of ABCG2 with bound imatinib. Imatinib is bound to the top of cavity 1 (green) under the leucine plug

(cyan) and is believed to act as a plug stopping conformational changes to allow substrate to pass into cavity 2 (magenta) to be effluxed. PDB: 7A6C (P-gp) and 6VXH (ABCG2)

ABCG2 is a homodimer of an NBD and 6 TMDs forming a Type II exporter. Interestingly, ABCG2 has been shown to have two cavities within its structure for substrate binding. Cavity 1 is exposed to the cytoplasmic side of the membrane allowing for substrate binding and is separated from cavity 2 by a leucine plug (residues L554 and L554').[54] Cavity 2 is not exposed to extracellular space in inward facing structures of ABCG2 and is capped by transmembrane helices 5b, 5c, and 6a from both monomers.[54] During transport substrate likely moves from cavity 1 to cavity 2 by conformational changes in the leucine plug. Further conformational changes shift transmembrane helices 5b, 5c, and 6a exposing the cavity to extracellular space. Derivatives of Ko143, an inhibitor of ABCG2, show inhibition through stabilization of the inward facing structures.[55] Further investigation in the transport of anticancer drugs shows imatinib stabilizes the open inward structure of ABCG2 inhibiting transport though not as well as more potent inhibitors such as Ko143.[56] Imatinib was able to bind directly under the leucine plug in cavity 1 and was sandwiched between F439 of both ABCG2 monomers potentially acting as a wedge to stabilize the inhibited, inward facing conformation [Figure 2B].

Advances in Defeating Multidrug Resistance in Cancer

After the discovery of P-gp, a number of inhibitors were identified including amiodarone, cyclosporine A, quinidine, and verapamil and implemented in chemotherapy regimes in clinical trials.[57] Promising results *in vitro* were not seen in patients as the first generation of inhibitors were not potent and potentially toxic.[5] Second generation inhibitors, such as valspodar, were more potent than the first generation but resulted in no better outcomes due to off target interactions. Valspodar specifically inhibits cytochrome p450 which required dose reductions leading to under dosing for defeating multidrug resistance.[58] Third generation inhibitors including biricodar, elacridar, dofequidar, tariquidar, and zosuquidar were designed specifically for P-gp in the hopes of better outcomes with coadministration with chemotherapeutics. However, coadministration with chemotherapeutics lead to increased toxicity likely due to increased inhibition of endogenous P-gp.[57] ABCG2 has also been shown to be inhibited by many inhibitors including some cross-reactivity with P-gp inhibitors cyclosporin A, elacridar, tariquidar but had similar outcomes in

clinical trials.[59] Though lamentable, the failure of inhibitors of ABC transporters have driven new research in battling multidrug resistance in cancer.

Despite the failure of early inhibitors many small molecule inhibitors and modulators continue to be developed for P-gp and ABCG2. The design around these modulators focus on different aspects of interrupting transport of ABC transporters through either direct interaction with the drug binding site, interaction with allosteric residues to modulate transport activity, inhibition of ATP binding, or interaction with the lipid bilayer to interrupt the membrane environment.[60–63] To this end a number of classes of inhibitors are currently being developed including aromatic or heterocyclic dimers[64,65], bifendates[66,67], condensed ring derivatives[68–70], 1,4-dihydropyridines[71–73], flavonoids[74–76], peptides[50,77,78], steroids[79–81], and tetrahydroisoquinolines.[82–84] Most inhibitors of P-gp stimulate ATPase activity while few fully inhibit ATPase function and transport.[63,85] New insight into inhibitor bound structures of P-gp and ABCG2 may give understanding into how inhibitors that are not transported interact with the transporters allowing for better rational drug design with new classes of P-gp and ABCG2 inhibitors.

In addition to slowing efflux function, some inhibitors have also been shown to modulate expression of P-gp and ABCG2 through inhibiting signaling pathways opening ideas about other possible mechanisms to defeat multidrug resistance in cancer. Dasatinib, a tyrosine kinase inhibitor, has been shown to inhibit the activation of ERK signaling which leads to downregulating P-gp expression.[86] Vacuolar H^+-ATPases, mTOR, and hypoxia-inducible factor 1α inhibition by proton pump inhibitors in MDR cell lines have shown decreased expression of P-gp.[87] Decreases in P-gp expression has also been observed in the suppression of the phosphatidylinositol 3-kinase/ Akt/ nuclear factor-κB singaling pathway with curcumin or tamoxifen.[88,89]

MicroRNAs (miRNAs) have recently become in interest for use in treatment of cancer and potentially regulating MDR deviating away from traditional small molecule inhibitors that have so far been unsuccessful. miRNAs are non-coding RNA molecules that bind mRNA to suppress protein regulation in translation. miRNA has been used to downregulate the JNK2/c-Jun pathway increasing sensitivity to chemotherapeutic drugs in MDR colorectal cancer tumor samples.[90] Direct downregulation of MDR ABC transporter translation can also be achieved through miRNAs specific for P-gp and ABCG2.[91,92] Small interfering RNAs (siRNAs) downregulate protein expression through operating in the RNA interference pathway which degrades mRNA after

translation. siRNAs have also been shown to downregulate expression of P-gp and ABCG2 restoring sensitivity of cancer cells to chemotherapeutics.[93–95]

P-gp and ABCG2 monoclonal antibodies could potentially reverse MDR. MRK16 and MRK17 were developed in the 1980s to reverse drug resistance.[96–98] MRK16 blocked efflux of actinomycin D and vincristine while MRK17 inhibited MDR cell proliferation. UIC2 was developed and had a greater extent in inhibiting P-gp through increased extracellular loop interactions compared to MRK16 and 17 and was able to suppress efflux of chemotherapeutics to a greater extent.[99] However, not much advancement in antibodies have been made due to the limitations of using antibodies or fragment antigen-binding in treatments *in vivo*.

Finally, nanotechnology-based approaches provide for efficient strategies in defeating MDR largely by circumventing interaction with ABC transporters at the plasma membrane. Many different types of nanoparticles including polymers, dendrimers, liposomes, micelles and quantum dots have been used to carry anti-cancer drugs and siRNA to specific targets.[100] Due to the nature in which nanoparticles enter the cell, mostly through endocytosis, they completely circumvent interactions with MDR ABC transporters.[101] Furthermore some polymer based nanoparticles can act as P-gp or ABCG2 modulators, such as polymers of N-(2-hydroxypropyl) methacrylamide, to inhibit efflux of substrate once it is released by the nanoparticle.[102] Nanoparticles can also be designed to carry P-gp and ABCG2 inhibitors or modulators to reduce intracellular ATP with chemotherapeutics to bypass ABC transporters and then modulate their activity after release of drug.[103,104] Targeting ABC transporter expression can also be coupled with nanoparticle design as seen in cancer cell membrane-coated silica particles containing miRNA-495 downregulating P-gp in MDR lung cancer cells.[105]

Conclusions

Much effort has been put into researching multidrug resistance in cancer over the past 60 years and has led to numerous discoveries including the superfamily of ABC transporters. While the role of ABC transporters, including P-gp and ABCG2, has been studied extensively *in vitro* there is still much to learn about the role of ABC transporter expression in cancer in clinical settings. Need for better understanding of MDR in cancer is driven by large percentages of patients with terminal stages of cancer developing the MDR phenotype making treatment extensively more difficult. While early discovery of P-gp and ABCG2 inhibitors were promising, there has yet to be

a modulator for P-gp or ABCG2 that has been FDA approved for the use in combating multidrug resistance. Regardless, the scientific community has pushed to expand the discovery of inhibitory molecules to many diverse classes of synthetic and natural products. Major advancements in cryo-EM in the last decade have begun to give great insight into the structure of human P-gp and ABCG2 and most recently insight into inhibitor bound structures. Alternative methods in defeating MDR are also continuing to be explored to a greater extent. Targeting signaling pathways controlling P-gp and ABCG2 expression, inhibiting expression with miRNAs and siRNAs, and circumventing ABC transporters through use of nanoparticles are all currently under investigation. Continued research interest in ABC transporter mediated MDR in cancer could potentially lead to new clinical applications of therapies to combat MDR.

Declarations

Authors' contributions
Contributed to writing and revision of the article: Jason Goebel
Contributed to review and revision of the article: Jean Chmielewski, Christine Hrycyna
Availability of data and materials
Not applicable.
Financial support and sponsorship
None.
Conflicts of interest
All authors declared that there are no conflicts of interest.
Ethical approval and consent to participate
Not applicable.
Consent for publication
Not applicable.

References

1. Patel NH, Rothenberg ML. Multidrug resistance in cancer chemotherapy. Invest New Drugs. 1994;12(1):1-13. doi:10.1007/BF00873229

2. Rosée PL, Corbin AS, Stoffregen EP, Deininger MW, Druker BJ. Activity of the Bcr-Abl Kinase Inhibitor PD180970 against Clinically Relevant Bcr-Abl Isoforms That Cause Resistance to Imatinib Mesylate (Gleevec, STI571). Cancer Res. 2002;62(24):7149-7153.

3. Sharom FJ, Tamaki A, Ierano C, Szakacs G, Robey RW, Bates SE. The controversial role of ABC transporters in clinical oncology. Essays Biochem. 2011;50:209-232. doi:10.1042/bse0500209

4. Sharom FJ. ABC multidrug transporters: structure, function and role in chemoresistance. Pharmacogenomics. 2007;9(1):105-127. doi:10.2217/14622416.9.1.105

5. Gottesman MM, Fojo T, Bates SE. Multidrug resistance in cancer: role of ATP–dependent transporters. Nat Rev Cancer. 2002;2(1):48-58. doi:10.1038/nrc706

6. Goldstein MN, Slotnick IJ, Journey LJ. In Vitro Studies with Hela Cell Lines Sensitive and Resistant to Actinomycin D. Ann N Y Acad Sci. 1960;89(2):474-483. doi:10.1111/j.1749-6632.1960.tb20171.x

7. Biedler JL, Riehm H. Cellular Resistance to Actinomycin D in Chinese Hamster Cells in Vitro: Cross-Resistance, Radioautographic, and Cytogenetic Studies. Cancer Res. 1970;30(4):1174-1184.

8. Danø K. Active outward transport of daunomycin in resistant ehrlich ascites tumor cells. Biochim Biophys Acta BBA - Biomembr. 1973;323(3):466-483. doi:10.1016/0005-2736(73)90191-0

9. Juliano RL, Ling V. A surface glycoprotein modulating drug permeability in Chinese hamster ovary cell mutants. Biochim Biophys Acta. 1976;455(1):152-162. doi:10.1016/0005-2736(76)90160-7

10. Riordan JR, Ling V. Purification of P-glycoprotein from plasma membrane vesicles of Chinese hamster ovary cell mutants with reduced colchicine permeability. J Biol Chem. 1979;254(24):12701-12705.

11. Gros P, Croop J, Roninson I, Varshavsky A, Housman DE. Isolation and characterization of DNA sequences amplified in multidrug-resistant hamster cells. Proc Natl Acad Sci. 1986;83(2):337-341. doi:10.1073/pnas.83.2.337

12. Roninson IB, Chin JE, Choi KG, et al. Isolation of human mdr DNA sequences amplified in multidrug-resistant KB carcinoma cells. Proc Natl Acad Sci. 1986;83(12):4538-4542. doi:10.1073/pnas.83.12.4538

13. Ueda K, Cornwell MM, Gottesman MM, et al. The mdrl gene, responsible for multidrug-resistance, codes for P-glycoprotein. Biochem Biophys Res Commun. 1986;141(3):956-962. doi:10.1016/S0006-291X(86)80136-X

14. Dean M, Hamon Y, Chimini G. The human ATP-binding cassette (ABC) transporter superfamily. J Lipid Res. 2001;42(7):1007-1017.

15. Higgins CF. ABC Transporters: From Microorganisms to Man. Annu Rev Cell Biol. 1992;8(1):67-113. doi:10.1146/annurev.cb.08.110192.000435

16. Gottesman MM, Ling V. The molecular basis of multidrug resistance in cancer: The early years of P-glycoprotein research. FEBS Lett. 2006;580(4):998-1009. doi:10.1016/j.febslet.2005.12.060

17. Miyake K, Mickley L, Litman T, et al. Molecular Cloning of cDNAs Which Are Highly Overexpressed in Mitoxantrone-resistant Cells: Demonstration of Homology to ABC Transport Genes. Cancer Res. 1999;59(1):8-13.

18. Allikmets R, Schriml LM, Hutchinson A, Romano-Spica V, Dean M. A Human Placenta-specific ATP-Binding Cassette Gene (ABCP) on Chromosome 4q22 That Is Involved in Multidrug Resistance. Cancer Res. 1998;58(23):5337-5339.

19. Doyle LA, Yang W, Abruzzo LV, et al. A multidrug resistance transporter from human MCF-7 breast cancer cells. Proc Natl Acad Sci. 1998;95(26):15665-15670. doi:10.1073/pnas.95.26.15665

20. Cox DS, Scott KR, Gao H, Raje S, Eddington ND. Influence of multidrug resistance (MDR) proteins at the blood-brain barrier on the transport and brain distribution of enaminone anticonvulsants. J Pharm Sci. 2001;90(10):1540-1552.

21. Banks WA. From blood-brain barrier to blood-brain interface: new opportunities for CNS drug delivery. Nat Rev Drug Discov. 2016;15(4):275-292. doi:10.1038/nrd.2015.21

22. Perez EA. Impact, mechanisms, and novel chemotherapy strategies for overcoming resistance to anthracyclines and taxanes in metastatic breast cancer. Breast Cancer Res Treat. 2008;114(2):195. doi:10.1007/s10549-008-0005-6

23. Yardley DA. Drug Resistance and the Role of Combination Chemotherapy in Improving Patient Outcomes. International Journal of Breast Cancer. doi:10.1155/2013/137414

24. Goldstein LJ, Galski H, Fojo A, et al. Expression of Multidrug Resistance Gene in Human Cancers. JNCI J Natl Cancer Inst. 1989;81(2):116-124. doi:10.1093/jnci/81.2.116

25. Amiri-Kordestani L, Basseville A, Kurdziel K, Fojo AT, Bates SE. Targeting MDR in breast and lung cancer: Discriminating its potential importance from the failure of drug resistance reversal studies. Drug Resist Updat. 2012;15(1):50-61. doi:10.1016/j.drup.2012.02.002

26. W. Robey R, R. Massey P, Amiri-Kordestani L, E. Bates S. ABC Transporters: Unvalidated Therapeutic Targets in Cancer and the CNS. Anti-Cancer Agents Med Chem- Anti-Cancer Agents. 2010;10(8):625-633. doi:10.2174/187152010794473957

27. Assaraf YG. Molecular basis of antifolate resistance. Cancer Metastasis Rev. 2007;26(1):153-181. doi:10.1007/s10555-007-9049-z

28. Wong ST, Goodin S. Overcoming Drug Resistance in Patients with Metastatic Breast Cancer. Pharmacother J Hum Pharmacol Drug Ther. 2009;29(8):954-965. doi:10.1592/phco.29.8.954

29. Gottesman MM, Ambudkar SV. Overview: ABC Transporters and Human Disease. J Bioenerg Biomembr. 2001;33(6):453-458. doi:10.1023/A:1012866803188

30. K. Tiwari A, Sodani K, Dai C-L, R. Ashby C, Chen Z-S. Revisiting the ABCs of Multidrug Resistance in Cancer Chemotherapy. Curr Pharm Biotechnol. 2011;12(4):570-594. doi:10.2174/138920111795164048

31. Schinkel AH, Jonker JW. Mammalian drug efflux transporters of the ATP binding cassette (ABC) family: an overview. Adv Drug Deliv Rev. 2012;64:138-153. doi:10.1016/j.addr.2012.09.027

32. Assaraf YG, Brozovic A, Gonçalves AC, et al. The multi-factorial nature of clinical multidrug resistance in cancer. Drug Resist Updat. 2019;46:100645. doi:10.1016/j.drup.2019.100645

33. Mao Q, Unadkat JD. Role of the Breast Cancer Resistance Protein (BCRP/ABCG2) in Drug Transport—an Update. AAPS J. 2015;17(1):65-82. doi:10.1208/s12248-014-9668-6

34. Hsia T, Lin C, Wang J, Ho S, Kao A. Relationship Between Chemotherapy Response of Small Cell Lung Cancer and P-glycoprotein or Multidrug Resistance-Related Protein Expression. Lung. 2002;180:173-179. doi:10.1007/s004080000091

35. Rinaldetti S, Pfirrmann M, Manz K, et al. Effect of ABCG2, OCT1, and ABCB1 (MDR1) Gene Expression on Treatment-Free Remission in a EURO-SKI Subtrial. Clin Lymphoma Myeloma Leuk. 2018;18(4):266-271. doi:10.1016/j.clml.2018.02.004

36. Chen L, Li Y, Zhao Q, Peng H, Hou T. ADME Evaluation in Drug Discovery. 10. Predictions of P-Glycoprotein Inhibitors Using Recursive Partitioning and Naive Bayesian Classification Techniques. Mol Pharm. 2011;8(3):889-900. doi:10.1021/mp100465q

37. Holland B, Cole S, Kuchlar K, Higgins C. ABC Proteins: From Bacteria to Man. Academic Press; 2003.

38. Thomas C, Tampé R. Structural and Mechanistic Principles of ABC Transporters. Annu Rev Biochem. 2020;89(1):605-636. doi:10.1146/annurev-biochem-011520-105201

39. Esser L, Zhou F, Pluchino KM, et al. Structures of the Multidrug Transporter P-glycoprotein Reveal Asymmetric ATP Binding and the Mechanism of Polyspecificity. J Biol Chem. 2017;292(2):446-461. doi:10.1074/jbc.M116.755884

40. Taylor NMI, Manolaridis I, Jackson SM, Kowal J, Stahlberg H, Locher KP. Structure of the human multidrug transporter ABCG2. Nature. 2017;546(7659):504-509. doi:10.1038/nature22345

41. Kim Y, Chen J. Molecular structure of human P-glycoprotein in the ATP-bound, outward-facing conformation. Science. Published online January 25, 2018:eaar7389. doi:10.1126/science.aar7389

42. Bai X, McMullan G, Scheres SHW. How cryo-EM is revolutionizing structural biology. Trends Biochem Sci. 2015;40(1):49-57. doi:10.1016/j.tibs.2014.10.005

43. Loo TW, Clarke DM. Determining the structure and mechanism of the human multidrug resistance P-glycoprotein using cysteine-scanning mutagenesis and thiol-modification techniques. Biochim Biophys Acta BBA - Biomembr. 1999;1461(2):315-325. doi:10.1016/S0005-2736(99)00165-0

44. Loo TW, Clarke DM. The Transmembrane Domains of the Human Multidrug Resistance P-glycoprotein Are Sufficient to Mediate Drug Binding and Trafficking to the Cell Surface. J Biol Chem. 1999;274(35):24759-24765. doi:10.1074/jbc.274.35.24759

45. Shapiro AB, Ling V. Positively cooperative sites for drug transport by P-glycoprotein with distinct drug specificities. Eur J Biochem. 1997;250(1):130–137.

46. Shapiro AB, Fox K, Lam P, Ling V. Stimulation of P-glycoprotein-mediated drug transport by prazosin and progesterone. Eur J Biochem. 1999;259(3):841-850. doi:10.1046/j.1432-1327.1999.00098.x

47. Martin C, Berridge G, Higgins CF, Mistry P, Charlton P, Callaghan R. Communication between Multiple Drug Binding Sites on P-glycoprotein. Mol Pharmacol. 2000;58(3):624-632. doi:10.1124/mol.58.3.624

48. Loo TW, Clarke DM. Location of the Rhodamine-binding Site in the Human Multidrug Resistance P-glycoprotein. J Biol Chem. 2002;277(46):44332-44338. doi:10.1074/jbc.M208433200

49. Mittra R, Pavy M, Subramanian N, et al. Location of contact residues in pharmacologically distinct drug binding sites on P-glycoprotein. Biochem Pharmacol. 2017;123:19-28. doi:10.1016/j.bcp.2016.10.002

50. Aller SG, Yu J, Ward A, et al. Structure of P-glycoprotein reveals a molecular basis for poly-specific drug binding. Science. 2009;323(5922):1718–1722.

51. Szewczyk P, Tao H, McGrath AP, et al. Snapshots of ligand entry, malleable binding and induced helical movement in P-glycoprotein. Acta Crystallogr D Biol Crystallogr. 2015;71(3):732-741. doi:10.1107/S1399004715000978

52. Alam A, Kowal J, Broude E, Roninson I, Locher KP. Structural insight into substrate and inhibitor discrimination by human P-glycoprotein. Science. 2019;363(6428):753-756. doi:10.1126/science.aav7102

53. Nosol K, Romane K, Irobalieva RN, et al. Cryo-EM structures reveal distinct mechanisms of inhibition of the human multidrug transporter ABCB1. Proc Natl Acad Sci. 2020;117(42):26245-26253. doi:10.1073/pnas.2010264117

54. Manolaridis I, Jackson SM, Taylor NMI, Kowal J, Stahlberg H, Locher KP. Cryo-EM structures of a human ABCG2 mutant trapped in ATP-bound and substrate-bound states. Nature. 2018;563(7731):426-430. doi:10.1038/s41586-018-0680-3

55. Jackson SM, Manolaridis I, Kowal J, et al. Structural basis of small-molecule inhibition of human multidrug transporter ABCG2. Nat Struct Mol Biol. 2018;25(4):333-340. doi:10.1038/s41594-018-0049-1

56. Orlando BJ, Liao M. ABCG2 transports anticancer drugs via a closed-to-open switch. Nat Commun. 2020;11(1):2264. doi:10.1038/s41467-020-16155-2

57. Binkhathlan Z, Lavasanifar A. P-glycoprotein Inhibition as a Therapeutic Approach for Overcoming Multidrug Resistance in Cancer: Current Status and Future Perspectives. Curr Cancer Drug Targets. 2013;13(3):326-346.

58. Leonard G, Polgar O, Bates SE. ABC transporters and inhibitors: new targets, new agents. Curr Opin Investig Drugs. 2002;(3):1652-1659.

59. de Bruin M, Miyake K, Litman T, Robey R, Bates SE. Reversal of resistance by GF120918 in cell lines expressing the ABC half-transporter, MXR. Cancer Lett. 1999;146(2):117-126. doi:10.1016/S0304-3835(99)00182-2

60. Drori S, Eytan GD, Assaraf YG. Potentiation of Anticancer-Drug Cytotoxicity by Multidrug-Resistance Chemosensitizers Involves Alterationsin Membrane Fluidity Leading to Increased Membrane Permeability. Eur J Biochem. 1995;228(3):1020-1029. doi:10.1111/j.1432-1033.1995.1020m.x

61. Regev R, Assaraf YG, Eytan GD. Membrane fluidization by ether, other anesthetics, and certain agents abolishes P-glycoprotein ATPase activity and modulates efflux from multidrug-resistant cells. Eur J Biochem. 1999;259(1-2):18-24. doi:10.1046/j.1432-1327.1999.00037.x

62. Varma MVS, Ashokraj Y, Dey CS, Panchagnula R. P-glycoprotein inhibitors and their screening: a perspective from bioavailability enhancement. Pharmacol Res. 2003;48(4):347-359. doi:10.1016/S1043-6618(03)00158-0

63. Palmeira A, Sousa E, H. Vasconcelos M, M. Pinto M. Three Decades of P-gp Inhibitors: Skimming Through Several Generations and Scaffolds. Curr Med Chem. 2012;19(13):1946-2025. doi:10.2174/092986712800167392

64. Laiolo J, Tomašič T, Vera DMA, et al. Analogues of the Lignan Pinoresinol as Novel Lead Compounds for P-glycoprotein (P-gp) Inhibitors. ACS Med Chem Lett. 2018;9(12):1186-1192. doi:10.1021/acsmedchemlett.8b00324

65. Sachs J, Kadioglu O, Weber A, et al. Selective inhibition of P-gp transporter by goniothalamin derivatives sensitizes resistant cancer cells to chemotherapy. J Nat Med. 2019;73(1):226-235. doi:10.1007/s11418-018-1230-x

66. Gu X, Ren Z, Peng H, Peng S, Zhang Y. Bifendate-chalcone hybrids: A new class of potential dual inhibitors of P-glycoprotein and breast cancer resistance protein. Biochem Biophys Res Commun. 2014;455(3):318-322. doi:10.1016/j.bbrc.2014.11.016

67. Chang JB, Wang Q, Li YF. Synthesis and Biological Activity of Wuweizisu C and Analogs. Curr Top Med Chem. 2009;9(17):1660-1675.

68. Chae SW, Lee J, Park JH, Kwon Y, Na Y, Lee HJ. Intestinal P-glycoprotein inhibitors, benzoxanthone analogues. J Pharm Pharmacol. 2018;70(2):234-241. doi:10.1111/jphp.12832

69. Chen C-Y, Liu N-Y, Lin H-C, Lee C-Y, Hung C-C, Chang C-S. Synthesis and bioevaluation of novel benzodipyranone derivatives as P-glycoprotein inhibitors for multidrug resistance reversal agents. Eur J Med Chem. 2016;118:219-229. doi:10.1016/j.ejmech.2016.03.070

70. Dinić J, Podolski-Renić A, Jovanović M, et al. Novel Heat Shock Protein 90 Inhibitors Suppress P-Glycoprotein Activity and Overcome Multidrug Resistance in Cancer Cells. Int J Mol Sci. 2019;20(18):4575. doi:10.3390/ijms20184575

71. Mollazadeh S, Sahebkar A, Kalalinia F, Behravan J, Hadizadeh F. Synthesis, in silico and in vitro studies of new 1,4-dihydropiridine derivatives for antitumor and P-glycoprotein inhibitory activity. Bioorganic Chem. 2019;91:103156. doi:10.1016/j.bioorg.2019.103156

72. Ranjbar S, Khonkarn R, Moreno A, et al. 5-Oxo-hexahydroquinoline derivatives as modulators of P-gp, MRP1 and BCRP transporters to overcome multidrug resistance in cancer cells. Toxicol Appl Pharmacol. 2019;362:136-149. doi:10.1016/j.taap.2018.10.025

73. Hemmer M, Krawczyk S, Simon I, Hilgeroth A. Discovery of substituted 1,4-dihydroquinolines as novel promising class of P-glycoprotein inhibitors: First structure–activity relationships and bioanalytical studies. Bioorg Med Chem Lett. 2015;25(15):3005-3008. doi:10.1016/j.bmcl.2015.05.018

74. Zhu X, Wong ILK, Chan K-F, et al. Triazole Bridged Flavonoid Dimers as Potent, Nontoxic, and Highly Selective Breast Cancer Resistance Protein (BCRP/ABCG2) Inhibitors. J Med Chem. 2019;62(18):8578-8608. doi:10.1021/acs.jmedchem.9b00963

75. Nile SH, Keum YS, Nile AS, Jalde SS, Patel RV. Antioxidant, anti-inflammatory, and enzyme inhibitory activity of natural plant flavonoids and their synthesized derivatives. J Biochem Mol Toxicol. 2018;32(1):e22002. doi:10.1002/jbt.22002

76. Bai J, Zhao S, Fan X, et al. Inhibitory effects of flavonoids on P-glycoprotein in vitro and in vivo: Food/herb-drug interactions and structure–activity relationships. Toxicol Appl Pharmacol. 2019;369:49-59. doi:10.1016/j.taap.2019.02.010

77. Singh S, Prasad NR, Chufan EE, et al. Design and Synthesis of Human ABCB1 (P-Glycoprotein) Inhibitors by Peptide Coupling of Diverse Chemical Scaffolds on Carboxyl and Amino Termini of (S)-Valine-Derived Thiazole Amino Acid. J Med Chem. 2014;57(10):4058-4072. doi:10.1021/jm401966m

78. Liu C-P, Xie C-Y, Zhao J-X, et al. Dysoxylactam A: A Macrocyclolipopeptide Reverses P-Glycoprotein-Mediated Multidrug Resistance in Cancer Cells. J Am Chem Soc. 2019;141(17):6812-6816. doi:10.1021/jacs.9b02259

79. Zeino M, Paulsen MS, Zehl M, Urban E, Kopp B, Efferth T. Identification of new P-glycoprotein inhibitors derived from cardiotonic steroids. Biochem Pharmacol. 2015;93(1):11-24. doi:10.1016/j.bcp.2014.10.009

80. Rocheblave L, de Ravel MR, Monniot E, et al. Deoxycholic acid derivatives as inhibitors of P-glycoprotein-mediated multidrug efflux. Steroids. 2016;116:5-12. doi:10.1016/j.steroids.2016.09.017

81. de Ravel MR, Alameh G, Melikian M, et al. Synthesis of New Steroidal Inhibitors of P-Glycoprotein-Mediated Multidrug Resistance and Biological Evaluation on K562/R7 Erythroleukemia Cells. J Med Chem. 2015;58(4):1832-1845. doi:10.1021/jm501676v

82. Mistry P, Stewart AJ, Dangerfield W, et al. In Vitro and in Vivo Reversal of P-Glycoprotein-mediated Multidrug Resistance by a Novel Potent Modulator, XR9576. Cancer Res. 2001;61(2):749-758.

83. Jekerle V, Klinkhammer W, Scollard DA, et al. In vitro and in vivo evaluation of WK-X-34, a novel inhibitor of P-glycoprotein and BCRP, using radio imaging techniques. Int J Cancer. 2006;119(2):414-422. doi:10.1002/ijc.21827

84. Bonandi E, Christodoulou MS, Fumagalli G, Perdicchia D, Rastelli G, Passarella D. The 1,2,3-triazole ring as a bioisostere in medicinal chemistry. Drug Discov Today. 2017;22(10):1572-1581. doi:10.1016/j.drudis.2017.05.014

85. Borgnia MJ, Eytan GD, Assaraf YG. Competition of Hydrophobic Peptides, Cytotoxic Drugs, and Chemosensitizers on a Common P-glycoprotein Pharmacophore as Revealed by Its ATPase Activity. J Biol Chem. 1996;271(6):3163-3171. doi:10.1074/jbc.271.6.3163

86. Chen T, Wang C, Liu Q, et al. Dasatinib reverses the multidrug resistance of breast cancer MCF-7 cells to doxorubicin by downregulating P-gp expression via inhibiting the activation of ERK signaling pathway. Cancer Biol Ther. 2015;16(1):106-114. doi:10.4161/15384047.2014.987062

87. Chen M, Huang S-L, Zhang X-Q, et al. Reversal effects of pantoprazole on multidrug resistance in human gastric adenocarcinoma cells by down-regulating the V-ATPases/mTOR/HIF-1α/P-gp and MRP1 signaling pathway in vitro and in vivo. J Cell Biochem. 2012;113(7):2474-2487. doi:10.1002/jcb.24122

88. Choi BH, Kim CG, Lim Y, Shin SY, Lee YH. Curcumin down-regulates the multidrug-resistance mdr1b gene by inhibiting the PI3K/Akt/NFκB pathway. Cancer Lett. 2008;259(1):111-118. doi:10.1016/j.canlet.2007.10.003

89. Mao Z, Zhou J, Luan J, Sheng W, Shen X, Dong X. Tamoxifen reduces P-gp-mediated multidrug resistance via inhibiting the PI3K/Akt signaling pathway in ER-negative human gastric cancer cells. Biomed Pharmacother. 2014;68(2):179-183. doi:10.1016/j.biopha.2013.10.003

90. Sui H, Cai G-X, Pan S-F, et al. miR200c Attenuates P-gp–Mediated MDR and Metastasis by Targeting JNK2/c-Jun Signaling Pathway in Colorectal Cancer. Mol Cancer Ther. 2014;13(12):3137-3151. doi:10.1158/1535-7163.MCT-14-0167

91. Hong L, Han Y, Zhang H, et al. The Prognostic and Chemotherapeutic Value of miR-296 in Esophageal Squamous Cell Carcinoma. Ann Surg. 2010;251(6):1056–1063. doi:10.1097/SLA.0b013e3181dd4ea9

92. Bao L, Hazari S, Mehra S, Kaushal D, Moroz K, Dash S. Increased Expression of P-Glycoprotein and Doxorubicin Chemoresistance of Metastatic Breast Cancer Is Regulated by miR-298. Am J Pathol. 2012;180(6):2490-2503. doi:10.1016/j.ajpath.2012.02.024

93. Fisher M, Abramov M, Van Aerschot A, Xu D, Juliano RL, Herdewijn P. Inhibition of MDR1 expression with altritol-modified siRNAs. Nucleic Acids Res. 2007;35(4):1064-1074. doi:10.1093/nar/gkl1126

94. Perez J, Bardin C, Rigal C, Anthony B, Rousseau R, Dutour A. Anti-MDR1 siRNA Restores Chemosensitivity in Chemoresistant Breast Carcinoma and Osteosarcoma Cell Lines. Anticancer Res. 2011;31(9):2813-2820.

95. Li H, Zhou S, Li T, et al. Suppression of BCRP expression and restoration of sensitivity to chemotherapy in multidrug-resistant HCC cell line HEPG2/ADM by RNA interference. Hepatogastroenterology. 2012;59(119):2238-2242. doi:10.5754/hge11781

96. Broxterman HJ, Kuiper CM, Schuurhuis GJ, Tsuruo T, Pinedo HM, Lankelma J. Increase of daunorubicin and vincristine accumulation in multidrug resistant human ovarian carcinoma cells by a monoclonal antibody reacting with P-glycoprotein. Biochem Pharmacol. 1988;37(12):2389-2393. doi:10.1016/0006-2952(88)90365-6

97. Pearson JW, Fogler WE, Volker K, et al. Reversal of Drug Resistance in a Human Colon Cancer Xenograft Expressing MDR1 Complementary DNA by In Vivo Administration of MRK-16 Monoclonal Antibody. JNCI J Natl Cancer Inst. 1991;83(19):1386-1391. doi:10.1093/jnci/83.19.1386

98. Tsuruo T, Hamada H, Sato S, Heike Y. Inhibition of Multidrug-resistant Human Tumor Growth in Athymic Mice by Anti-P-glycoprotein Monoclonal Antibodies. Jpn J Cancer Res. 1989;80(7):627-631. doi:10.1111/j.1349-7006.1989.tb01688.x

99. Mechetner EB, Roninson IB. Efficient inhibition of P-glycoprotein-mediated multidrug resistance with a monoclonal antibody. Proc Natl Acad Sci U S A. 1992;89(13):5824-5828. doi:10.1073/pnas.89.13.5824

100. Livney YD, Assaraf YG. Rationally designed nanovehicles to overcome cancer chemoresistance. Adv Drug Deliv Rev. 2013;65(13-14):1716-1730. doi:10.1016/j.addr.2013.08.006

101. Murakami M, Cabral H, Matsumoto Y, et al. Improving Drug Potency and Efficacy by Nanocarrier-Mediated Subcellular Targeting. Sci Transl Med. 2011;3(64):64ra2-64ra2. doi:10.1126/scitranslmed.3001385

102. Braunová A, Kostka L, Sivák L, et al. Tumor-targeted micelle-forming block copolymers for overcoming of multidrug resistance. J Controlled Release. 2017;245:41-51. doi:10.1016/j.jconrel.2016.11.020

103. Emilienne Soma C, Dubernet C, Bentolila D, Benita S, Couvreur P. Reversion of multidrug resistance by co-encapsulation of doxorubicin and cyclosporin A in polyalkylcyanoacrylate nanoparticles. Biomaterials. 2000;21(1):1-7. doi:10.1016/S0142-9612(99)00125-8

104. Wang H, Gao Z, Liu X, et al. Targeted production of reactive oxygen species in mitochondria to overcome cancer drug resistance. Nat Commun. 2018;9(1):562. doi:10.1038/s41467-018-02915-8

105. He J, Gong C, Qin J, Li M, Huang S. Cancer Cell Membrane Decorated Silica Nanoparticle Loaded with miR495 and Doxorubicin to Overcome Drug Resistance for Effective Lung Cancer Therapy. Nanoscale Res Lett. 2019;14(1):339. doi:10.1186/s11671-019-3143-3